Characterization of rapid neurite manipulation for building an artificial neural network with neurons

Matthew Rigby

Physics Department, McGill University

Montreal, Québec, Canada

August 2019

A thesis submitted to McGill University in partial fulfillment of the requirements of the degree of Doctor of Philosophy

Table of contents

Contents

Abstract

This thesis presents an approach for how to build an artificial neural network with neurons for the purpose of comparing how artificial and biological neural networks process information. Image recognition of hand-written digits using a multi-layer perceptron is chosen because the task is complex but well studied, and the network does not have too many neurons. To wire an artificial neural network with neurons, a technique for rapid manipulation of neurites is used and characterized. Reliable, rapid pulling speeds and the maximum forces required to manipulate neurites are determined. Using these parameters, multiple magnetic pole pieces are chosen to be the technique most suitable to build a neural network and the total amount of time it will take to wire the network is calculated. An approach for training the biological neural network to recognize hand-written digits is proposed. The ability to test the robustness of a trained neural network is shown by axotomizing and reconnecting live axons. To further understand this remarkably fast neurite manipulation, the neurite's mechanical properties are determined. The initiation of the neurite is modelled as a catenoid which transitions to a long cylindrical tube once the catenoid is no longer stable. The viscoelastic extension of the neurite is phenomenologically modelled during constant velocity elongation as a Maxwell element with a viscosity and an elasticity. When the neurite is elongated in steps, the slightly more complex model consisting of many flowing springs in series is used to estimate the neurite's elastic modulus and composition. It is determined that during this initial period of elongation, the neurite is mainly plasma membrane with a small amount of cytoskeleton. However, over the course of tens of minutes, the actin cytoskeleton is shown to arrive in the neurite, making it more structurally stable. The flowing of actin cytoskeleton is used as a proxy for growth and is modelled with a Maxwell viscoelastic element, giving a characteristic time for the arrival of actin and an effective growth rate of the neurite.

Résumé

Cette thèse présente une approche sur la façon de construire un réseau de neurones artificiels avec des neurones dans le but de comparer la manière dont les réseaux de neurones artificiels et biologiques traitent les informations. La reconnaissance d'image de chiffres écrits à la main à l'aide d'un perceptron multicouche est choisie parce que la tâche est complexe mais bien étudiée et parce que le réseau ne comporte pas trop de neurones. Pour connecter un réseau de neurones artificiel avec des neurones, une technique de manipulation rapide des neurites est utilisée et caractérisée. Des vitesses de traction fiables et rapides ainsi que les forces maximales requises pour manipuler les neurites sont déterminées. En utilisant ces paramètres, plusieurs pièces de pôles magnétiques sont choisies comme la technique la plus appropriée pour construire un réseau de neurones et le temps total nécessaire pour connecter le réseau est calculé. Une approche pour entrainer le réseau de neurones biologiques à reconnaître les chiffres écrits à la main est proposée. La capacité à tester la robustesse d'un réseau neuronal formé est illustrée par l'axotomisation et la reconnexion d'axones vivants. Pour mieux comprendre cette manipulation de neurites remarquablement rapide, les propriétés mécaniques du neurite sont déterminées. L'initiation du neurite est modélisée comme un caténoïde qui se transforme en un long tube cylindrique une fois que le caténoïde n'est plus stable. L'extension viscoélastique du neurite est modélisée de manière phénoménologique au cours d'un allongement à vitesse constante sous la forme d'un élément de Maxwell ayant une viscosité et une élasticité. Lorsque le neurite est allongé en distances discrètes, un modèle légèrement plus complexe, composé de nombreux ressorts coulants en série, est utilisé pour estimer le module d'élasticité et la composition du neurite. Il est déterminé que pendant cette période initiale d'élongation, le neurite est principalement constitué de membrane plasmique avec une petite quantité de cytosquelette. Cependant, au bout de quelques dizaines de minutes, le cytosquelette d'actine arrive dans le neurite, le rendant plus structurellement stable. L'écoulement du cytosquelette d'actine est utilisé comme indicateur de la croissance et est modélisé avec un élément viscoélastique de Maxwell, donnant un temps caractéristique pour l'arrivée de l'actine et un taux de croissance effectif du neurite.

Acknowledgements

I would like to thank my supervisor, Peter Grütter, for his guidance, insight and patience. It was a pleasure meeting and discussing research and the world every week with someone who is so intelligent, passionate and friendly. Thank you.

I would like to thank the entire Grütter group for the daily interactions I had with them, whether it was to troubleshoot an issue, discuss science or take a break. In Particular, Yoichi Miyahara, who was always there to help.

I would like to thank everyone in the Fournier lab for welcoming me into their neuroscience lab even though I was a physicist. The collaboration I had with your lab was extremely important for my PhD.

Thanks also to the supporting staff who were patient and industrious whenever I needed their help. Thank you, Robert, John, Richard, Pascal, Juan, Paul, Janney, Philippe and Isabel.

Thanks to my siblings, Mireille, Jamie and Peter, and my close friends for the emotional support during this long journey.

And of course, to my Mom and Dad. To my Mom, whose only concern is that I'm happy and believes the rest will come naturally, and my Dad, who is so interested and excited to talk to me about physics and life. Thank you so much for both of your support, I appreciate it so much.

Matthew Rigby

McGill University

August 2019

Preface and statement of originality

The author, Matthew Rigby, claims the following aspects of the work contained herein to constitute original scholarship and an advancement of knowledge. Currently, this thesis contains results from one publication. The first two points are from this publication.

- Presenting an approach for building, training and testing the robustness of an artificial neural network with biological neurons (chapter 3). M. Rigby, M. Anthonisen, X.Y. Chua, A. Kaplan, A.E. Fournier, and P. Grütter, AIP Adv. **9**, 075009 (2019).
- Characterizing the neurite as a Maxwell viscoelastic material and showing that the mechanically pulled neurite acts as a guiding structure for the actin network to flow into (chapter 3). M. Rigby, M. Anthonisen, X.Y. Chua, A. Kaplan, A.E. Fournier, and P. Grütter, AIP Adv. **9**, 075009 (2019).
- Estimating the elastic modulus and determining the composition of the neurite following initiation by modelling it as many springs in series that flow (chapter 4).
- Method for subtracting the crosstalk between temperature fluctuations and the AFM cantilever deflection for AFM normal force measurements (chapter 2).
- Method for reducing the lateral spring constant of the cantilever, improving measurement sensitivity and reducing uncertainty for AFM lateral force measurements (chapter 2).

Contribution of co-authors

This thesis is largely based on the following publication: Rigby, M. et al. 2019. “Building an Artificial Neural Network with Neurons.” *AIP Advances* 9(7): 075009., which was co-authored by Madeleine Anthonisen, Xue Ying Chua, Andrew Kaplan, Alyson Fournier and Peter Grütter. Their contributions to the thesis are as follows:

- Madeleine Anthonisen discussed the design of experiments and analysis of the data (all chapters). Assisted in the culturing of neurons.
- Xue Ying Chua discussed the design of experiments and analysis of the data (all chapters). Assisted in the culturing of neurons.
- Andrew Kaplan discussed the design of experiments and analysis of all the data in chapter 3. Assisted in the culturing of neurons. Provided the neuron fixation protocol (section 2.4.1). Assisted with preparing and troubleshooting the setup described in section 2.3.3.
- Alyson Fournier discussed the design of experiments and analysis of all the data in chapter 3.
- Peter Grütter supervised all the work in this thesis. Discussed the design of experiments and analysis of all the data. Revised the manuscript.

1

1. Introduction

1.1 Biological neural networks

The brain is an amazing organ capable of rapidly processing information, giving rise to consciousness and emotions, and allowing the completion of complex tasks. It is composed mainly of neurons and glial cells, where approximately 86 billion neurons[1] make about 100 trillion connections. There are about equal number glia and neurons in the brain,[1] but glia are viewed to have a mainly supportive role such as forming myelin, maintaining homeostasis and forming the blood brain barrier. Glia have also been shown to potentially play a role in information processing, although this is a heated subject of debate.[2–5]

The brain transmits information by sending electrical signals between neurons. Each neuron consists of a cell body with a nucleus and many long, thin, protruding cytoplasmic processes called dendrites and one axon (see figure 1.2). The electrical signal is sent from the nucleus by locally depolarizing the cell membrane in a transient wave which propagates down the axon. Each wave is known as an action potential and propagates at *in vivo* speeds of about 1-120m/s.

The axon extends much further than the dendrites and transmits outgoing signals only. At the end of the axon, it splits into many branches and forms synapses with other neurons' dendrites.

When the action potential reaches the synapse, the pre-synaptic membrane is depolarized, causing the release of neurotransmitters across the synaptic cleft (a small gap separating the pre- and post- synapses). Neurotransmitters diffuse across the gap and bind to specific receptors on the post-synapse, causing ion channels to open. Depending on the nature of the synapse, this can either cause a de-polarization or a polarization of the next axon, with these being known as excitatory or inhibitory connections respectively. If the accumulation of changes to the potential difference of the cell body depolarizes the membrane beyond a specific threshold, another action potential will be initiated in the post-synaptic neuron. This is a highly non-linear process because action potentials do not have a gradient of strengths. An action potential either occurs or it does not, and each one has the same strength. The requirement to reach a threshold to fire is similar to transistor-transistor logic pulses in digital electronics.

Each neuron is connected on average to 1000 other neurons, making for an extremely complex interconnected network. The more interconnected the network, the more opportunity for signal processing, allowing for more complex learning. As connectivity increases, circuit complexity increases. Some of the basic building blocks which are observed throughout the brain are the feedforward and feedback loop (see figure 1.1). In the feedforward circuit, one neuron is connected to two neurons which are also connected themselves.[6] The axon can also grow an axon collateral, which can act similarly to the axon by connecting with another neuron, or can connect back to itself. This type of feedback loop can aid in the modulation of parallel processes.[7]

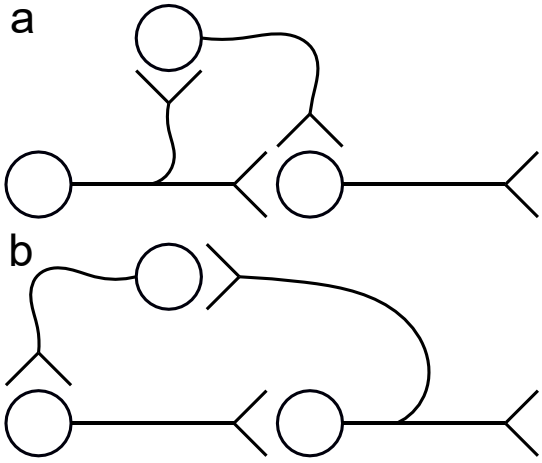

Figure 1.0.1 Examples of simple circuits found in the brain and in artificial neural networks. (a) Feedforward circuit (b)

Learning is achieved by the process of forming, strengthening or weakening specific connections such that the spatio-temporal organization of electrical signals is changed. Hebbian theory says that this can be done by altering the number or nature of synaptic connections.[8–10] A

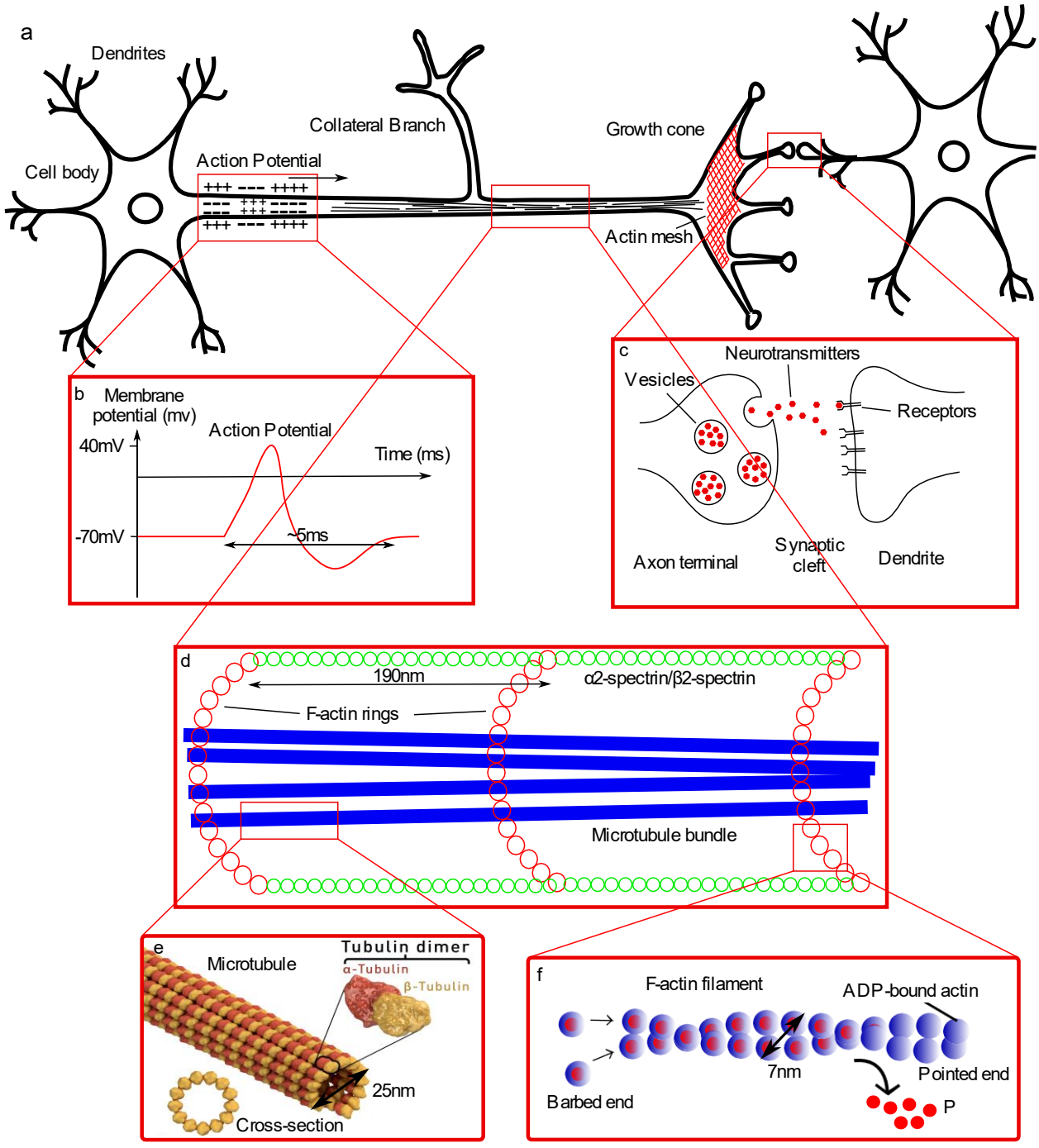

Figure 1.2 Neuron architecture and function (a) Neuron with a collateral branch has formed a synapse with another neuron. (b) Action potential propagates distally, changing the local polarization of the axon from -70mV to +40mV for a transient time of a few milliseconds. (c) When an action potential arrives at the axon terminal, this triggers the release of neurotransmitters across the synaptic cleft which bind to receptors on the post-synaptic dendrite. (d) The cytoskeletal structure of an axon has microtubules bundles and an actin scaffolding which is formed of actin rings connected by spectrin. (e-f) Microtubules are formed by tubulin dimer subunits while F-actin filaments are formed by actin monomers (e-f are adapted from Wikipedia, 2019).

pre-synaptic neuron whose action potentials correlate with those in the post-synaptic neuron will likely strengthen the synaptic connection in a process called long-term potentiation. The functional opposite of this is long-term depression and can be induced when the post-synaptic neuron does not fire following pre-synaptic action potentials.[10–13]

1.2 Artificial neural networks

Artificial neural networks used in machine learning were initially based on mathematical models of biological neural networks.[14] In comparison with a brain (as far as we are aware), a computer has no autonomy, consciousness or free will, so it is not intelligent in that regard. However, whereas classical computer programs could only perform the task exactly as specified by the programmer, artificial neural networks can improve their performance over time, displaying the capacity to 'learn'.

Initially, artificial neural networks had little success, but as the processing power of the computer increased, the number of nodes or 'neurons' available to put in a network has also drastically increased, allowing the network to solve increasingly difficult tasks. Interestingly, algorithms that existed in the 1980s work quite well, but the computational power wasn't strong enough until the late 2000s to test them.[14] Also, the necessary training sets really only existed once social media started to be broadly used. It is unsurprising that the brain still outperforms artificial neural networks in many tasks as the total number of nodes in the biggest artificial neural networks is 10 million, which is about four orders of magnitude smaller than the human brain (see figure 1.3). The computational power of a computer is linked to the number of transistors it has, so it is not a coincidence that the doubling of transistors occurs every 2 years and the total number of nodes in artificial neural networks doubles every 2.4 years. At this rate, the number of nodes in the artificial neural network will equal that in the human brain by about 2050. Perhaps when this level of complexity is achieved, the network will achieve the same level of autonomy as a human.

Each 'neuron' or node in an artificial neural network holds some information encoded by bits which are physically held by transistors. The value of a node is operated on and sent to another node by passing through logic gates. The bit rate, or the rate at which the signal propagates to

the next node is almost the speed of light, so it is about 1 million times faster than the fastest action potentials, allowing very fast computation. In contrast to an action potential which either fires or it does not, the value passed from one node to the next can take on any value, meaning it can be linear or highly non-linear. Training a network can be done very quickly as the strengthening of connections between nodes can be varied immediately since it is not limited by the slow physiological process of strengthening or weakening a synapse. Since the early 2010s, connectivity of thousands of connections per neuron (as in the brain) has been achieved.[15] Many of the same types of circuits present in the brain are also present in an artificial neural network such as feedforward and feedback loops (see figure 1.1). However, there may be ways in which the neuron processes information which is not captured in an artificial neural network computer model, such as differences in diameter of the axon.

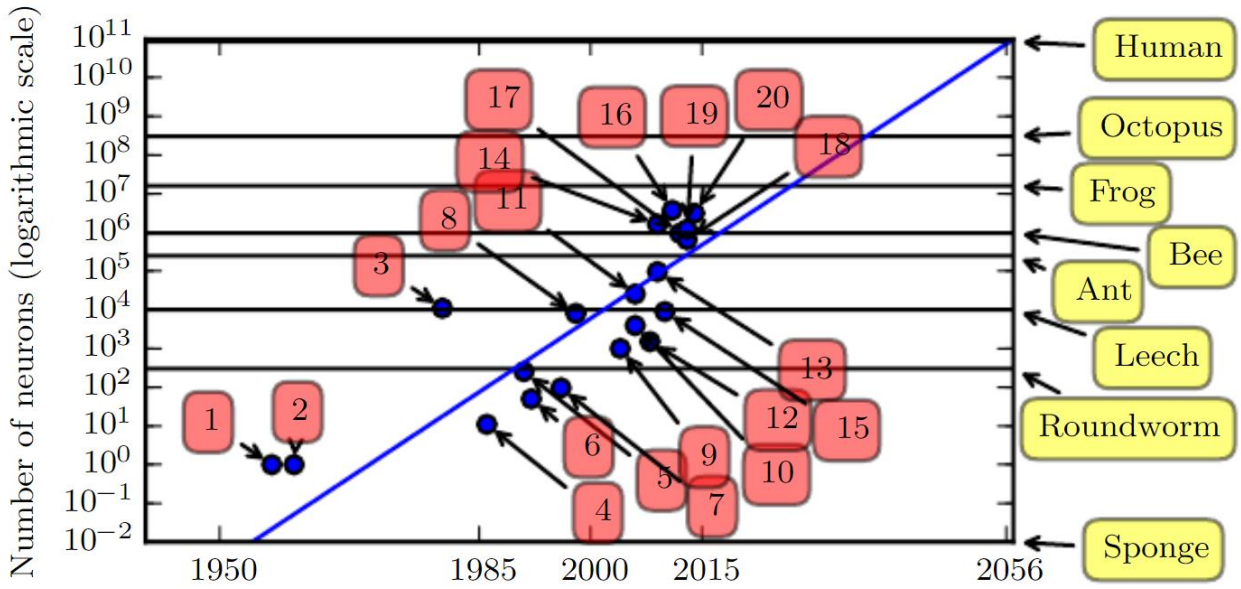

Figure 1.3 Increase in neural network size with time. According to the trendline, the neural network size doubles every 2.4 years and will reach human brain size by approximately 2050. The numbers correspond to specific neural networks referenced in Goodfellow et al. 2016. Figure reproduced from Goodfellow et. al, 2016.

Inspired by the quote "What I cannot create, I do not understand" (written on Richard Feynman's blackboard at the time of death in February 1988), we believe that by building an artificial neural network from biological neurons, we will be able to understand what is fundamentally different between a brain and a machine. In order to build an artificial neural network from biological neurons, we require a method to connect hundreds of neurons to

thousands of specific targets and the ability to both record and stimulate each neuron in the network.

1.3 Building biological neural networks

Many groups have attempted to build biological neural networks and study their connectivity. The approaches usually constitute either taking slices of the brain to look at a circuit of interest or dissecting the neurons and allowing them to form a circuit.[16] In dissected cultures, neurons can be encouraged to form synapses with specific targets, but there is still an element of randomness in the circuits. Some rules can be followed to increase the chances of them forming the desired connections. For example, it was discovered that neurons that are close to each other are more likely to make a connection in sparse cultures than in dense cultures.[17]

The distribution, density and neuronal growth cues given to neurons are important components when trying to wire a neuronal network with known topology. Using sparse cultures is essential to be sure that neurons do not make any undesired connections. This presents a significant challenge because neurons grow much better when they are surrounded by other neurons. By using patterned surfaces of cell adhesive molecules such as poly-lysine[18] (and by preventing non-specific attachment[19]), it is possible to keep separate populations of neurons from connecting to each other. At least two groups have even managed to get single neuron confinement. One group used disposable PDMS stencils in a "NeuroArray"[20] while the other used physical confinement called neurochips,[21] which essentially had cages over individual micro electrode array electrodes. The electrodes are an essential part of being able to record and train the network. By connecting single neurons with adhesive strips, up to 90% of neurons have been able to make monosynaptic connections separated by only 50um.[22] The use of other confinement devices also allowed single neurons to make single connections.[23,24] However, connecting one neuron to multiple targets while not allowing it to make connections with other nearby targets has not yet been achieved to our knowledge.

Using confinement devices, Feinerman and colleagues[25] have been able to show that groups of neurons can work together to act as a Boolean logic gate such as the AND gate and another circuit that was similar to a diode. This is impressive, although it is still unclear whether large

groups of neurons form in the brain to operate as single Boolean logic circuits. Treating the neurons as individual computational units would be more efficient for the brain but could be more susceptible to noise or cell death. Using individual neurons to form a more complex circuit based on artificial neural networks to complete more complex tasks such as recognizing images would help to understand how the brain computes information. For this, we require a method for building biological neural networks on a micro electrode array and the capability of connecting any neuron to as many target neurons as we'd like.

Rather than allowing the neurons to grow randomly and hope that they make the desired connections, Fass et al. 2003[26] proposed using a magnetic pole piece to tow axons to connect any two neurons. Unfortunately, this method appears to be limited by the maximum neurite elongation speed of 0.055µm/s, above which the axon thins and breaks. A large speed up is thus required to wire a large neural network, without which this method is prohibitively slow because the neurons will not survive long enough to form the network.

1.4 Neurite growth

Average axonal growth occurs at a rate of 0.0017µm/s but can increase significantly in bursts. Growth depends strongly on the growth cone providing tension to the rest of the axon (see figure 1.2).[27] The growth cone is dynamic and motile and is constantly using small extrusions at its periphery called filopodia to find the correct path during development.[28–30] The growth cone and the entire axonal shaft is made of plasma membrane and contains actin, microtubules and associated proteins which work together for axonal growth and to give the axon its properties.

G-actin monomers polymerize to form a filament called F-actin which has a diameter of 7nm and can assemble into lengths of many micrometers (see figure 1.2f). F-actin polymers are present throughout the axon. In the axolemmal space (in the outer 50-100nm of the axon), they form rings which are periodically spaced 190nm apart, and are linked together by spectrin to form a scaffold (see figure 1.2d).[31] There are also patches of actin filaments found throughout the axon which seem to be precursors for filopodia as well as trails and hot-spots.[32,33] In the growth cone, they form a dense mesh.[34] F-actin filaments are polarized such that a concentration which gives polymerization at the barbed end leads to depolymerization at the pointed end. This

can lead to a steady state known as treadmilling where the length of the polymer is constant because polymerization and depolymerization occur at the same rate.[34] Associated binding proteins regulate the organization of F-actin in many ways (e.g. by binding with actin and inhibiting the addition or removal of subunits to the polymer).

Microtubules are made of 12-15 tubulin dimers in circumference and form to make a long cylindrical polymer with a diameter of 25nm and lengths of many micrometers up to 50um (see figure 1.2e).[35] They form a central bundle all along the length of the axon until the growth cone where they end spread out at the base of the growth cone. In the axon, all microtubules are polarized with their plus ends pointed distally (i.e. away from the nucleus), allowing for polymerization in that direction. Microtubules have a dynamic instability which depends on the concentration of tubulin dimer subunits, where they can quickly switch between growing (polymerization in the plus direction) and shrinking (loss of tubulin dimers off the plus side). It is also possible for the polymer to become hydrolysed, at which point the entire polymer can undergo a dramatic shrinkage in length called catastrophe.

Neurofilaments are formed from a family of different proteins and measure about 10nm in diameter and many micrometers in length. Similarly to actin and microtubules, they help to give structural stability to the axon. They are also believed to have a crucial role in determining the caliber of the axon, which affects action potential propagation speeds.[36]

Filopodia protrude from the cell body or axon through actin polymerization which applies a force on the membrane with the help of myosin.[32] If the filopodia makes an adhesive contact, this can sustain the tension of the membrane. A neurite is consolidated when microtubules enter the filopodial protrusion. It is unclear whether the microtubules polymerize into the protrusion or whether it is only preformed, acetylated, stable microtubules which translocate into the protrusion.[34,37] Experiments by Smith et al. 1994 used taxol and nocodazole to prevent new polymerization, but the neurite still formed,[37] while Slaughter et al. 1997 labeled new tubulin dimers, and showed in this way that none of these tubulin dimers were present in microtubules in a new neurite of 50µm length.[38] This seems to indicate that microtubules are pushed or pulled into the protrusion to form a new neurite.

Growth cones have a network of meshed actin which are very dynamic and their polymerization is constantly pushing out the leading edge. They work with myosin II to exert a force on the rest of the axon.[39] Similarly to neurite initiation, a protrusion of actin extends, adheres, and exerts a force, creating cytoplasmic space for microtubules and associated organelles to fill.[40,41] The engorgement of cytoplasmic space just described is one possible mechanism by which the axon may be elongating. This theory is further supported by work showing that branch points and marks along the axon are stationary during axonal elongation.[42–46] It is also possible that the forces applied by the growth cone cause bulk transport all along the axon by stretching along its length. This has been shown by tracking docked materials which seem to move at low velocity transport speeds along the length of the axon.[47] In addition, in the tip growth model, microtubules should be polymerizing into the cytoplasmic space, but the microtubule polymerizing drug taxol does not induce more elongation.[48] It was also shown that by stretching the entire length of the axon, remarkable growth rates of 8mm/day could be attained, which are not sustainable by tip growth only.[49–51] The cytoskeleton has been shown to have anterograde movement during growth by using photobleached and photoactivated microtubules, although the effect diminishes in the proximal part of the axon.[52,53] It is possible that adhesion influences the mechanism by which axons grow. Xenopus neurons grown on a highly adhesive substrate (concanavalin A) display tip growth, whereas growth along the body occurs when they were grown on more permissive substrates (laminin).[54] Furthermore, low velocity transport of docked mitochondria in an axon detached from the substrate was shown to move much quicker in the part of the axon no longer adhered to the substrate.[55] The effect of adhesion on growth is further discussed in the following section.

Following initiation, we expect a mature axon to have neurofilaments, microtubules and F-actin. F-actin forms a scaffold with spectrin dimers which bind to axolemmal proteins and resists mechanical forces.[56] C. elegans axons that do not have β-spectrin break.[57] Actin also stabilizes synapses by increasing the concentration of F-actin relative to the rest of the axon, and maintaining the same F-actin ring structure it has elsewhere.[34,58,59] Microtubules mainly contribute to active axonal transport, which is important given the length of the axon, and

neurofilaments determine the axon caliber. Without these cytoskeletal components, we expect the neurite to be more prone to breakage.

The importance of forces for the initiation and elongation of neurites has been well studied. In 1984, Bray showed that by adhering to the cell body using a pipette coated with collagen and polylysine, neurites could be initiated *de novo* and extended faster than normal growth at 0.017μm/s.[43] He noted that the neurite had a growth cone-like structure with axon-like caliber and showed using electron microscopy that it contained microtubules and neurofilaments. When the neurites were released, they grew similarly to a growth cone. When he added colchicine, a microtubule depolymerization drug, only tether-like structures formed, showing that the neurite needed microtubules to form.

A series of excellent studies performed by Heidemann's group quantified the forces needed to initiate and extend neurites and axons. This was done by using force sensitive needles with spring constants between 0.01-0.1N/m. The needle was coated with polylysine, collagen and laminin or polylysine and concavalin A to adhere the needle to the neurites. After adhering, the neurite was initiated and extended, while the bending of the force sensitive needle was compared to a rigid reference needle, allowing the force applied to the neurite to be quantified. They typically pulled the neurites with feedback on the force signal such that a constant force was applied. The speed of elongation was then the speed at which the axon could adapt (presumably by adding material) to maintain a constant force. They determined that neurite elongation speed had a linear dependence on the force which ranged between 0 and 0.6 micrometers per hour per piconewton of force applied. It was also determined that there was a threshold force for elongation under which the neurite would retract.

They initiated and elongated neurites from a variety of different neuronal types: chick sensory and cortical neurons[27,60–62], NGF treated PC 12 cells[61] and rat hippocampal neurons.[63] The initiation force for neurites depended on the type of neuron: for chick forebrain neurites, the force required was on the order of hundreds of piconewtons, sensory neurites required between 1-2nN and PC-12 cells required between 1-10nN.

Force sensitive needles require a very stable setup with limited drift and a lot of user experience to get an accurate measurement of force, so Fass et al. 2003 used a simpler magnetic

trap setup to pull neurites.[64] They coated magnetic beads in netrin and used a magnetic pole piece to apply and measure forces while initiating the neurites.[26] This method allowed the measurement of forces down to tens of piconewtons, and allowed them to determine that the threshold force for extension of neurites was between 15-100pN. This was significantly smaller than the forces required for initiation of the neurites which was hundreds of piconewtons. However, no explanation was proposed for this higher force. In addition, the mechanism by which neurites are naturally initiated require actin polymerization to form a small protrusion followed by the insertion of microtubules to consolidate the neurite. Powers et al. 2002 and Derenyi et al. 2002, modelled the formation of tethers.[65,66] Although tethers are mainly plasma membrane, so the exact details of the resistance to neurite formation is different, the situation is similar because actin polymerizes into plasma membrane to form a protrusion. They show that the tension is highest when the protrusion is small while the neurite is in the form of a catenoid (see figure 1.4c). However, the catenoid is only stable for a few micrometers, after which the neurite forms a long cylindrical process, causing the tension to decrease. As the cylindrical neurite is stretched however, the force increases again, but it is no longer necessary to overcome the same energy barrier posed by the catenoid. This may be why the minimum force extension for neurites is 15-100pN whereas initiation requires hundreds of piconewtons.

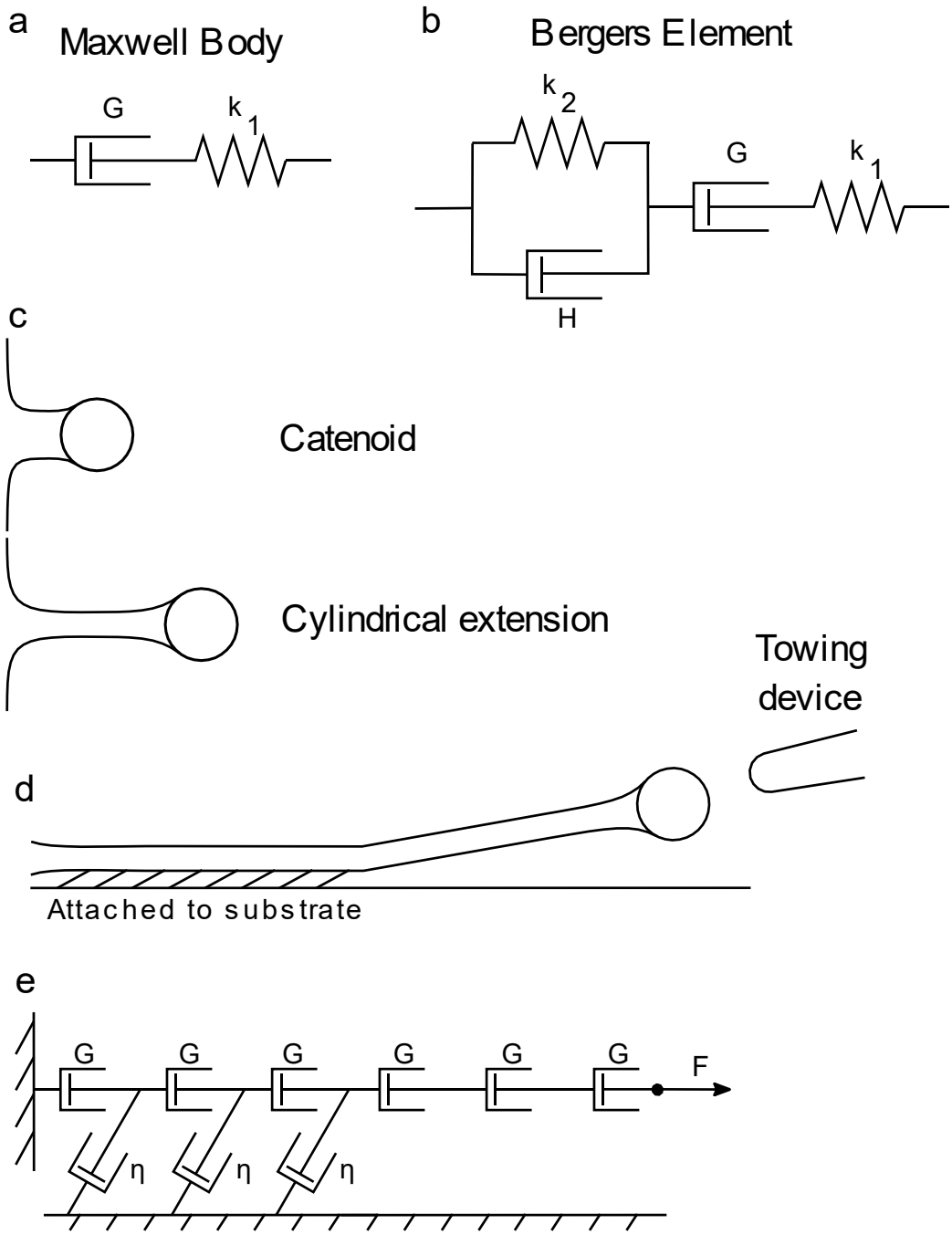

Figure 1.4 Modelling neurite extension. (a) Basic viscoelastic element called the Maxwell body with a spring and dashpot in series. (b) A slightly more complex viscoelastic element called the Bergers element, used by Dennerll et al. 1989 to model axons. (c) During initation, the neurite is initially a catenoid, causing the force of initiation to be higher than the force to extend the cylindrical neurite. (d) Neurite is towed at the tip in all towing experiments. Here, the proximal part of the neurite is adhered to the surface, while the distal end is not. (e) The model used by O'Toole et al. 2008 uses dissipation dashpots to model the adhesion of the neurite to the surface proximally, while the entire neurite is modelled by many growth dashpots in series.

1.5 Modelling neurite growth

To wire a neural network one neurite at a time will take a very long time. The feasibility of this approach will depend on how fast the neurites can be initiated and elongated. Understanding what parameters optimize this speed are crucial for building a neural network using neurons.

Bray pulled neurites out of the cell body after being in contact with polylysine coated pipette only "10 minutes or so".[43] He typically pulled the neurites at a rate of 0.0067-0.027μm/s but made a few attempts to pull much faster. At 0.28μm/s, there was either no neurite formation or the neurite would fail. Heidemann's group either adhered to the growth cone to extend axons or initiated neurites using polylysine, collagen and laminin or polylysine and concavalin A from the cell body. They initiated the neurites immediately after contacting the cell. They noted a linear increase between elongation rate and force, with an upper limit on speeds of about 0.05μm/s.[26] Fass et al. 2003 used netrin coated beads to initiate neurites from the cell body and initiated the neurites immediately following addition of the beads to the neurons. They observed that at speeds above 0.055μm/s, the neurite thinned and broke.[26] Lucido et al. 2009 showed that axons will form synapses if left in contact for longer than 30 minutes with an adhesive molecule (e.g. polylysine).[67] None of the pipettes nor the beads in the experiments by Bray, Heidemann's group or Fass were left in contact this long, and they initiated neurites from the cell bodies, so it is unlikely that the neurons formed synapses with them. This may be one reason why the neurites broke when extended too quickly.

When deforming an axon or neurite, the deformations will be both elastic and viscous. On short time scales, the elastic component dominates, but axons and neurites are made of viscous materials, so the viscous component will eventually be observed for long time scales. The viscous response of a mature axon takes tens of minutes to relax.[60] The most basic phenomenological model which captures viscoelastic behaviour is a Maxwell element (see figure 1.4a). This combines a simple elastic spring and a viscous dashpot. In this simple model, a force applied to the material with a constant strain will initially cause the spring to stretch, with the dashpot element viscously flowing to relieve some of the force on the spring. However, if the force is applied through constant velocity elongation, then the elastic deformation will initially increase

linearly and eventually plateau when the dashpot starts to flow at the same velocity as the elongation.

Dennerll et al. 1989 were the first to propose a phenomenological model to describe the elongation of neurites.[27] Using force needles to measure the force, they extended the neurite, and allowed them to relax. For their data, they found that the Maxwell model was too simplistic to describe the force profile. They needed an extra spring and dashpot to add to the Maxwell model in order to capture neurite growth, and not just the viscoelastic response. The model is a Burgers element (see figure 1.4b) and consists of a Maxwell element in series with a Kelvin-Voigt element (a spring and dashpot in parallel). After an initial stretch, there is a period of delayed stretch, followed by elongation at a constant rate.

Aeschlimann proposed a model that attempted to describe different segments of the axon.[68,69] She used springs all along the length of the axon to describe the elastic behaviour and one growth dashpot to describe the growth due to material being added at the growth cone. She also had the insight to incorporate viscous drag due to adhesion between the axon and the surface. She treated the axon as a viscoelastic solid where growth only occurred through the growth cone. However, this neglects the possibility of growth occurring through the addition of material all along the body of the axon and through viscoelastic flow.[49,60] Low velocity transport which occurs following increased tension cannot be described only by adding material at the tip.[47,55] Also, in a viscoelastic solid flow would stop whenever the growth stopped advancing, but this is not what is observed.[55]

O'Toole used a similar approach, but modelled the axon instead as a viscoelastic fluid.[55,70] He used the model proposed by Dennerll et al. 1989 to describe the entire length of the axon by putting many Burgers elements in series. As in Aeschlimann's model, this allows the axon to be treated in segments. This is useful when modelling the adhesion of the axon to the surface because frictional dashpots can be added to the Burgers elements wherever the axon is adhered to the surface (see figure 1.4e). By pulling at a constant force, the Burgers elements simplifies to a number of growth dashpots in series adhered to the surface by frictional dashpots. This describes the low velocity transport of docked mitochondria through the axon very well. They showed that, in portions where the axon was detached from the surface, the low velocity

transport was significantly increased. Growth dashpots have a high viscosity if the cytoskeleton is well developed (i.e. with a significant amount of cross-linkage). In this case, the growth is predicted to be quite slow. When the axon is strongly adhered to the surface, the frictional dashpot coefficient is high, which means that the tension generated at the growth cone will dissipate along the length of the axon, which also causes the growth dashpots to flow slowly. This is shown by a slowing of low velocity transport when axons are grown on very adhesive substrates.[54,55] Further evidence for this model is observed when the proximal part of the axon is dislodged from the surface and pulled. Low velocity transport was significantly higher in the proximal part where there was no adhesion. In addition, the velocity profile when no adhesions are present is linear, whereas in sections where the axon was adhered to the surface, the velocity profile was nonlinear, which is predicted by the model.

To wire a complex neural network, fast neurite elongation is required to be able to manually connect all the neurons to their targets. The criteria for maximizing elongation speed are:

1) Strongly adhering to the distal part of the neurite to be able to apply large forces without detachment or breakage.

2) Minimizing the viscosity of the growth dashpots.

3) Minimizing dissipation along the length of the neurite by preventing adhesion of the neurite to the surface.

Synapses are reinforced significantly by increased actin concentrations, so the formation of a synapse on the large surface of a bead would be a very strong point of adhesion from which to apply large forces. By initiating a neurite from the axon rather than the cell body, there would be less material available to immediately make a thick branch, meaning that the growth dashpot would be smaller. Additionally, due to minimization of surface area and the condition that the transition from axon to neurite must be smooth,[65,66] we expect the neurite coming out of the side of an axon to be smaller than the axon itself, whereas neurites formed from the cell body could be much bigger (as is the case in the axon initial segment). These branches are still able to become as thick and strong as an axon as shown by collateral branch formation. By forming a neurite *de novo* from another axon, the elongation of the neurite can be suspended in solution to avoid adhering to the surface and to minimize friction which opposes low velocity transport.

Lopez et al. 2016 has indeed shown that neurites grown in this way can be pulled at high speeds (0.33µm/s) and are physiologically indistinguishable from regular axons in that they contain microtubules, F-actin and neurofilament and are able to send action potentials to neighbouring neurons.[71,72] She does not give an explanation for why this may be possible, which could be useful when optimizing growth speeds for wiring a neural network. By using a similar model to O'Toole but without adhesive frictional dashpots, and assuming that the cytoskeleton is a good proxy for the growth dashpot parameter and neurite maturation, we can confirm whether this model is appropriate for these neurites and maximize growth speeds with the goal of wiring up a biological neural network using neurons.

2

2. Experimental techniques and procedures

2.1 Atomic force microscopy

Atomic force microscopy (AFM) uses a local probe (a sharp tip) to obtain images of the surface with angstrom resolution. It has comparable resolution to scanning tunneling microscopy and transmission electron microscopy and has approximately 1000 times better resolution than diffraction limited optical microscopy. Binnig et al. invented AFM in 1986 with the motivation of investigating insulators on the atomic scale because the scanning tunneling microscope could only probe conductive samples.[73] In addition to high resolution topographic images, AFM can be used to manipulate the sample or measure a variety of sample properties. Since AFM measures surface forces, an appropriate choice of sample and tip can be used to measure almost any force. Unfortunately, this versatility also makes AFM measurements susceptible to crosstalk with other forces.

Conceptually, making an AFM image is analogous to closing your eyes and building an image in your mind by feeling the surface with your hands. By replacing your fingers with a sharp

tip and your sensory neurons with a force sensitive lever, an image is constructed. A cantilever is a force sensitive lever with one end rigidly fixed while the other end has a sharp tip and is free to interact with the sample. The cantilever can be modeled as a spring such that the deflection of the cantilever x can be converted into a force F via the spring constant k following Hooke's law: $F = kx$.[74] The cantilever deflection is usually measured using optical beam deflection,[75] but interferometry or piezo-resistive sensing are also popular. Optical beam deflection works by shining a laser on the back of a cantilever and measuring a change in the position of the reflected beam using a photodiode. As the cantilever scans over the sample, the beam position is typically compared to a user-defined value and kept constant such that the image is constructed based on the movements made to keep this value constant. Piezoelectric elements quickly move the cantilever angstrom to micrometer sized distances to maintain this value constant regardless of the size of the features being imaged. AFMs all share the same basic components (i.e. a force sensitive lever for probing forces in the sample), but the setup can vary greatly depending on the sample. For atomic resolution, ultra high vacuums are needed, to keep certain molecules from diffusing around on the surface, liquid Helium and a low temperature rig are required and in bio-AFM, we have a completely unique set of requirements for probing live neurons.

2.1.1 Bioscope and Asylum AFM design

The primary AFMs used in this work are the Bruker Bioscope III (formerly Digital Instruments) and the Asylum MFP3D (See figure 2.1). In both AFMs, the z-piezoelectric element, laser, photodiode and cantilever are all located in the AFM head (see figure 2.2) which lowers down to bring the cantilever in contact with the sample. The sample sits on a Zeiss s100 TV (Bioscope) or an Olympus IX-71 (Asylum) optical microscope, ideal for alignment purposes and capable of fluorescence microscopy using a mercury lamp (Bioscope) or laser diode (Asylum). One major difference between the Bioscope and the Asylum is that the x- and y- piezoelectric actuators (piezos) are located in the head (Bioscope) and the stage (Asylum) as shown in figure 2.2. For the Bioscope, this allows it to have a higher bandwidth when imaging large samples in petri dishes.[76] Unfortunately, this luxury comes at a big cost. Since the cantilever moves with respect to the laser during x-, y- and z- piezo movements, an additional Tracking Lens must be used to ensure that the alignment of the laser does not change during these movements (see figure 2.2a). For

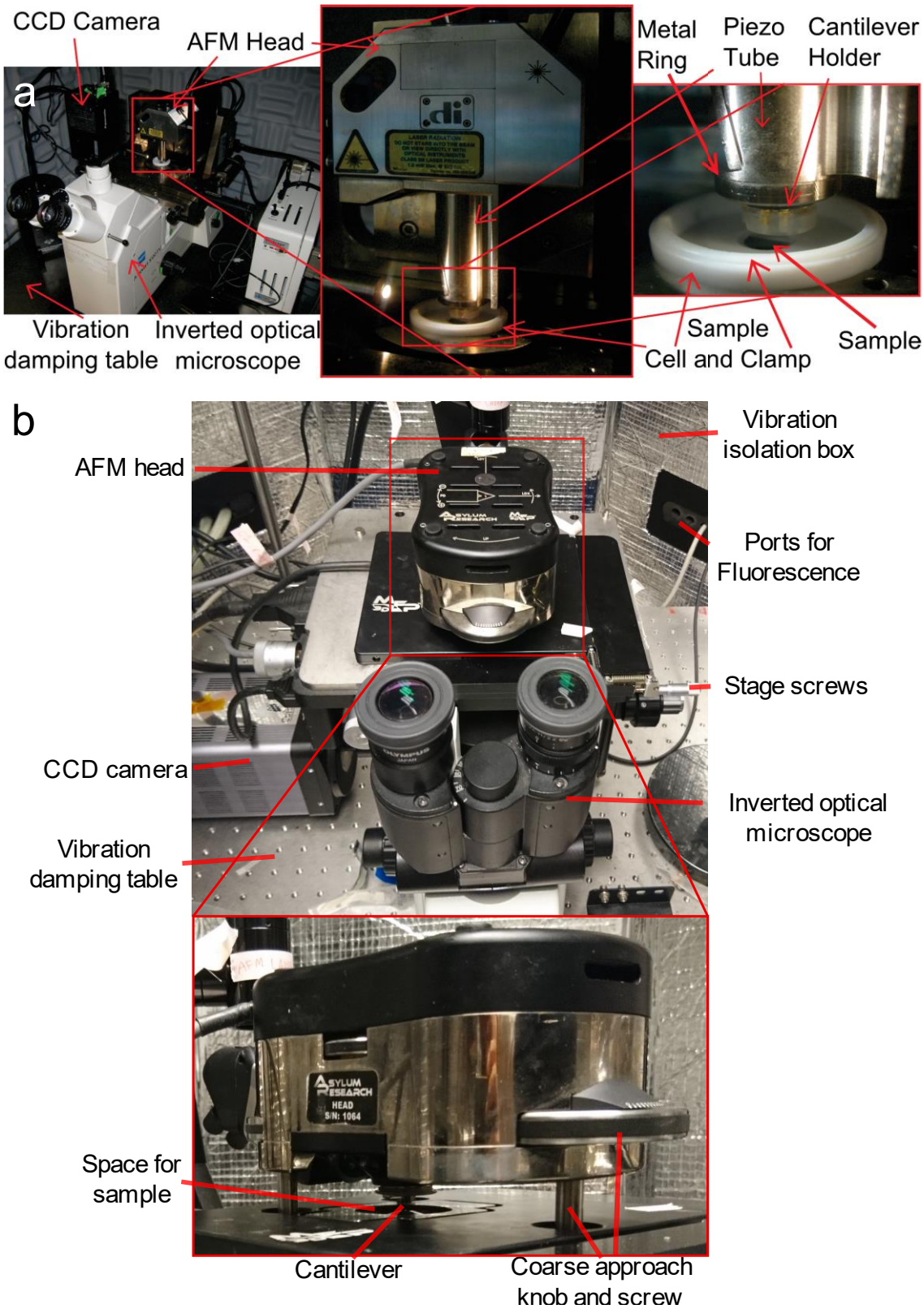

Figure 2.1 Bruker Bioscope and Asylum MFP3D Setups (a) Bioscope with a zoomed image of the AFM head and sample holder (adapted from Matthew Rigby's Master's Thesis). (b) Asylum with a zoomed image of the AFM head.

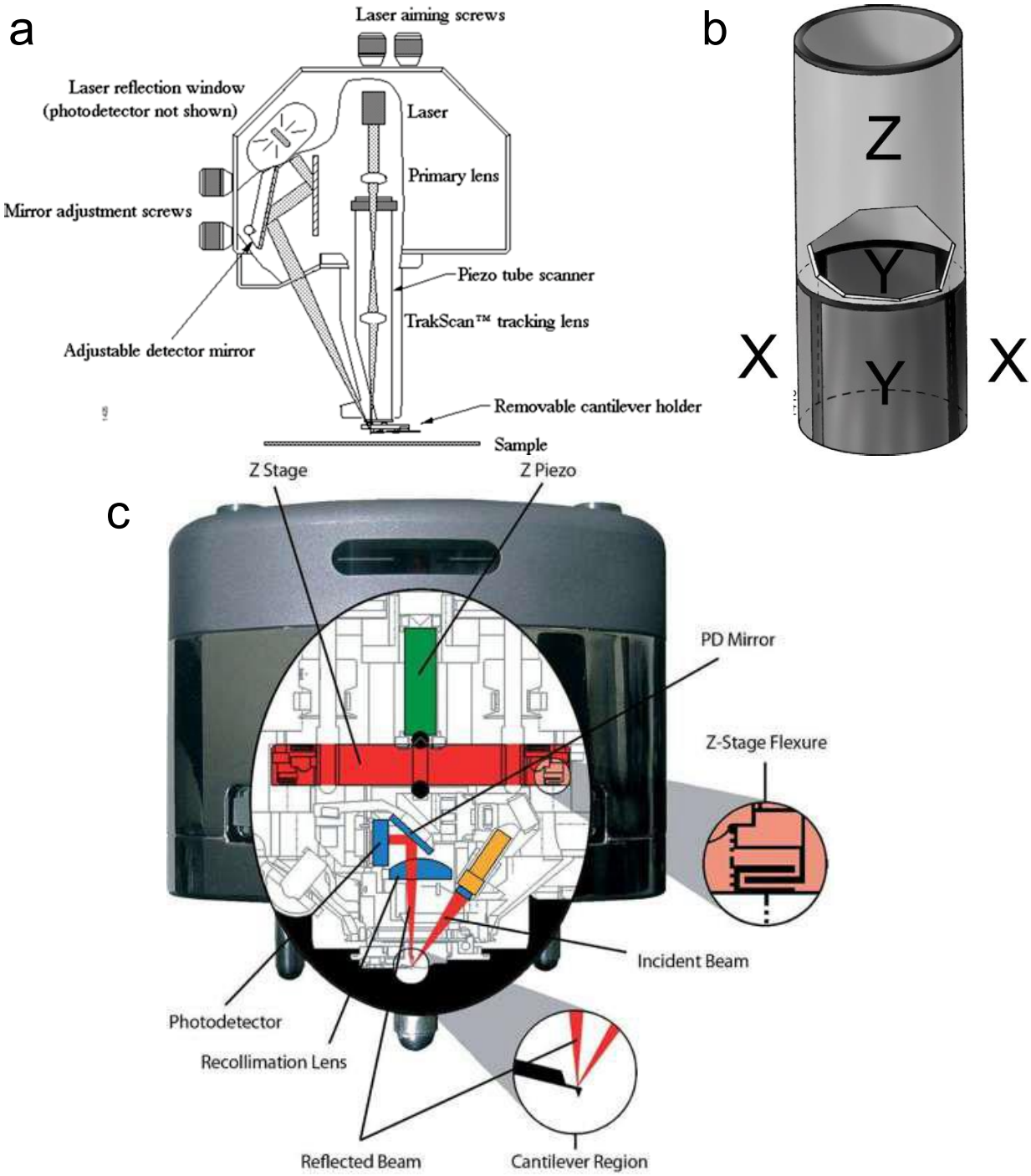

Figure 2.2 Bioscope and Asylum Schematics (adapted from the Nanoscope IIIa manual and the MFP3D User Guide) (a) Bioscope head schematic. The laser passes through (b) the piezo tube scanner en route to the cantilever, causing much more crosstalk than in the Asylum. (c) Asylum head schematic shows how the laser does not pass through the z-piezo, while the x- and y- piezos are not even located in the AFM head (they are in the stage), minimizing crosstalk between piezo movements and cantilever deflection.

the Asylum, the z-piezo is located in the AFM head (see figure 2.2c) so the laser does not pass through it, meaning that the laser pathway is not changed. In our experience, the Asylum design introduces much less crosstalk between piezo movements and cantilever deflection than the Bioscope, even with its Tracking Lens. Figure 2.3 shows the crosstalk between z-piezo and cantilever deflection in the Asylum and Bioscope. Furthermore, the z-piezo range on the Asylum is 18µm whereas the Bioscope has a range of only 5µm.

Both AFMs also sit on vibration damping tables and are enclosed in acoustically isolated boxes to minimize noise from low frequency building vibrations and sound waves. In bio-AFM, the low frequency noise components are most detrimental to measurements because the cantilevers and samples are relatively soft (and thus have low resonant frequencies). Typical bio-AFM cantilevers have resonant frequencies on the order of tens of kHz. Once in contact, the cantilever is moved exclusively by the piezoelectric actuators, but initially, the tip and sample are separated by millimeters. The coarse approach of the cantilever to the sample is accomplished with a motor (Bioscope) or approach screws (Asylum). The Bioscope is more convenient to use because it is

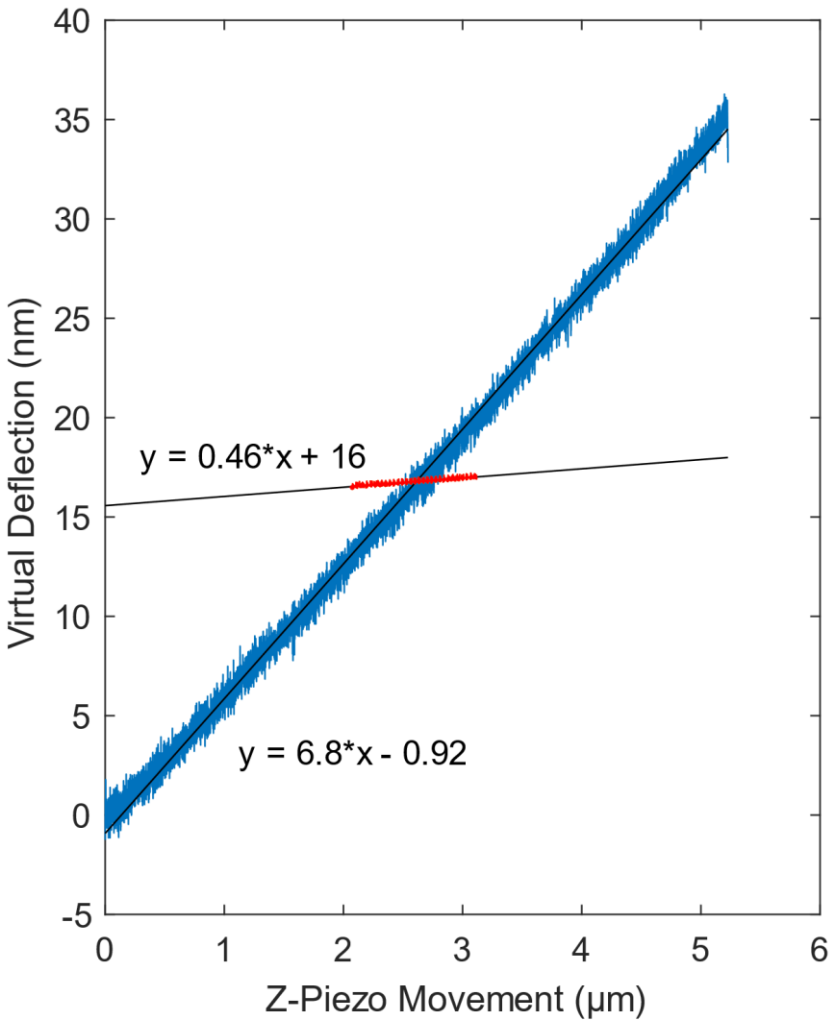

Figure 2.3 Crosstalk between the z-piezo movement and the deflection signal (ie. virtual deflection) for the Bioscope (blue) and the Asylum (red) with fits in black. The Bioscope has 15 times more virtual deflection than the Asylum, making measurements much more difficult on the Bioscope.

possible to approach in increments as small as 0.137μm and the step distance is well controlled, making it possible to use the motor for measurements. Additionally, since the Asylum uses a manual screw located on the head during the approach, the user must be careful not to move the head while approaching (in practice, the head will always move a little even if the user is extremely careful and skillful). In our experiments, a large movement may lead to making contact with the wrong neuron, or laterally shearing an axon, and it is certainly not possible to touch the screws during data acquisition. Since it is difficult to control distances and one must touch the screws to do coarse adjustments, this means that using the screws to do a force distance curve is not possible.

2.1.2 Force measurements

Forces are measured using Hooke's law $F = kz$, where z is the deflection of the cantilever, k is the spring constant and F is the force. A vertical force can be measured using the normal (flexural) mode of the cantilever or a lateral force can be measured using the lateral (torsional) mode of the cantilever. Stoney's formula $z = (3s(1-\nu)L^2/Et^2$ gives the cantilever's normal deflection z as a function of stress s where ν, L, E and t are the cantilever's Poisson ratio, length, elastic modulus and thickness respectively. Dividing by the force gives the spring constant which depends only on intrinsic properties and its dimensions:

$$k_N = \frac{Ewt^3}{4L^3} \tag{2.1}$$

For bio-AFM, a lower spring constant is desired. Since the spring constant has a strong cubic dependence on the thickness of the cantilever, it is easiest to decrease the spring constant by making it thinner. Bio-AFM cantilevers are typically made using Silicon Nitride rather than Silicon. This is because it is much easier to use Silicon Nitride to microfabricate a thin cantilever, despite the two materials having comparable elastic moduli. Using equation 2.1, manufacturers are typically able to specify the cantilever spring constant to about 10%. We used the Sader method to reduce this calibration error to about 4%.[77] Sader's method uses the width, length, resonant frequency, quality factor and hydrodynamic damping factor to calibrate the spring constant. It works because a higher spring constant gives a higher resonant frequency.[78] The improvement

in error of this method compared to many others (including the manufacturer's estimate) is largely due to the fact that it does not use the thickness to calibrate and the percent uncertainty on the thickness is high. Sader's method is a convenient, accurate and precise method for determining the spring constant.

The torsional deflection is measured as a change in angle of the cantilever $\theta = TL/GJ$ where T is the torsion, G is the shear modulus and J is the torsion constant. Similarly to the flexural mode, the lateral spring constant is given by:

$$k_T = \frac{Gwt^3}{3Lh^2} \tag{2.2}$$

Where h is the tip height. The spring constant is given by intrinsic properties and cantilever dimensions as before except for the tip height, h. The reason the lateral spring constant depends on the tip height is that the tip height changes the torsional lever arm of the cantilever. The torsional spring constant is harder to control than the flexural spring constant, meaning that it is usually not specified by the manufacturer. Sader's method can typically specify the lateral spring constant to about 9% uncertainty.[79]

2.1.3 Cantilever drift

When measurements are made in DC mode AFM (i.e. using a static deflection of the cantilever) and these measurements take a long time (on the order of tens of seconds), then cantilever drift due to temperature changes starts to be a significant issue. Because cantilevers are so thin (particularly for bio-applications), they are quite transparent and the intensity of the reflected laser on an uncoated cantilever is very small. For this reason, cantilevers often have a gold coating to improve reflectivity. Unfortunately, this gold coating has a different thermal expansion from Silicon Nitride (Si_3N_4) such that the two materials will expand or contract at different rates when heated or cooled. This means that the deflection signal of the cantilever will change with any temperature change (see figure 2.4a).

To form a synapse on a PDL coated bead, the axon must be in contact with the bead for at least 30 minutes. During this time, the temperature may have changed significantly, which will change the neutral position of the cantilever. This means that if the temperature changes in 30

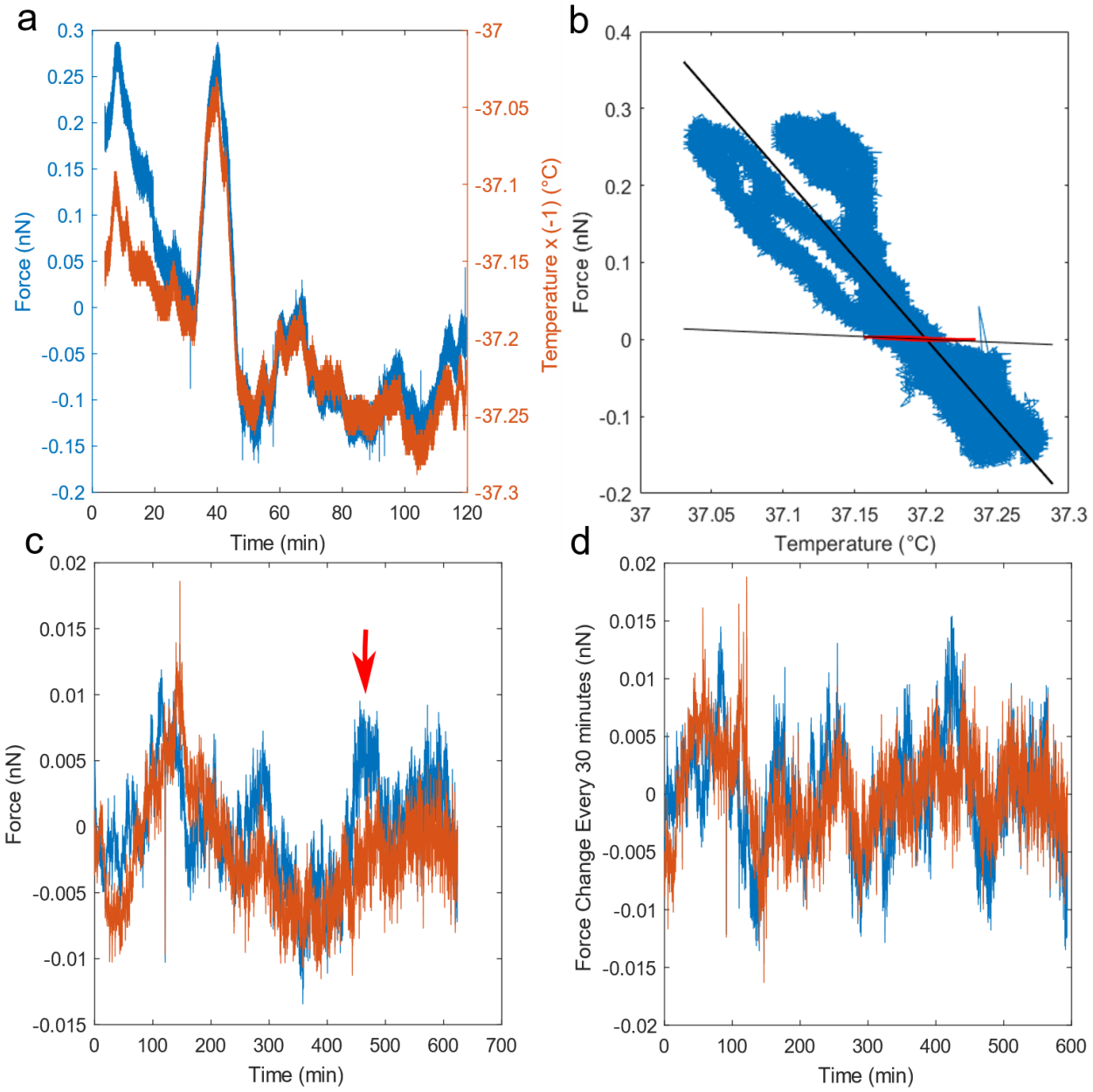

Figure 2.4. Effect of temperature on cantilever deflection converted to force. (a) Fully coated MLCT-C cantilever deflection and temperature of the cell media plotted as a function of time. The fluctuations in temperature cause the cantilever to deflect. (b) MLCT-C cantilever (in blue) and a partially coated cantilever (in red) with linear fits to both (in black). Clearly the partially coated cantilever is much less sensitive to temperature fluctuations. (c) Using the fit in (b), the partially coated cantilever fluctuations (blue) can be minimized by subtracting the effect caused by temperature (the corrected curve is in red). The red arrow shows an example of how correcting for the temperature reduces the uncertainty in the force. However, because we are using a partially coated cantilever, the red curve is only marginally better than the blue curve as other sources of error now dominate. (d) Running average of the difference in deflection every 30 minutes plotted as a function of time. This allows us to estimate the uncertainty in static force following neurite initiation.

minutes, we will no longer know what amount of deflection corresponds to 0nN, and the absolute tension value for the neurite will be unknown. As much as possible, it is best to eliminate this source of uncertainty by designing the experiment better, and then to remove the remaining uncertainty through post-processing. To minimize the error, we used a partially coated cantilever, where the coating was only at the end of the cantilever. Not only is it best to align the laser on the end of the cantilever for the best deflection sensitivity, it is also the part of the cantilever which, when heated, will contribute the least to the deflection of the cantilever. A small expansion at the base of the cantilever will cause a large deflection at the end of the cantilever due to the lever arm (see Stoney's formula). Switching from a Bruker MLCT-C cantilever to a partially coated cantilever (Uniqprobe QP-SCONT) with a 60nm Gold coating thickness and a coating which covers 30µm out of 125µm total length, reduces the temperature sensitivity from 2.1±0.8nN/°C to 0.14±0.07nN/°C (see figure 2.4b). This is a 15-fold decrease in crosstalk between temperature and cantilever and thus reduces the systematic error introduced by temperature significantly.

By correlating temperature changes with cantilever deflection, it is possible to reduce the noise caused by the crosstalk even further. We placed a sterilized thermocouple into the cell dish to measure the temperature and cantilever deflection simultaneously. By crosscorrelating the two signals, it was found that the thermocouple temperature (which was at the edge of the dish) lags behind the cantilever change in temperature by about 60 seconds. Once the two signals are temporally aligned, we can use the temperature sensitivity measurement to subtract the noise introduced by temperature to the cantilever deflection. The red arrow in figure 2.2c shows an example of fluctuations caused by temperature which are removed using this method. After about 4 hours, the temperature of the dish has usually come to an equilibrium (with the improvements made in section 2.2.1, the cells live in the dish for more than 24 hours, so waiting 4 hours to make a measurement is reasonable). Once in equilibrium, the temperature should not change much, so the correction is quite minimal.

We would like to know how much the deflection changes over 30 minutes because this is the amount of time the bead must stay in contact with an axon to form a synapse. We use the data in figure 2.2c to measure the running average of the difference in deflection every 30 minutes

and plot this as a function of time in figure 2.2d. By taking the root mean squared value of the force difference from figure 2.2d, we can get an estimate of the uncertainty we will have on our zero point in tension during a pull. Here we have reduced the uncertainty from 0.005nN to 0.004nN by correcting for the temperature changes. While in this case, the difference is very small, it is still important to monitor the changes in temperature in case there is a large, unexpected fluctuation in temperature, as this would give a completely erroneous absolute value for the tension. The most important improvement here is in switching from completely coated to partially coated cantilevers as this reduces the crosstalk by a factor of 15. The resting tension in the neurite is typically about 0.15nN (see section 5.1), which is only 2 times larger than the uncertainty using completely coated cantilevers (~0.075nN), whereas using partially coated cantilevers, the uncertainty is 60 times smaller than the signal.

2.1.4 Neurite initiation

To initiate neurites, we moved the cantilever at a constant velocity using the z-piezo on both the Bioscope and the Asylum. Using the motor on the Bioscope was not possible because the minimum step size was 0.137µm and because each step introduced noise, meaning that pulling at a constant velocity was not possible without automating the motor and acquiring a very noisy signal. Using the screws on the Asylum to move in the z-direction was not possible as the user introduces noise because it is necessary to touch the head to move the screws. Moving the z-piezo on the Bioscope introduces much more crosstalk than on the Asylum as shown in figure 2.3. Because of this, the Asylum was much more convenient to use as it only requires a simple virtual deflection calibration step before making a measurement.[1] The crosstalk on the Bioscope is best removed by first making a null measurement without a neurite, and then subtracting this from the actual signal (see figure 2.5a). This is important to do in the Bioscope instead of making a simple linear subtraction because non-linearities in the piezo give a crosstalk signal comparable in size with the actual signal in the neurite initiation.

[1] To subtract the systematic error introduced by the crosstalk of the z-piezo with the cantilever deflection on the Asylum, a force distance curve (z-piezo extension and retraction) is performed far away from the sample. The resultant z-piezo position vs deflection curve is then fit and subtracted from all future force distance curves.

2.1.5 Neurite extension

We performed both constant velocity extensions as well as constant steps extensions to elongate the neurite and measure its viscoelastic properties. It is possible to step the piezo on the Bioscope, but even after subtracting an extremely large crosstalk signal between piezo and cantilever deflection, there was still the additional problem of creep in the piezo, such that the pull would continue after the initial step was made. For these reasons, the motor was used to pull the neurite in constant steps. In figure 2.5b, the red curve shows how there is no crosstalk between the motor and the cantilever. The step occurs at 6 seconds, and there is some noise introduced by the motor into the measurement (as seen by the vertical line at 6 seconds), but the signal returns to the baseline as soon as the motor is finished stepping. This means that in the data acquired when pulling a real neurite (the blue curve in figure 2.3b), there is no correction needed.

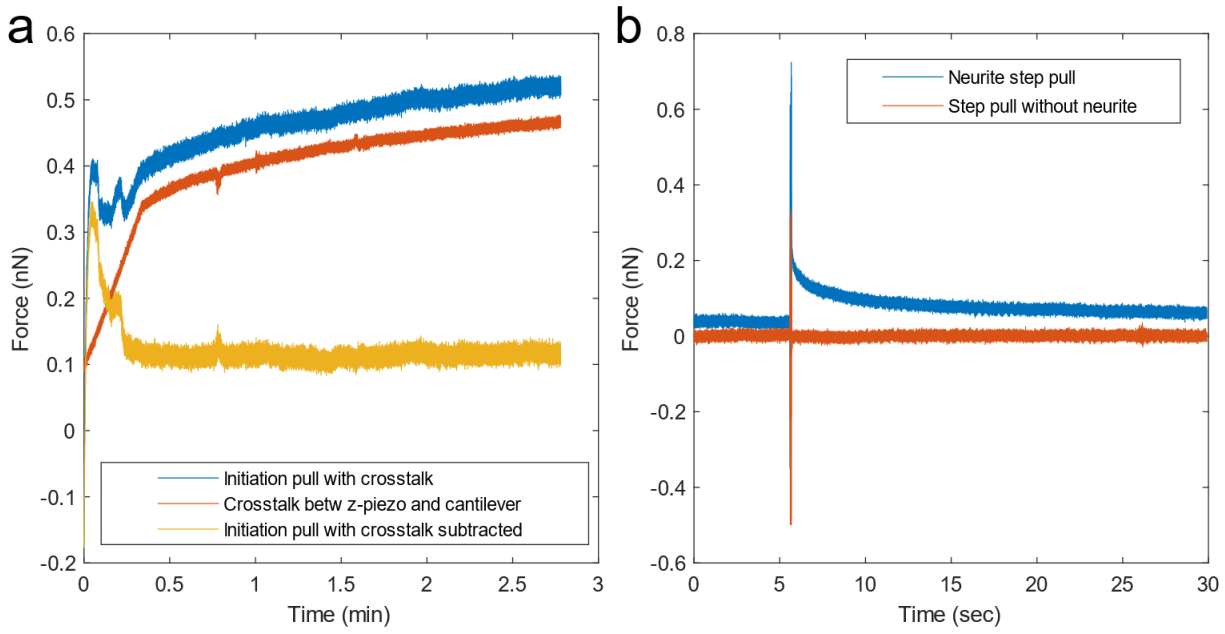

Figure 2.5 Initiation and Step Pulls (a) The initiation of the neurite is done by moving the piezo at a constant velocity. The crosstalk between z-piezo and cantilever force must be subtracted from a pull with a neurite in order to get the true cantilever force with crosstalk removed. (b) There is no crosstalk between the motor and the cantilever that interferes with the measurement shown by the step pull without neurite (in red), such that no correction is needed on the true data (in blue). The steps occur at 6 seconds.

Constant velocity pulls can be made in the same way as in the neurite initiation in section 2.1.3. The z-piezo has a range of 5.227µm on the Bioscope and 18µm on the Asylum. However,

the x- and y- piezos have ranges of 70µm on the Bioscope and 100µm on the Asylum. Pulling laterally thus allows a much longer measurement, which is necessary to see viscoelastic effects.[80] On short distance and time scales, the neurite tension depends linearly on distance. However, with time, the material will flow, causing the force distance dependence to become non-linear. Since we are pulling the neurites quickly, it is necessary to pull a long distance to observe the viscoelastic effects.

Pulling laterally uses the lateral (torsional) mode of the cantilever as opposed to vertical pulling which uses the normal (flexural) mode as described in section 2.1.2. The lateral spring constant depends on the square of the tip height (or in this case the bead height) as shown in equation 2.2. We typically use a bead of diameter 10µm, but with this small lever arm, the spring constant is 0.9N/m. This is significantly stiffer (and thus noisier) than the normal spring constant of 0.01N/m which we have used in all previous experiments. By increasing the lever arm by gluing additional beads of whatever size we would like, we can tune our spring constant accordingly (see figure 2.6a). In our experiments, we glued two 60µm beads and another 10µm bead on top of each other to increase the lever arm and decrease the lateral spring constant to 0.02N/m. We still make contact with the same size bead (10µm) as before because we would like to keep the indentation radius of curvature between the bead and the axon constant and also to try to keep the number of axons being contacted constant.

In addition to decreasing the spring constant of the bead, gluing extra 60µm beads on the bottom of the cantilever has the additional advantage of being more convenient and precise for measuring the lateral deflection sensitivity. To obtain the lateral deflection sensitivity, the 60µm bead is laterally deflected into a cleaved GaAs surface.[81] This is analogous to obtaining the normal deflection sensitivity by performing a force distance curve into an infinitely hard surface (i.e. InvOLS – called the inverse optical lever sensitivity, in the Asylum MFP3D manual). In the procedure by Cannara et al. 2006[81] they glue a 60µm bead onto a reference cantilever and deflect it laterally into the GaAs surface to obtain a reference deflection sensitivity. They then assume that another cantilever without the bead will have the same deflection sensitivity to within a dimensional conversion factor and use this in the experiment. In our case, the bead serves two purposes: it decreases the lateral spring constant and is used to obtain the lateral deflection

sensitivity without the need for a reference cantilever. This is more convenient and avoids the additional uncertainty added by the uncertainty on the conversion factor. Typically the uncertainty on the deflection sensitivity is about 7.5% using their method, where the conversion factor contributes 1% or more to the uncertainty.[81]

Another significant advantage with lateral measurements is that there is no crosstalk between the piezo movement and the lateral deflection (see the red curve in figure 2.4b) because the sample is scanned while the cantilever is held stationary (for the Asylum). Unfortunately, this is not true for the Bioscope as lateral scans introduce even more crosstalk than pulls using the z-piezo. The z-piezo crosstalk on the Asylum is minimal, but in the lateral direction, there is none. In addition to this, there are no thermal issues because the gold coating is equally distributed along the width of the cantilever. Since there is no lateral asymmetry on the cantilever, the expansion of the gold coating relative to the Silicon Nitride base will not cause the cantilever to rotate. These advantages make it easy to get high quality data without the need for subtracting a null curve or correcting for fluctuations in temperature (see figure 2.6).

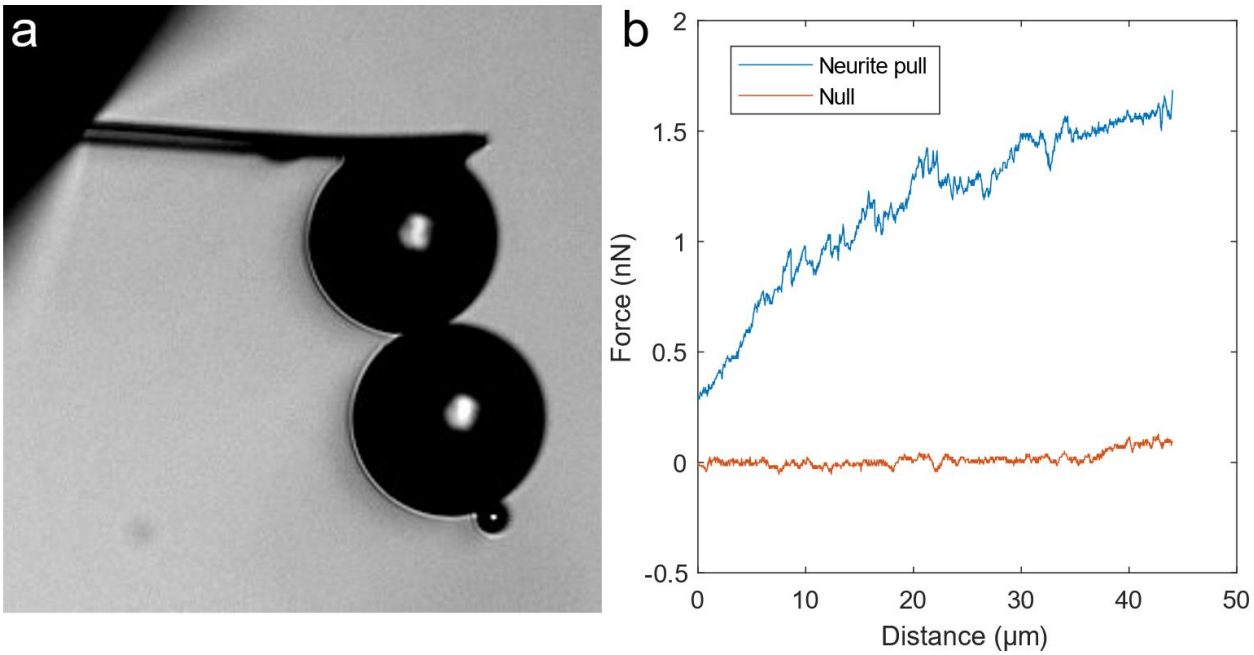

Figure 2.6 Lateral Force Measurements. (a) Two 60 μm beads and a 10μm bead glued onto a partially coated cantilever to decrease the lateral spring constant of the cantilever. (b) Force measurement for constant velocity extension in the lateral direction of a neurite using the cantilever shown in (a). There is no crosstalk between the y-piezo and the force as shown by the null pull.

2.2 Pipette manipulation

Micropipettes are ubiquitous in research labs, in particular in the biosciences. They typically consist of a glass tube with a microscopic opening that seals either partially or fully on the sample. Because the sealing end is quite small and the other end large, microscopic measurements can be made without too much noise. To name a few applications; electrophysiologists use them for patch clamp to measure action potentials and for iontophoresis to inject dyes, battery research can be done using pipettes in scanning ion conductance microscopy and biophysicists use them to make force measurements on cells. Pipettes are inexpensive and the size and dimensions of the small end are easily tuned such that they can be optimized for the experiment with minimal effort and cost. Typically, the back side of the pipette will be filled with solution and is connected to a macroscopic syringe, which gives the user control over the pressure at the other end. In addition, a micropipette setup is relatively inexpensive and simple to implement. All that is needed is a pipette puller, a vibration isolation table and a micromanipulator.

2.2.1 Neurite manipulation

For pipette manipulation of neurites, a similar setup as used for the Asylum AFM described in section 2.1.1 was used, but with the addition of a micromanipulator. The neurons were imaged using a Xeiss Axiovert 200M microscope, a Zeiss 63x objective and a QImaging Retiga Exi camera. The microscope was sitting on a vibration isolation table which gave just enough stability to perform neurite manipulations. The micromanipulator used to position the pipettes was an Eppendorf InjectMan NI 2 which attached to the microscope. Once in contact with the beads, negative suction was applied via tubing connected to the pipette on one end and the syringe on the other. The fan for the heater to keep the cells at 37°C needed to be turned off during manipulations because the vibrations introduced by the fan caused the pipette to vibrate too much to pick up the bead.

In the following, all excerpts in «» are from the paper “Building an artificial neural network with neurons”: «Cell media for 7-21 DIV neurons was replaced with 100nM of the live cell fluorogenic F-actin labeling probe (Si-R actin, Spirochrome) in 2mL of cell media. Immediately

after, 10µm beads coated for 24 hours with 100µg/ml PDL as described previously[82] were added such that the probe and the beads were incubated with the neurons for 6-9 hours. The medium containing the probe was removed along with most unattached PDL-coated beads and replaced by physiological saline solution. The neurons were imaged using a Zeiss Axiovert 200M microscope and a 63x objective (Zeiss), with the F-actin probe illuminated by a xenon arc bulb (Sutter Instruments). Pipettes (King Precision Glass) of inner and outer diameters of 1mm and 1.5mm respectively were pulled using a Sutter Instruments P-87 pipette puller to a tapered opening of between 2-6µm.» The pipette puller works by simultaneously melting and pulling on the pipette. By varying the type of pipette and the pulling parameters of heat, pull strength, velocity and pressure, we can obtain pipettes with openings as small as 100nm. Using a laser puller and quartz pipettes, it is possible to get the opening down to about 10nm.[83]

Due to capillary forces there will be a negative pressure which pull liquid, debris or loose beads into the pipette when it is submerged in liquid (even though the pressure difference is 0 in air). Before experimenting on cells, the amount of positive pressure needed to balance the negative pressure due to capillary forces was found. This was done by simply placing beads in solution and varying the pressure at which nearby beads neither flow towards nor away from the pipette. When performing experiments on cells, we thus knew how much initial positive pressure was needed to overcome the negative pressure due to capillary forces and to avoid debris accumulating at the opening of the pipette. Once the pipette was in contact with a bead adhered to a bundle of axons, a negative pressure was applied, allowing the bead to be picked up and a neurite to be initiated (see figure 2.7). If too much negative pressure is applied, the axons can be sucked up into the pipette. If insufficient negative pressure is applied, the neurite tension will overcome the suction on the bead, and the neurite will retract. For this reason, it is important to know how much pressure to apply to compensate for capillary forces and to get as good a seal as possible on the bead. The bead was manipulated vertically by ~3µm to avoid rubbing the neurite on the surface of the dish, then it was laterally extended 100-250µm at a speed of 0.1-0.5µm/s parallel to the glass before depositing the bead on another bundle of axons. Since the neurite is under a lot of tension, it is necessary to adhere the bead to another bundle of axons by leaving them in contact for a few minutes. Ideally, the bead is positioned behind another bead

which is already adhered on the bundle. Applying a positive pressure is usually sufficient to release the bead, but the bead can stick to the pipette (likely due to debris which sticks the bead to the pipette). In this case, it is necessary to break the pipette on the glass surface to release the bead.

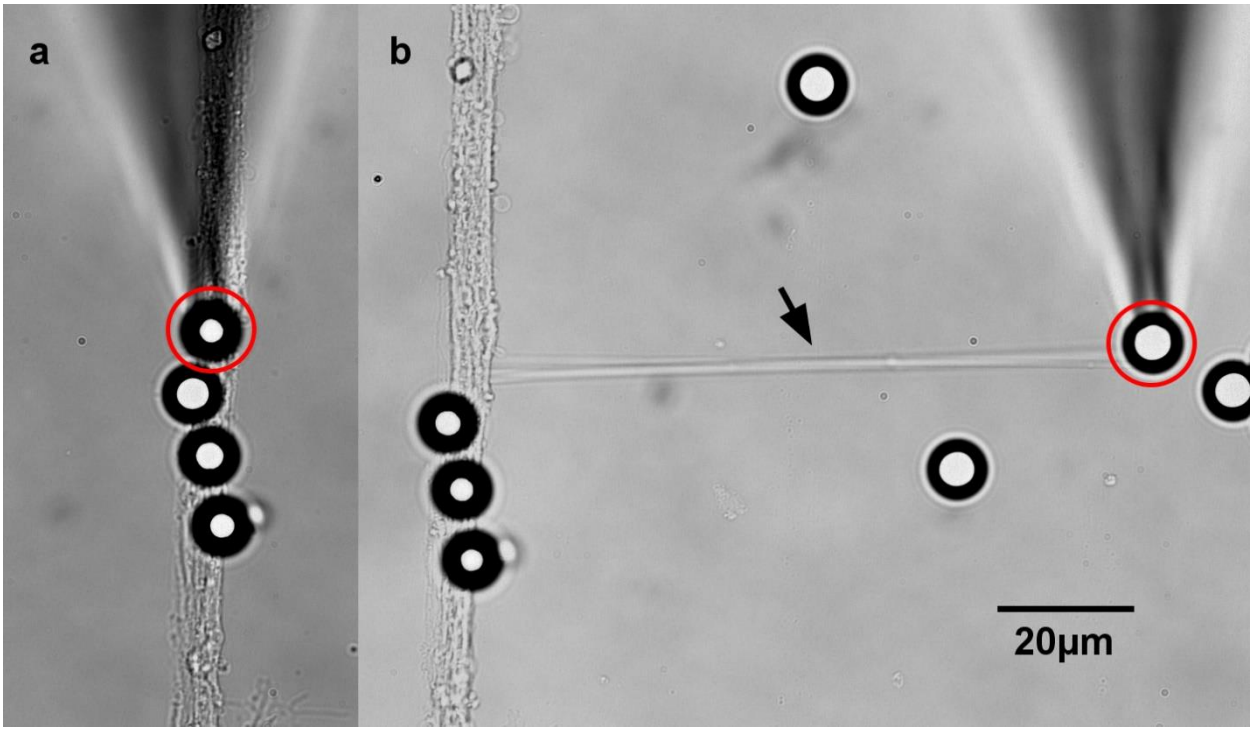

FIG. 2.7 Initiation of a neurite using a pipette (a) A pulled pipette (triangular shadow at top of image) applies suction to a PDL-coated bead (circled) and initiates a neurite by pulling upwards ~3µm. (b) By pulling horizontally on the bead (circled) at a constant velocity of 0.1-0.5µm/s, the neurite (indicated by the arrow) is extended.

The neurites were kept in focus by manual adjustment of the objective and fluorescent images were taken every ~4 seconds. «The image stack was analyzed by drawing a line on top of the neurite and using the ImageJ Multi Kymograph plug-in v3.0.1. This produced a kymograph, which is constructed from one intensity line profile of a stack of images. It is an image of position as a function of time, allowing the measurement of the speeds of F-actin polymers in the neurite as a function of time elapsed since pulling (see section 3.3). These were analyzed by hand by tracing 15-30 actin trajectories per kymograph (each kymograph was generated from one neurite).»

2.2.2 Axotomy, reconnection and patch clamp

Axotomies can be performed in many ways including a high-power laser, but we opted for axotomizing the axons using hardware readily available in the lab. Using an AFM cantilever to axotomize and reconnect the axon can work, but it is not possible to release the bead during reconnection, so we did only a small number of experiments using the AFM. It is also possible to use a pulled pipette or a scalpel to axotomize the axons. All three of these methods have the disadvantage of sometimes stretching the axon rather than slicing it cleanly but cutting them quickly helps to reduce this issue. Cutting using a pulled pipette or a scalpel was optimal because it requires only a micromanipulator, which is already being used for the reconnection of the axotomized axon. To evaluate the success of the scalpel and pipette axotomy methods, we used the criteria that a successful axotomy was one which displayed regeneration 24 hours after axotomy. Any axons which displayed regeneration (top arrow in figure 2.8B) were assumed to

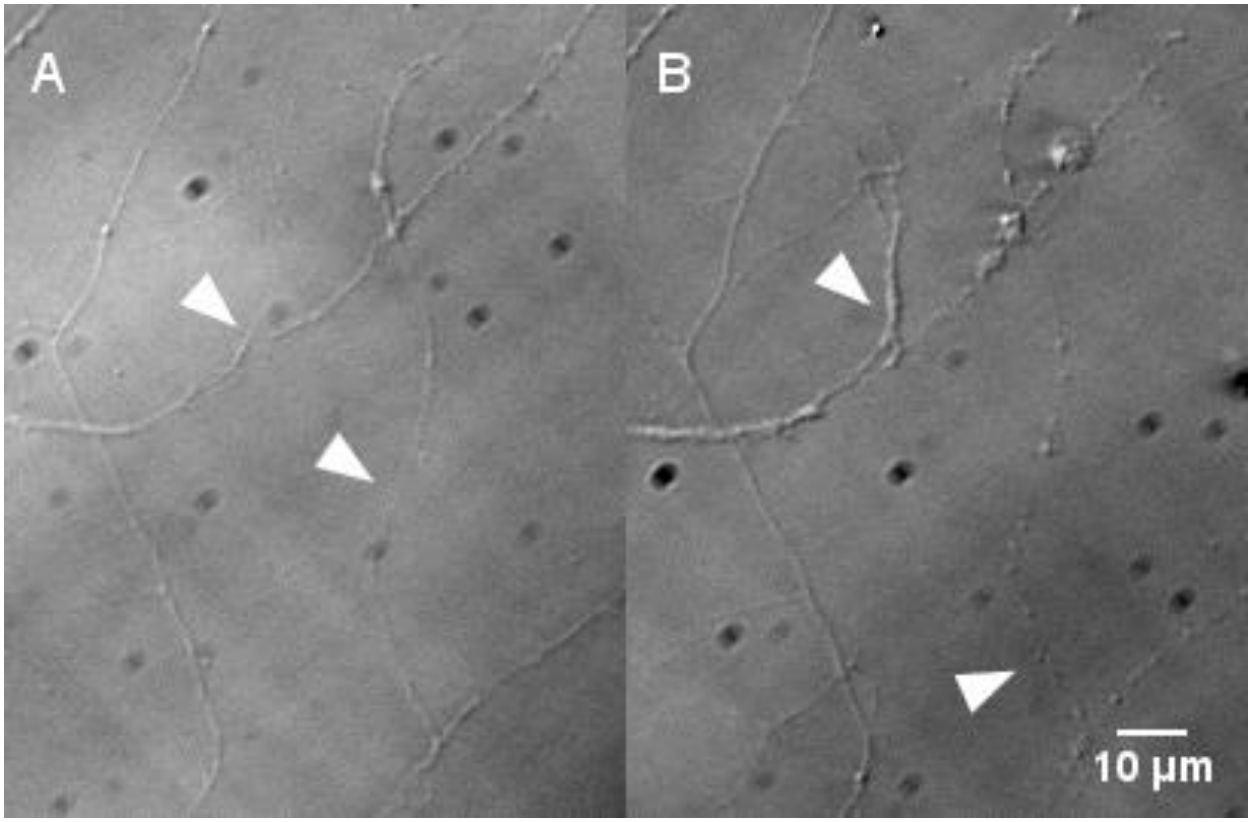

Figure 2.8 Regeneration for axotomies of single axons and small bundles (A) Both arrows indicate locations where an axotomy was just performed using a scalpel. (B) Image of neurons 24 hours after axotomies. The top arrow shows active neural regeneration and Wallerian degeneration in the proximal end of the axon. The bottom arrow shows Wallerian degeneration in both the proximal and distal ends of the axotomized axon.

have been cleanly cut. By this metric, both methods performed similarly well. Using the pipette, 9/20 axons displayed regeneration, whereas using the scalpel, 8/17 displayed regeneration giving a 45% and 47% success rate respectively. Another group using the same method with pipettes but on mice hippocampal neurons have reported up to a maximum of 80% survival rate, depending on proximity to the soma, sharpness of the cut and general health of the cells.[84]

To avoid stretching the axons, the sample stage piezo was moved using a step function, moving the sample as fast as possible to make a clean cut. When using the Bioscope to axotomize using a cantilever, the stage was quickly moved using a stepper motor. An adjacent cantilever on the same substrate with a PDL-coated bead was then used to initiate a neurite out of the proximal end for reconnection (axotomy was performed using the MLCT-C cantilever and the manipulation using the MLCT-D cantilever). For pipette axotomy and reconnection, the axotomy was always performed slightly distally with respect to a PDL coated bead adhered to the axon such that this bead could be immediately used to initiate a neurite for reconnection. The neurite is pulled as described in section 2.2.1, but in this case, the neurite is deposited on top of the (recently axotomized) distal part of the axon with the hope that the two ends reconnect and fuse.

For dye injection via patch clamp, a third pipette is used and a second micromanipulator to speed up the experiment. The third pipette is pulled with a 2-6µm opening and filled with intracellular solution as previously described[71] and a membrane impermeable dye (AlexaFluor 488 hydrazide at 10mM concentration). A ground electrode is placed in the solution as well as an electrode in the pipette to measure and/or change the potential difference across the membrane of the neuron. This pipette is micromanipulated into contact with the cell while applying a positive pressure to avoid debris gathering on the pipette opening. It is possible to see the cell body change shape slightly upon contact. This is the moment to apply a sudden negative pressure using your mouth to break the cell and get a seal around the pipette opening. Once the membrane has been punctured, the strength of the seal can be determined by measuring the amount of current flow and given a voltage difference applied through the two electrodes. This is done using an Axopatch 200-B system (Molecular Devices), and it is be possible to elicit action potentials by depolarizing the membrane with a change in applied voltage. Once the cell is patched, the dye should take less than a minute to diffuse down the axon (and across the

reconnection if the membrane has fused). Being extremely careful not to move the pipette (as it is patched to the cell body), one must move the stage to fluorescently image the proximal and distal end of the axon to see if the membrane fused at the reconnection.

2.3 Cell viability

Experimental data obtained on stressed, dying, dead, or the wrong type of neurons is at best useless and at worst, misleading. This means that a significant amount of time is spent trying to optimize the conditions in which the cells are dissected, grown and finally experimented on. Firstly, there are many different types of neurons in different regions of the brain. The neurons used throughout this thesis are rat hippocampal neurons. However, the hippocampus is surrounded by cortical neurons and is quite small, meaning that many hippocampi are required to get enough neurons. The neurons are plated on a poly-D-lysine coated glass dishes and are kept alive for 7-21 days before experiments can be performed. The are kept in a sterile incubator which maintains the environment at 37°C, 100% relative humidity and 5% CO_2.

The natural temperature for cells to operate is logically the same temperature as our internal body temperature. However, lowering the temperature of cells for a couple of days will not kill them and once returned to 37°C, the cells are even more resistant to adverse events.[85] Increasing the temperature a few degrees above 37°C is however fatal for the cells. Conveniently, since the lab room temperature is always below 37°C, so the only instance where the temperature will go above 37°C is if the temperature controller is broken or if the user does not set it at the correct temperature.

The cell media contains a buffer which uses CO_2 in the atmosphere to maintain the pH in the optimal range (pH 7.3-7.4) for the cells. If the CO_2 goes too far below or above 5%, the pH will increase or decrease respectively. Since the solution is buffered, it slowly increases, but if left long enough, the pH will change too much and will kill the cells. We measured the pH over time when the solution was left in regular atmosphere (i.e. almost no CO_2) and the pH increased exponentially with time (see figure 2.9). This makes sense since the pH scale is a log scale, and we would expect the CO_2 to react with the media in a linear way. If the cells do not die during this time, and the CO_2 levels are fixed, the cells will make a full recovery. The cell is stressed above

pH 8, and lethal at pH 8.5 so any manipulations should be done within an hour of switching off the CO_2.[86]

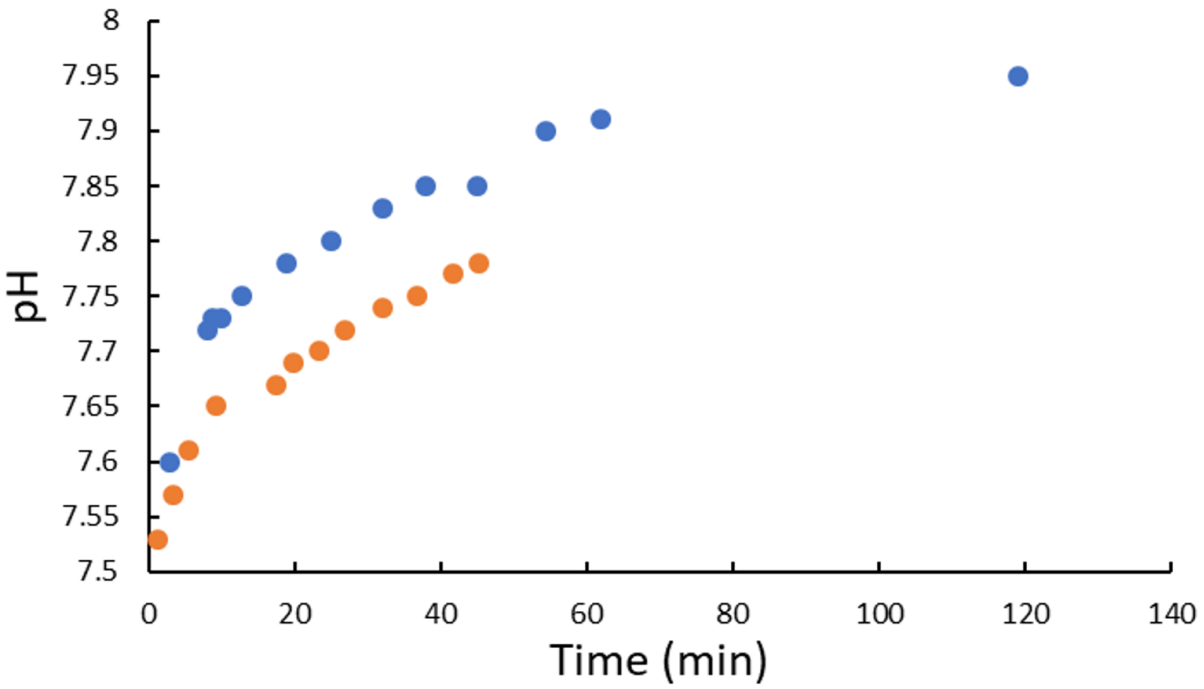

Figure 2.9 pH of media as a function of time after it was removed from an incubator with 5% CO_2 concentration in the atmosphere and placed in regular atmospheric conditions.

When the cell media is too salty, the cell will shrivel up due to osmotic pressure differences. Conversely, if the media does not have enough salt, the cell will swell. The optimal range for osmolarity is between 260-320mOsm/kg.[87] The further the osmolarity is from this range, the more stressed the cell is and the faster it will die.[86] Even in the case where the cell is not dead yet, experimenting on a stressed cell is not ideal. The problem is that water is constantly evaporating out of the cell dish, meaning that the osmolarity always tends to move away from the optimal range. This is particularly a problem when the cells are being kept at 37°C because the water evaporates quickly unless the relative humidity in the surrounding environment is close to 100%. If the temperature is below 37°C or the CO_2 percentage is off temporarily, the cells will make a full recovery once the conditions are corrected. This is not the case for relative humidity. If the relative humidity falls below 100%, the osmolarity change caused by the increased evaporation will not be fixed when 100% humidity is restored. Since the osmolarity is always drifting away from the optimal range due to evaporation, this may be the biggest challenge for keeping the cells alive indefinitely. One group showed that by weighing the dish to keep track of

how much solution evaporates and countering this by adding the correct amount of water, they were able to keep the cells alive for 30 days.[86] This goes against conventional wisdom which says that the main reason we replace a third of the media every two days is to remove cell by-products.

2.3.1 Bioscope setup

With the help of Pascal Bourseguin (head of the machine shop), we machined a cell chamber compatible with the Bioscope for live cell experimentation (see figure 2.10a). This consists of a plexiglass chamber which is secured to the microscope stage with screws, has small holes for the heater wires, and a large opening in the top for AFM access. The cells are placed in the heated microscope stage with a sterilized thermocouple in the cell media to ensure it is kept at 37°C. This is an improvement on previous experiments where the only thermocouple was one which was in the stage, used by the temperature controller to keep the temperature constant. The problem is that this thermocouple was consistently 3-4°C above the true temperature of the media. To maintain the correct pH in the media, 5% CO_2 is continuously flowed into the cell chamber. To minimize noise caused by the CO_2 air flow, the outlet was directed into a damp Kim wipe.

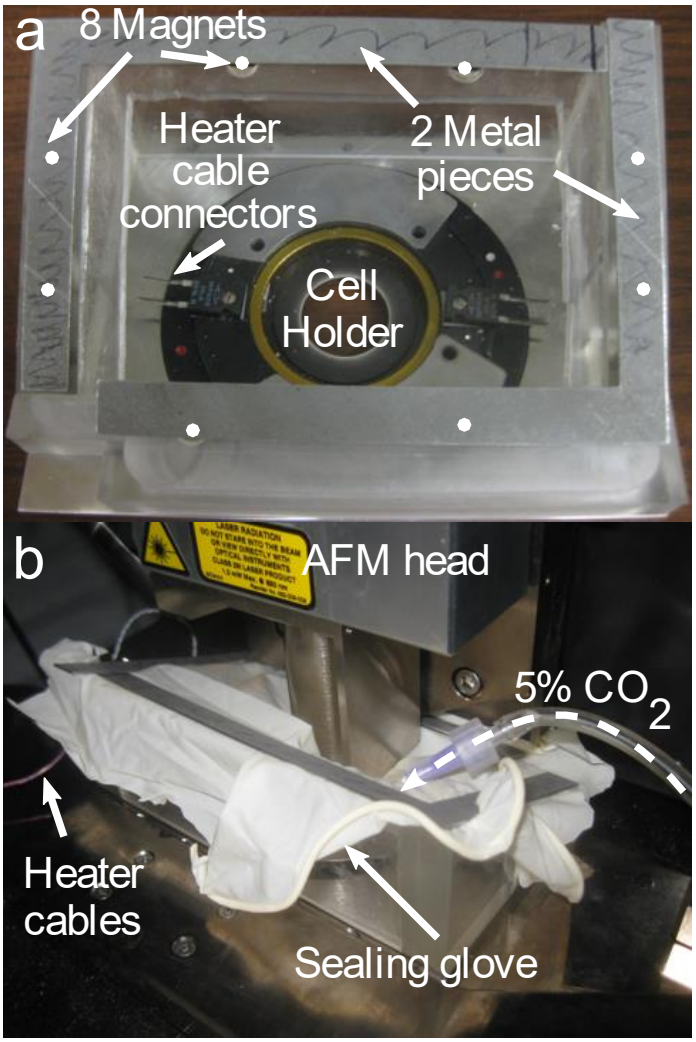

Figure 2.10 Bioscope live cell setup. (a) Cell chamber secured on microscope stage with heater. The cell chamber has 8 magnets and 2 metal pieces to seal a glove in place as shown in (b) the AFM integrated with the cell chamber and 5% CO_2.

The most difficult challenge in this setup is minimizing evaporation. In order to seal the top of the cell chamber where the AFM accesses the cells, we first cut a

Latex glove such that it is essentially a flat piece, and then cut a hole in the middle. The glove is elastic, so it seals tightly around the AFM head (see figure 2.10b). The glove seals onto the AFM skirt, which is placed on the end of the piezo. The piezo is an expensive piece of the microscope and sensitive, so it is crucial to be careful as too much strain from the glove on the piezo can cause it to crack. Many live cell microscopes build an incubator around the entire microscope so that the temperature is very stable (as in the microscope used for pipette manipulations in chapter 4). However, this was not done with the Bioscope setup as the piezoelectric tubes and electronics inside the head of the AFM would corrode due to humidity and eventually cause electrical shorting. The outer edges of the glove seal the cell chamber using strips of aluminum and magnets (2 magnets were glued into the top of each wall of the cell chamber). Once the glove is in place, the chamber is sealed so that the relative humidity can be kept as high as possible and 5% CO_2 in the air can be maintained. A crucial improvement on our previous setup is that we now place kim wipes soaked in boiling hot water inside the chamber. It is essential that they be very hot so that they increase the relative humidity to as close to 100% as possible as quickly as possible. Following this implementation, the cells went from living about 3-6 hours in the setup to well over 24 hours.

2.3.2 Asylum setup

While performing Asylum AFM manipulations, we did not have a cell chamber to maintain a high relative humidity to avoid evaporation, so the experiments were performed at ambient temperature (~26°C). We used a buffer as described in Magdesian et al. 2016[71] which kept the cells alive for more than 24 hours and does not require 5% CO_2 in the atmosphere. During AFM manipulations, the lid was off, causing evaporation to happen quite quickly. We measured the evaporation rate by putting a culture dish filled with media on a scale and quantifying the amount of water lost to evaporation by converting the decrease in weight to volume (see figure 2.11a). The evaporation rate was measured to be 0.24mL/hr. At this evaporation rate, we see that the osmolarity moves out of the optimal range (0.26-0.32mOsm/mL) in about 1.25 hours (figure 2.11c). By frequently replacing the solution, the osmolarity can be kept in the optimal range. Exactly how much and how frequently the solution needs to be replaced can be calculated by understanding how the osmolarity ρ of the solution changes with a constant evaporation rate r:

$$\rho(t) = \frac{\rho_0 V_0}{V_0 - rt} \tag{2.3}$$

Where V_0 is the initial volume (usually 3mL in our experiments) and t is the time. To ensure that the osmolarity does not drift out of the optimal range as in the blue curve in figure 2.11a (plotted using equation 2.3), we must replace the media periodically. After a time t_1, the volume and the osmolarity have changed to ρ_1 and V_1. When a volume V_{rep} of media is replaced, then the new osmolarity ρ' is given by the formula:

$$\rho' = \left(\rho_1\left(V_1 - V_{rep}\right) + \rho_0 V_{rep}\right)/V_1 \tag{2.4}$$

Equations 2.3 and 2.4 can be used to generate the sawtooth looking curves in figure 2.11 c and d. The portion of the curve which slowly increases corresponds to the gradual evaporation given by equation 2.3. Each time the media is replaced, the osmolarity decreases in a stepwise fashion which is given by equation 2.4. The osmolarity will never decrease all the way down to the initial osmolarity, but with the appropriate initial volume and replacement rate, it will stay inside the optimal range until, after a long time, the total volume has decreased by so much that even replacing media will not maintain the solution in the optimal range.

With a 3mL initial volume and 1mL of solution being replaced, we used equations 2.3 and 2.4 to find the maximum time interval between media replacement to keep the osmolarity in the optimal range is 24 minutes (purple curve in figure 2.11c). So as to keep the media well in the optimal range, in our experiments, we replaced 1mL of media every 5 minutes (yellow curve in figure 2.11c). Another approach would be to replace the exact amount of water lost due to evaporation rather than replacing large quantities of solution. However, this method is much more susceptible to mistakes in timing or differences in evaporation rate from day to day (due to differences in humidity or temperature). For this reason, we opted to simply replace the media periodically.

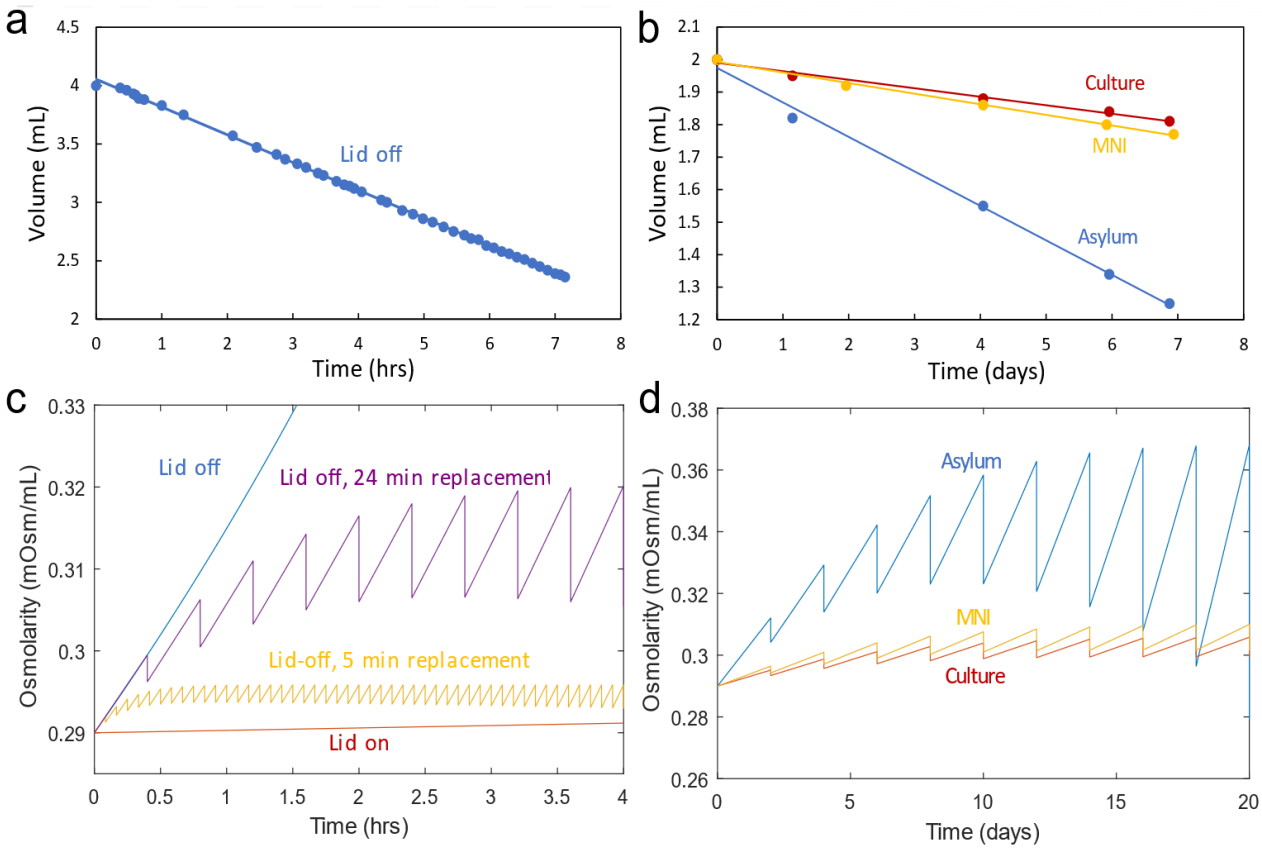

Figure 2.11 Evaporation of Cell Media. Uncertainty on data in (a-b) is smaller than the data points. (a) Evaporation of cell media at 26°C with the lid off so that cells can be accessed either by AFM or with micropipettes. Evaporation with the lid on was so minimal that it was essentially constant on the time frame of hours and was not included here. (b) Evaporation of cell media in three separate incubators for long term cultures. (c) Using equation 3.3 and 3.4, the theoretical osmolarity of the media is plotted vs time by using the calculated evaporation rate obtained in (a) for the lid off and lid on. By replacing the media every 24 minutes (or less), the media will remain isotonic (between 0.26-0.32mOsm/mL) for a long time. In experiments, we typically replaced the media every 5 minutes (yellow curve). (d) Using equations 3.3 and 3.4, we can see that the evaporation rate for the incubator in the Asylum was too high to keep isotonic even with replacement of solution every 2 days. We noticed the cells were not surviving long in this incubator, so only cultured cells in the 'Culture' and 'MNI' incubators.

2.3.3 Fluorescent microscopy setup

The microscope was enclosed entirely inside an incubator to give the option of keeping the cells at 37°C. We filled the incubator with boiling hot water to keep the humidity high to limit evaporation, and there was a stage lid which allowed 5% CO_2 to be supplied to the media to keep the pH at physiological levels. The cells were treated in the same way as those in the Asylum setup (section 2.2.2) by continuously replacing the media during manipulations. Evaporation at 37°C was estimated to be 0.2mL/hr, which is less than the evaporation at 26°C. Evaporation

would normally have been about two times higher at 37°C, but this was compensated by the increased humidity in the chamber. Since the evaporation was approximately the same here as in the Asylum, we replaced 1mL of media every 5 minutes as before. Some experiments were run overnight in this setup, so a lid was placed on the dish to limit evaporation and the total volume was increased from 3mL to 7mL to limit the changes in osmolarity due to evaporation. With the lid on and 7mL volume, the osmolarity changed very slowly as shown in the red curve in figure 2.11c.

2.3.4 Long-term cell incubation, culturing tricks and microfluidics

Since animal lives are sacrificed, experiments take weeks to perform and cost a lot of lab resources, lab practices change very slowly because no one wants to deviate from a protocol that has been shown to work. However, when your protocol suddenly and inexplicably stops working, it is necessary to be systematic while troubleshooting such that parts of the protocol can sometimes be improved as a consequence of attempting to find the problem. The standard practice of cleaning the incubator and being extra careful with your cultures does not always work and are common knowledge. Here are a few things which I have found to be less well known.

Based on Potter et al. 2001[86] and ignoring contamination problems, one of the main reasons for cell death in long-term incubation is changes in osmolarity. The assumption made is that by ensuring the incubator water jacket and water bath are full and by not opening the incubator too often, that the humidity will remain close to 100% and evaporation will be limited. This is not always the case and should be verified experimentally by weighing a test dish filled with media to quantify evaporation. We use three different incubators, and each had a different evaporation rate. Indeed, in one case, in the 'Asylum' incubator, we realized that the reason the cells were not surviving was probably because the evaporation rate was too high, causing the cell media to no longer be isotonic (see figure 2.3 b and d). In the other two incubators, the evaporation rate was approximately equal, meaning that the media could simply be replaced every two days without the osmolarity changing too much.

We used ANANDA microfluidic devices to ensure that we were experimenting on axons. Axons grow longer than dendrites, so by experimenting on neurites which have grown at least 400µm into a channel, we are sure we are experimenting on axons, not dendrites. The standard way to load the devices is to fill one of the wells with neurons such that some neurons will gather in the chamber (i.e. the space between the two wells). The recommended amount of media to add with the cells is 50µL. Unfortunately, this makes a large pressure gradient across the loading chambers, meaning cells flow through the chambers too quickly and accumulate close to or inside the wells, rather than being evenly distributed throughout the chamber. By removing all solution from the wells (leaving only enough to keep the chamber wet) and by pipetting less than 10µL of solution with cells into both wells, the cells flow much slower into the device, and will be well distributed in the chamber such that neurons will grow in all the channels.

To reduce costs, we have been reusing our microfluidic devices. The method we have found to work best is to rinse the microfluidics immediately using water (not ethanol, as this is a fixative and will make it harder to remove cell debris). We then sonicate the microfluidics for about 10 minutes, sterilize using ethanol, UV treat for 30 minutes and reuse. Following sonication, it is useful to visually inspect the microfluidic under a 10 times objective to make sure all debris has been removed. After multiple usages, it may be difficult to remove all residue. Increasing sonication time and adding an additional step of using Scotch tape to manually remove the cell residue may be necessary. However, after about 5-10 uses, the microfluidics will no longer be cleanable (by the methods described here).

This last trick is quite common, but not universally known. Media is always heated before using it to replace the old cell media. However, the media is generally heated in a water bath and is therefore not at the correct pH. This can be a shock for the cells, especially if a large proportion of the media is being replaced (typically about 1/3-1/2 of the media is replaced). It can therefore be good to heat the media up inside the incubator where the environment has 5% CO_2 so that the cells are not shocked by a change in pH.

2.4 Fluorescence microscopy

Lopez et al. 2009[71] showed that our neurites are structurally and functionally indistinguishable from regular axons. They showed that the neurites are functional at least 24 hours after initiation and that they contain actin, microtubules and tau neurofilaments a few hours after initiation. How is it possible to pull the neurite 300 times faster than average axonal growth speeds? How and when elements of the cytoskeleton arrive is important to understanding this puzzle. The cytoskeleton is visualized using fluorescence microscopy. Usually it is done with fixed cells, but new fluorescent probes have allowed certain elements of the cytoskeleton to be visualized in live cells.

2.4.1 Neurite fixation

In previous attempts, our group was never able to fix pulled neurites less than hours after initiation.[71] This may be in part because it can take tens of minutes for the cytoskeleton to arrive (see section 3.3) and can take hours for the neurite to fully mature (see section 4.4). Since this is the case, finding the least perturbative way to fix neurites was crucial. Using the protocol recommended by ThermoFisher Scientific to fix and image the cells using the AlexaFluor 488 Phalloidin F-actin probe was too rough on the neurites because adding and removing the fixative solutions introduced too much turbulent flow in the dish. By keeping the dish under the optical microscope during the fixation process, it was possible to see during exactly which step the neurite breaks and to minimize movement of the dish (which also introduces turbulent flow).

The procedure used was shown to us by Andrew Kaplan of Alyson Fournier's lab. It helps to reduce the turbulent flow of liquids during the removal and addition of new solutions. Rather than using a solution of 4% PFA/PBS which is typical for fixation before phalloidin labeling, a new solution of 4% PFA/20% sucrose/PBS was added directly to the bottom of the well. The sucrose makes the media denser, so it stays at the bottom of the well, meaning that we don't have to remove any media before fixing the cells. The rest of the procedure is otherwise equivalent, but this step helps to significantly reduce the amount of turbulent flow in the solution.

Having imaged the neurite throughout the fixation process, we identified the addition of 0.2% Triton-X/PBS to be another major reason for neurite breakage. This solution dissolves the plasma

membrane, so a neurite which does not have a strong supporting structure/cytoskeleton would likely break. An indication that there is some strengthening occurring in the neurite is that all four neurites where the neurite was fixed in 3 minutes or less after initiation broke, whereas 4/6 neurites of the neurites fixed after 30 minutes or more remained intact (see figure 2.12). This result provided the motivation to perform experiments using a live F-actin dye which are presented in section 3.3 and show that the arrival of F-actin into the neurite has a time constant on the order of tens of minutes.

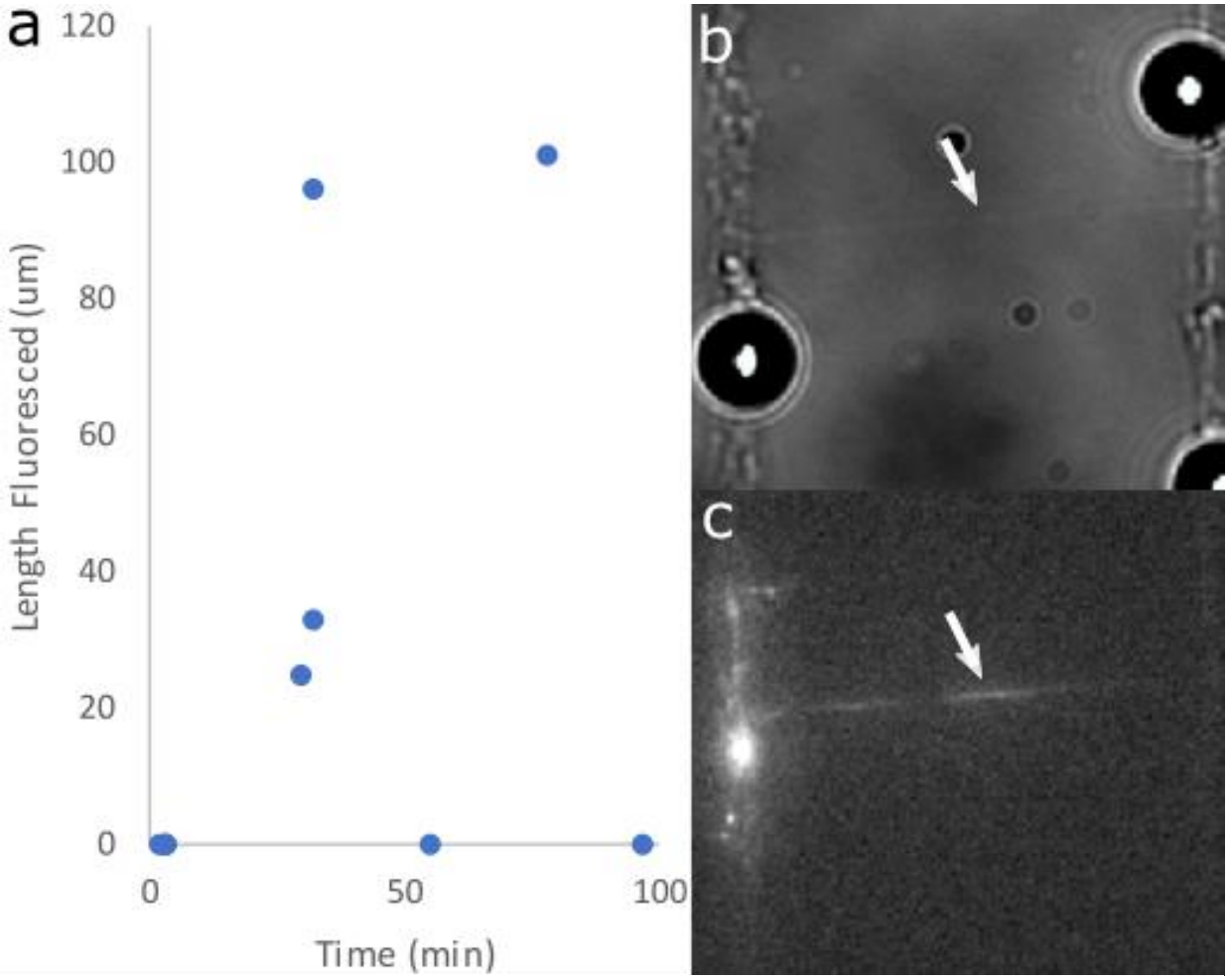

Figure 2.12. Fixed neurites to see F-actin. (a) Length of the fluorescent neurite as a function of the amount of time between initiation of the neurite and fixation (time=0min is the moment the neurite was initiated). Every neurite which did not break during fixation had F-actin fluorescence. All four neurites fixed less than three minutes after initiation broke. (b) Bright field image of a fixed neurite and (c) fluorescent image labeled with phalloidin to see F-actin.

2.4.2 Live fluorescence microscopy

To image F-actin in live neurons, we used the live cell fluorogenic F-actin labeling probe (Si-R actin, Spirochrome). Cell media for 7-21 DIV neurons was replaced with cell media containing 100nM Si-R actin. As described in section 2.2.1, 10µm beads coated with PDL were added to the cells. In this case, the beads were incubated with the fluorogenic probe for 6-9 hours. After this time, the media was again replaced with regular cell media to remove the fluorogenic probe and then the dish was put in the MNI micropipette setup.

Theoretically, a linear increase in fluorescence indicates a linear increase in F-actin such that two F-actin polymers of equal length should be twice as bright as one. This could be used to measure the increase in the number of F-actin polymers in the neurite, indicating the maturation of the neurite. It could potentially also be correlated with tension, thickness of the neurite, strength or a measure of neurite developmental stage. In practice, this is very difficult to do because the fluorescent signal of a neurite is actually convoluted with bleaching, focal plane changes and the fluorescent probe being actively pumped out of the neuron (see figure 2.13). Although axons are quite dynamic and F-actin is continuously moving throughout, we can assume that a large bundle of axons should maintain an approximately constant amount of F-actin. We can thus use bundles of axons in the same field of view as the neurite to estimate how these three issues affect the signal inside the neurite.

We systematically varied the objective's focal plane from focusing below to above a bundle of axons. We varied it by 15µm, which is slightly larger than the amount the focus changes during experiments. We can see from figure 2.13b that the change in fluorescence appears to be approximately linear over 15µm. This is independent of whether the focal plane is above or below the axons. This is important because the neurites are typically suspended slightly above the surface of a glass slide. If we hope to use axons in the same field of view, but in a slightly different focal plane to correct for the neurite signal, then we would like the changes in the fluorescence of the axons to be the same as that of the neurite.

In figure 2.13c, the normalized intensity of three different bundles of axons are plotted with time. At the beginning of the experiment, the intensity is dominated by large changes in the focal length. However, over time, the microscope comes to a thermal equilibrium such that the

focal length barely changes. At long times (i.e. greater than about 2 hours), the dominating effects are bleaching of the fluorescent probes and the neuron actively pumping the dye out. These are both exponential effects, giving an explanation for why the raw signal in the neurite in figure 2.13a appears to be following an exponential fit with a plateau. By normalizing the intensity of the bundles of axons, we can use this as a transfer function for the raw neurite signal by simply dividing the raw neurite signal by the bundle signal. This approximates the true intensity in the neurite and is shown in figure 2.13d.

Unfortunately, there is significant variation in the transfer function (up to 35% difference), meaning that it is difficult to draw conclusions as to the type of increase of signal (e.g. linear, exponential, etc.). We can conclude that the signal increases, meaning that more F-actin polymers are being added to the neurite for many hours after pulling. We would expect the number of new F-actin polymers to eventually reach some equilibrium and stop increasing, but for this noise level and length of experiment, we cannot say when or if this occurs.

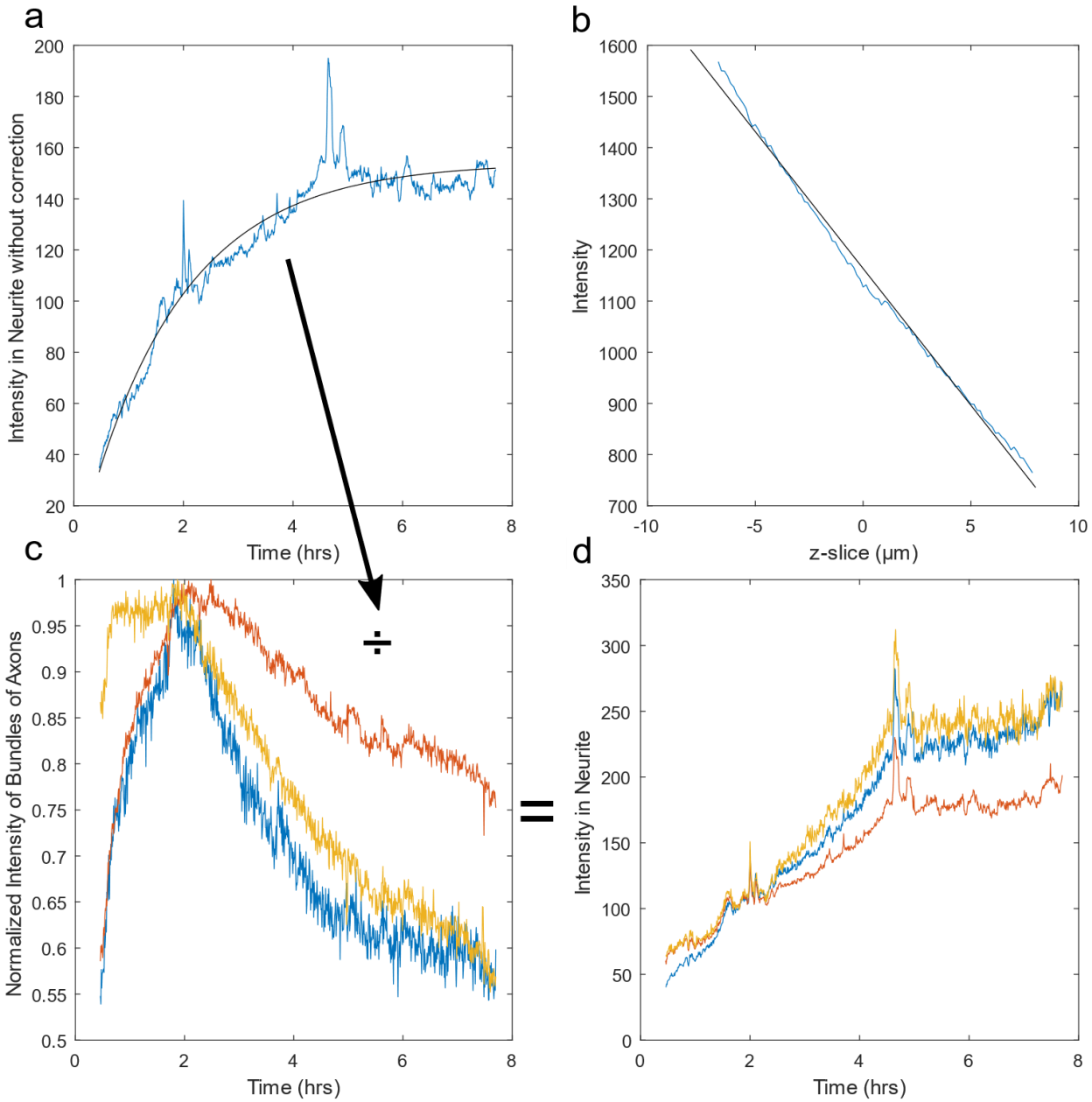

Figure 2.13 Fluorescent signal of a neurite with time. (a) Intensity of the neurite as a function of time. The F-actin signal seems to fit quite well to an exponential which reaches a plateau after a few hours, but systematic noise needs to be removed from the signal before this can be confirmed. (b) The effect on the fluorescent intensity as a function of focal position. At 0μm, the object is in optimal focus. (c) The normalized intensity of different bundles of axons in the same field of view as the neurite (which should not be changing with time, but is due to changing focal length, bleaching and the neuron pumping the dye out of the axon). The raw signal in (a) is corrected by dividing by (c) to get (d) the true fluorescence signal. Unfortunately, there is quite a bit of variation in the fluorescence of these axons, meaning that there is quite a lot of variation. It is hard to draw any conclusions from this data other than that the fluorescent signal increases with time.

3

3. Building an artificial neural network with neurons

This chapter is a combination of results from the paper "Building an artificial neural network with neurons" published in the journal AIP Advances with some other complimentary results added in. Everything inside angle quotes («») is from the paper. Otherwise, it is additional work.

Building an artificial neural network from neurons will help to understand what is fundamentally different between a brain and a computer. Neural networks which perform complex tasks have a high number of neurons and connections.[14] Even building a simple multi-layer perceptron (which for artificial neural networks can recognize hand-written digits) requires 496 neurons and 4215 connections.[88,89] The neuronal system of *C. elegans* would be interesting to build as the connectome is completely known, but this has a far more complex network with 320 neurons, 6393 chemical synapses, 890 gap junctions and 1410 neuromuscular junctions.[90] To manually wire a network of such complexity, we require very fast manipulation speeds. We have shown in previous work that by pulling poly-D-lysine or netrin coated beads which have formed a synapse with an axon,[67] we can initiate and extend neurites at speeds of 0.33µm/s or

greater over millimeter scale distances![71,91] This is about 300 times faster than average natural outgrowth of 0.0017µm/s. The maximum speeds attained and forces applied will determine how long it will take and which technology to use to wire the biological neural network. It is both biologically interesting and important for the optimization of wiring speeds to model the neurite physically and to look at the neurite's cytoskeletal structure over time. Once the network is wired, the non-trivial step of training the neural network to recognize hand-written digits must be performed.

3.1 Building a multi-layer perceptron from neurons

«A simple artificial neural network for image recognition of the hand-written numbers 0-9 consists of 16x16 inputs,[89] 2 deep layers of 15 neurons each and 10 outputs.[88] The same configuration of neurons was then chosen as shown in figure 3.1 to get an estimate of how long it would take to build a neuronal network from neurons. In a perceptron, every neuron from a previous layer is connected to every neuron from the next layer. This means that the total manipulation distance for the setup proposed would be given by:

$$d = s\sum_{i,j,k}\sqrt{(n+1-i)^2+(j-k-1)^2} + s\sum_{j,k}\sqrt{1+(j-k)^2} + s\sum_{j,k}\sqrt{1+(j-k-2)^2} \tag{3.1}$$

Where the variable i represents the indices for the rows, j and k represent the indices for subsequent layers of columns in figure 3.1 and n is the total number of rows in the first layer. The first term in equation 3.1 corresponds to the total amount of neurite needed to be manipulated to connect every neuron from the layer of input neurons to the first deep layer of neurons. Similarly, the second and third terms in the equation correspond to the two remaining layers being connected. The reason we sum over i, j and k in the first term, but only j and k in the second terms is that the first layer of input neurons has multiple rows (n rows) whereas the others only have one row. On a high-density multi-electrode array, separating the neurons by s=30 µm would allow recording from each neuron. This means that the total manipulation distance for the

requisite 4215 connections is 1.288 meters. In the following we will investigate if this is theoretically feasible using mechanical pulling of neurons.

From a bio-engineering perspective, there is no reason to choose this task and neural network over another. However, the identification of hand-written digits has been extensively studied in the machine learning community, and deep learning techniques have been very successful at performing this task. This has led to it being called "the drosophila of machine learning" by Geoffrey Hinton[14], so it makes a simple, but good candidate for making an artificial neural network from a biological one. We do not intend on building this network ourselves but would simply like to show that it is possible to build a neural network from neurons which can solve a real task.

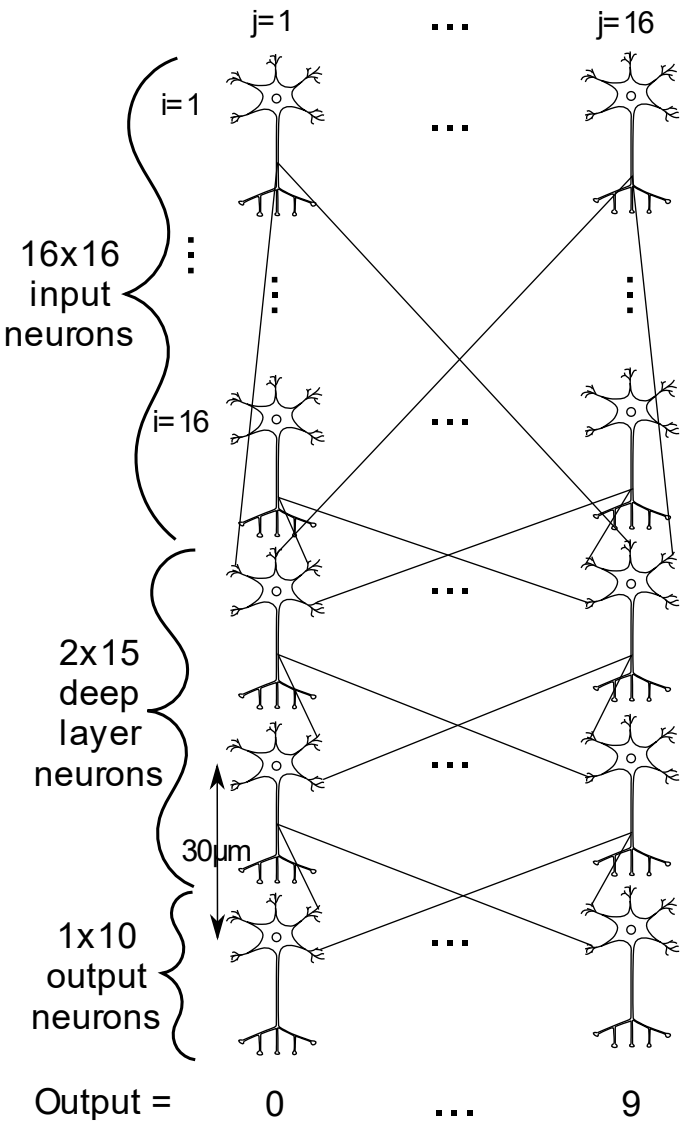

Figure 3.1 Multilayer Perceptron: Each neuron from the 16x16 block of input neurons will connect with each neuron from the first deep layer of 15 neurons. This is true for all adjacent layers (ie. all neurons in one layer are connected to all neurons in the next layer).

3.2 Force requirements

In order to wire a neural network, the manipulation method must be able to exert a large enough force to initiate and extend the neurites. Using an atomic force microscope to measure mechanical properties,[92] we found that the force required to initiate and extend a neurite varies significantly. To initiate a neurite, the maximum force was 1.1±0.7nN (+/-SD) (figure 3.2a) and to

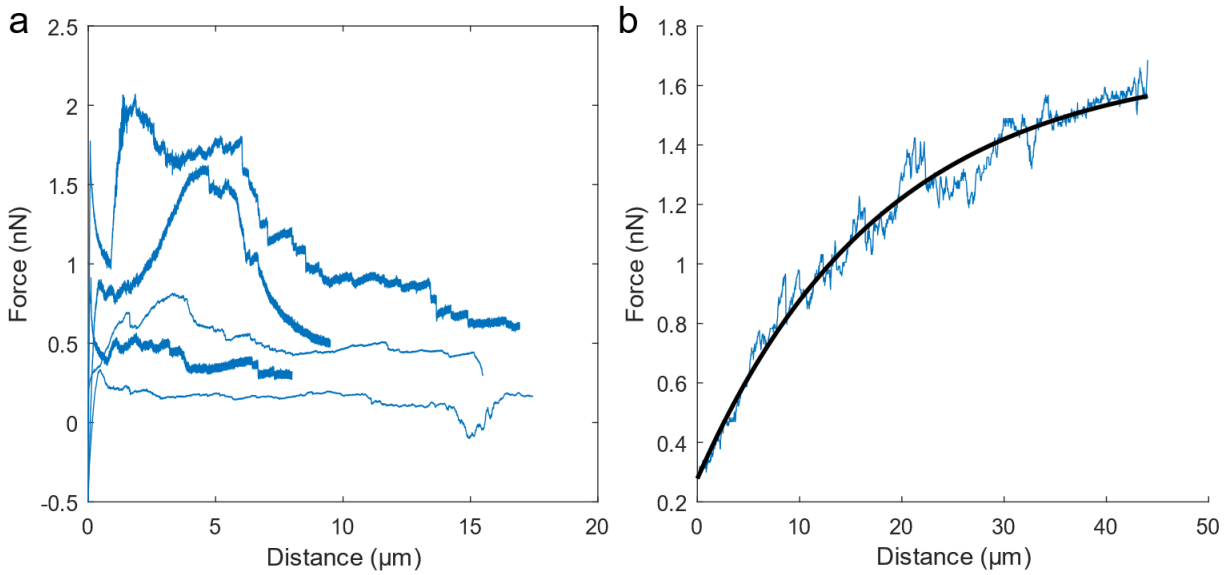

Figure 3.2 (a) Initiation of Neurites from 5 different experiments (maximum forces are F=1.98nN, 1.60nN, 0.81nN, 0.85nN, 0.24nN). (b) Following initiation, the neurite is elongated, and the force is fit with a Maxwell viscoelastic model.

continue extending the neurite, the average force was 1.1±0.8nN (+/-SD) (figure 3.2b) for 5 different experiments at the pulling speed 0.5μm/s. The large variability in the force needed is likely due to the variation in number of neurites being pulled. For these experiments, we often initiated neurites from bundles of neurons, possibly initiating the pulling of several neurites. The values quoted above are thus the maximum forces needed to initiate pulling of single neurites because the maximum force to initiate and pull one neurite will be less than or equal to the force obtained when pulling multiple neurites.

During the initiation of a neurite, the force does not simply increase with stretch as in Hooke's law.[74] The force initially increases very quickly, followed by a decrease in force, then finally after much more extension, the force begins to increase gradually again. According to both Powers et al. 2002 and Derenyi et al. 2002,

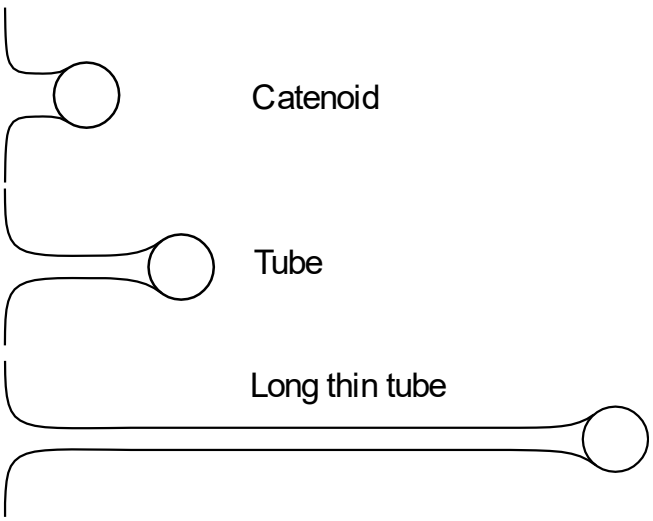

Figure 3.3 The neurite is initially a catenoid until the boundary conditions become unstable, and it collapses into a tube. The tube stretches with elongation but maintains the same approximately cylindrical shape.

the bead initially pulls out a portion of the axon into a catenoid as shown in figure 3.3. However, the boundary conditions of a catenoid are only stable when the neurite is below a specific length such that the neurite starts to collapse into a thin tube beyond this length and the force decreases.[65,66] As the pull continues, the tube starts to stretch, and the force increases again.[93] Over the first 10µm,[80] this increase is approximately linear, but is clearly viscoelastic on longer length scales (figure 3.2b). The simplest model that exhibits both viscous and elastic behavior is the Maxwell viscoelastic body and consists of a dashpot with viscosity μ and a spring with stiffness constant k. The force F as a function of extension x for a neurite being pulled at a constant velocity v is then:[94, 95]

$$F(x) = \mu v\left(1 - e^{-\frac{k}{\mu v}x}\right) \tag{3.2}$$

The spring constant and viscosity obtained from fits as in figure 3.2b from 5 different neurites is 56±35µN/m and 2.8±2.2mNs/m respectively. The significant variation in these values is again likely due to the variation of the number or diameter of neurites initiated.

3.3 Pulling speeds

Using our micromanipulation technique, we can pull at a remarkably fast 0.5µm/s to wire any two neurons together. Previous work has been done to show that the neurite is functional after 24 hours. The neurite contains actin, tubulin and neurofilament and it has been shown to be electrically connected to another neuron.[71] As far as we can determine, these 'pulled' neurons are structurally and functionally not distinguishable from naturally grown ones. An intriguing question is why is it possible to pull so fast? Is the neurite growing at this speed or is the plasma membrane stretched and the neurite subsequently filled with cytoskeletal elements? These are biologically interesting questions that are important to understand the limits to how fast we can build a complex neuronal network.

To answer this question, we fluorescently labelled F-actin, an important cytoskeletal element, and used it as a proxy for growth leading to biologically relevant structure and functionality. After

stretching / extending the neurite hundreds of micrometers at 0.1-0.5μm/s, the neurite is held at a constant length, and the maturation of the neurite can be observed. Immediately after stopping the extension, actin appears to be pulled into the neurite. This can be seen in the kymograph in figure 3.4a.

As in section 2, we can model the actin in the neurite as a Maxwell material, but this time with many Maxwell elements in series[95] (the exact details for the model are given in section 3.6). We thus derived the position of the i^{th} element of F-actin cytoskeleton in the neurite as a function of time to be:

$$d_i(t) = A\left(1 - e^{-\frac{t}{\tau}}\right) \tag{3.3}$$

Where A is the displacement of the actin and τ is the characteristic time it takes for the actin to arrive to its final position in the neurite. We fit equation (3.3) to the data in figure 3.4b, and we see that the characteristic time τ is a constant independent of the actin position in the neurite (figure 3.4c). Since τ is a constant throughout the neurite, we can use the average τ to determine the growth rate of the whole neurite. The average τ for all the actin movement in a neurite, measured in 7 different experiments, is 15.5±9min (±SD). Using actin cytoskeleton as a proxy for growth, where the growth is assumed to be finished after $t = 3\tau$ (when the distance the actin travelled is 95% of the total distance the actin will travel), these values translate to an effective growth rate of 0.048±0.02μm/s. This is calculated by dividing the total length of the neurite by 3τ plus the pull time. The maximum growth rate achieved without neurite thinning and breaking for Fass et al. 2003 was 0.055μm/s, indicating that the actual biological growth speed in our experiments is similar to the growth rates seen by others.[26] In their experiments however, they were not able to pull faster without the neurite breaking.

There are two main differences between the initiation of neurites in our experiments and those by others.[26,27,55,60,61] The first is that we initiate the neurites *de novo* from axons whereas normally neurites are initiated *de novo* from the cell body. The second is that our axon forms a pre-synapse with the bead before initiation whereas we do not believe that is the case in other experiments. We believe that others initiate neurites using simple adhesion because they all initiate their neurites from the cell body, whereas pre-synapses are formed on axons. In addition

to this, it takes at least 30 minutes to form a synapse with a PDL-coated bead.[67] Bray left the polylysine coated pipette in contact only "10 minutes or so",[43] Heidemann's group initiate

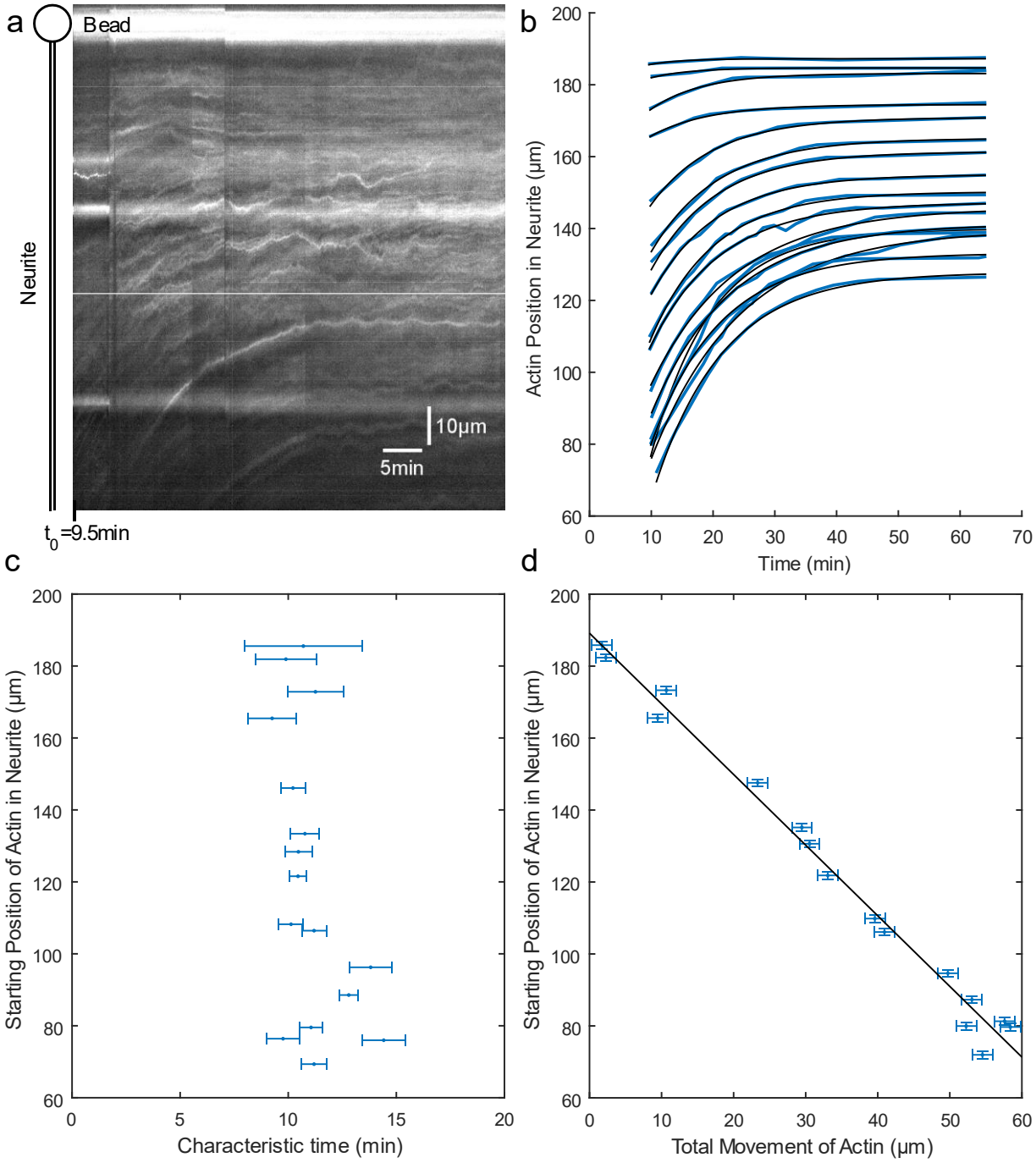

Figure 3.4 Movement of actin in the neurite after extension: (a) Kymograph of the actin starting 9.5min after extending neurite. The bead is at the top of the image, and the neurite extends straight down as in the drawing on the left. (b) Traces of actin from the kymograph in (a) with equation 4 fit to the data. (c) The characteristic time τ, a fit parameter in equation 4, is independent of the starting position of actin in the neurite. The characteristic time is equal to the spring constant divided by the viscosity of the neurite. (d) The total movement of actin has an inverse linear dependence on the starting position of actin in the neurite.

neurites immediately after coming in contact with the cell,[60,27,61] and the Integrin-coated beads added to the cells by Fass et al. 2003 were added once the neurons were in the manipulation setup, meaning they were not in contact long before the neurites were initiated (the exact time was not specified).[26] Heidemann's group also frequently pulls the growth cone of already formed axons, however, the fact that the axon is adhered to the surface slows the growth rate down because the adhesion increases its viscosity.[62] In our experiments, the neurite is always suspended in the solution, so we do not have this issue. It is possible that, in our experiments, the presence of an already formed axon adjacent to the neurite with a strong connection in the form of a synapse is better able to provide cytoskeleton and plasma membrane than a cell nucleus on its own, allowing for quicker pulling and the generation of a 'guiding structure' which later fills with the cytoskeletal components present in all axons.» The fast growth reported here seems to fulfill the criteria that the neurite-bead connection be strong, growth viscosity of the neurite be small and that there is no adhesion to the surface, causing dissipation of the force applied at the tip.[55]

3.4 Neurite Maturation

This section is not quoted from the paper:

We showed in the previous section that the actin cytoskeleton which arrives in the neurite can be modeled by a simple viscoelastic model, and that the characteristic time can give an estimate for how long it takes for the actin to arrive in the neurite. Actin is one of the main cytoskeletal components, providing stability to the neurite. By crosslinking with other actin filaments or by adding new filaments, the neurite can strengthen. The more F-actin present in the neurite, the stronger the fluorescence signal.

What is clear in figure 3.5 is that the fluorescent signal in the neurite increases over time. A mature axon has actin rings spaced 190nm apart, and a finite number of patches, hot spots and rings,[96] so it would make sense that the actin signal strength would have a characteristic time where the actin reaches some stable equilibrium with actin being removed at the same rate as it

is added. Indeed, it is common for actin filaments to enter into a steady state where their length is constant called treadmilling.[34] Here, we describe briefly again why, due to several important factors contributing to the noise, all that can be concluded is that the fluorescent signal definitively increases over time on the order of hours (see section 3.4.2 in chapter 3 on live fluorescence microscopy for more details). The live actin probe is being pumped out by the neuron, such that the signal decreases exponentially over time with a characteristic time on the order of hours. The dye is bleaching, another effect leading to an exponential decrease in fluorescent signal. Lastly, as the microscope's focal plane changes with temperature drift, so does the fluorescent signal. As the microscope heats up slowly, the focus drifts upwards, causing the fluorescent signal to decrease. Despite the fact that these effects usually act to reduce the fluorescent signal over time, all 10 data sets acquired increase systematically in the same way as the set of unprocessed

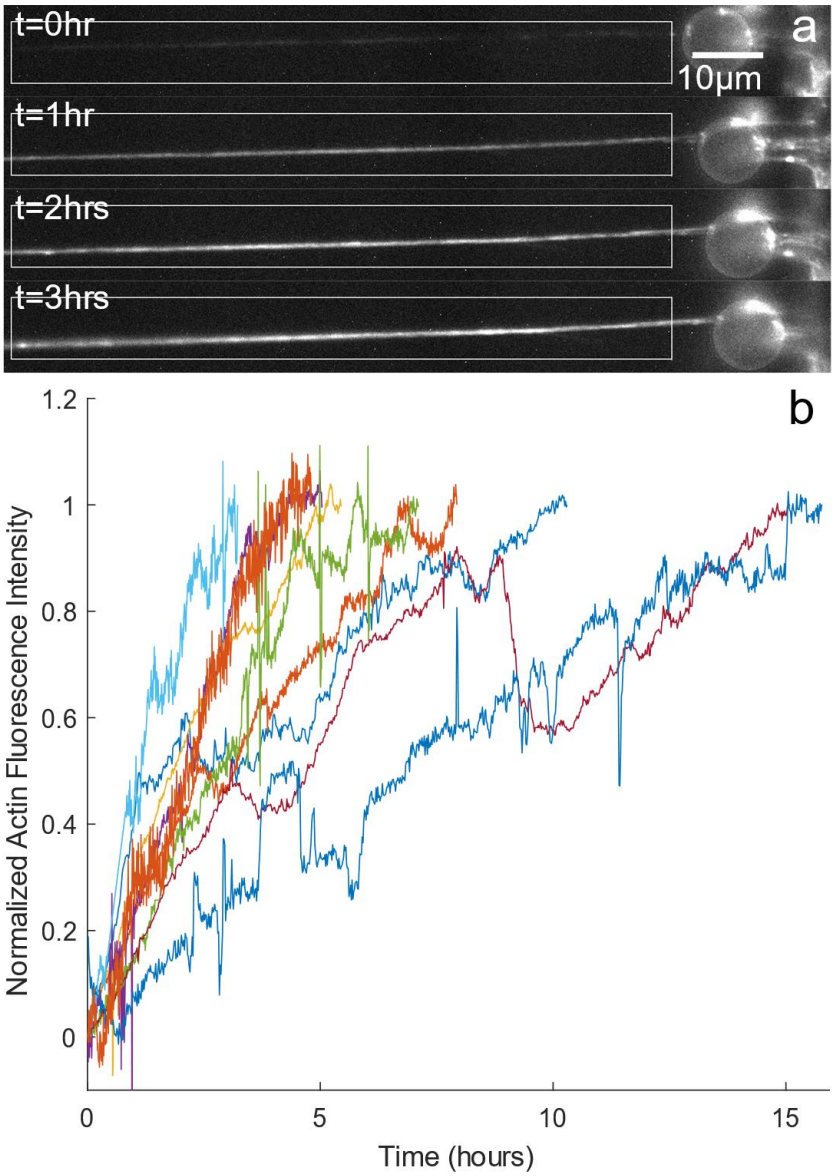

Figure 3.5. Neurite Maturation (a) Time series showing how the actin fluorescent signal increases with time. By summing the intensity for all pixels inside the rectangular box, and subtracting the background, we obtain the neurite's fluorescence as a function of time. (b) Zeroed and normalized actin fluorescence signal from 10 different neurites. The signal clearly increases over many hours, indicating an increase in actin in the neurites.

images show in figure 3.5a. We can thus say definitively that the amount of F-actin in the neurite is increasing with time. We can attempt to correct for these systematic effects by dividing by the fluorescent signal of nearby axons in the same field of view as the neurite. Their actin concentrations should be roughly constant with time, but their signal is also affected by bleaching, dye depletion and focal changes. After correcting for these effects, the resulting fluorescent increase appears to be linear (figure 3.5b). However, by looking at the fluorescent signal with time from different bundles of axons (see figure 3.5c), we can see that there are large differences between their correction factors. In figure 3.5c, the relative value of correction factors differs by as much as 35%. An underlying exponential with a long characteristic time will cause only a slight deviation from a linear curve, so it could easily be lost in the noise. For this reason, we cannot be certain that the curve is linear nor use this data to discover some maturation time to F-actin equilibrium.

3.5 Network robustness

«Once the neural network has been trained using images provided openly in the NIST database,[89] we would be able to determine the contribution of each neuron and its connections to the success of the network. To test this experimentally, we could sever individual axons (axotomy) and then reconnect them. In figure 3.6, we axotomized an axon using an atomic force microscope (AFM) cantilever, then used a PDL-coated bead glued to another AFM cantilever to micromanipulate one axotomized end into contact with the other. Subsequent experiments were encouraging but inconclusive as to whether the two axotomized ends fused. The newly grown neurites did show transport in both the proximal and distal ends, but it is unclear whether there is transport across the reconnection.

In further experiments designed to see if fusion between the two axotomized ends of the axon can occur simply by pressing the two ends together, we used patch clamp to input a membrane impermeable dye into the nucleus following axotomy and reconnection.» In figure 3.7a, the axon bundle was axotomized and reconnected using our micromanipulation technique,

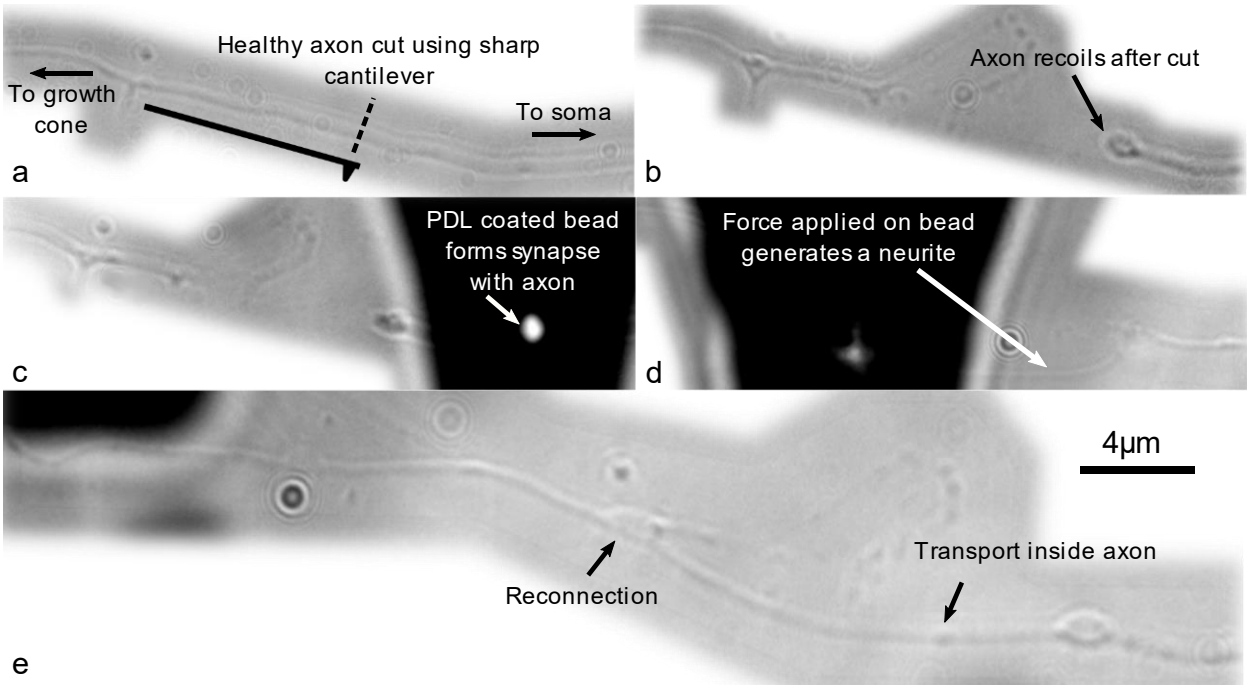

Figure 3.6. Axotomy and Reconnection. (a) A single healthy axon is cut along the dash line using a sharp cantilever. (b) Axon following axotomy. (c) A PDL-coated bead glued to bottom of cantilever (large black object) forms a synapse with proximal end of the axotomized axon. (d) Force applied by cantilever and bead on axon generates a new neurite. (e) Neurite reconnects the axon's proximal and distal ends. The axon appears to be reconnected and has transport in the proximal end, but not definitively in the distal end.

and we can faintly see the reconnected portion of the axon. In figure 3.7b, the distal end of the axon is fluorescing. Since the dye is membrane impermeable, this indicates that the proximal and distal ends must have undergone fusion in this case. Unfortunately, we were unable to show this again. «There are a few reasons why fusion may not be observed: the axon forms a synapse with the bead (so wouldn't fuse with the distal part of the axon), the cell would sometimes undergo Wallerian degeneration following axotomy, finding the correct nucleus to patch to experimentally demonstrate successful fusion was difficult as there were many axons taking similar paths, and it is possible that the fusion does not occur every time. The fact that we did not observe routine fusion following axotomy is unsurprising due to the above-mentioned challenges. Furthermore, it has also not been observed in mammalian axons to our knowledge (except by using methods which break down the membrane structure).[97] It has been observed to occur by axonal regeneration in *C. elegans*, crayfish, earthworm and leech.[98] Irrespective of whether the proximal and distal ends of the severed neuron can fuse using our micromanipulation technique and by pressing the two ends together, it has been routinely shown

that the two ends can be fused by using a technique called microelectrofusion.[97,99] This method works by dissolving the membrane using high electric pulses such that the membrane fuses into a single tube when it re-solidifies. We have showed here that by using microelectrofusion and our micromanipulation technique, we can systematically study the role of individual connections in the neural network.

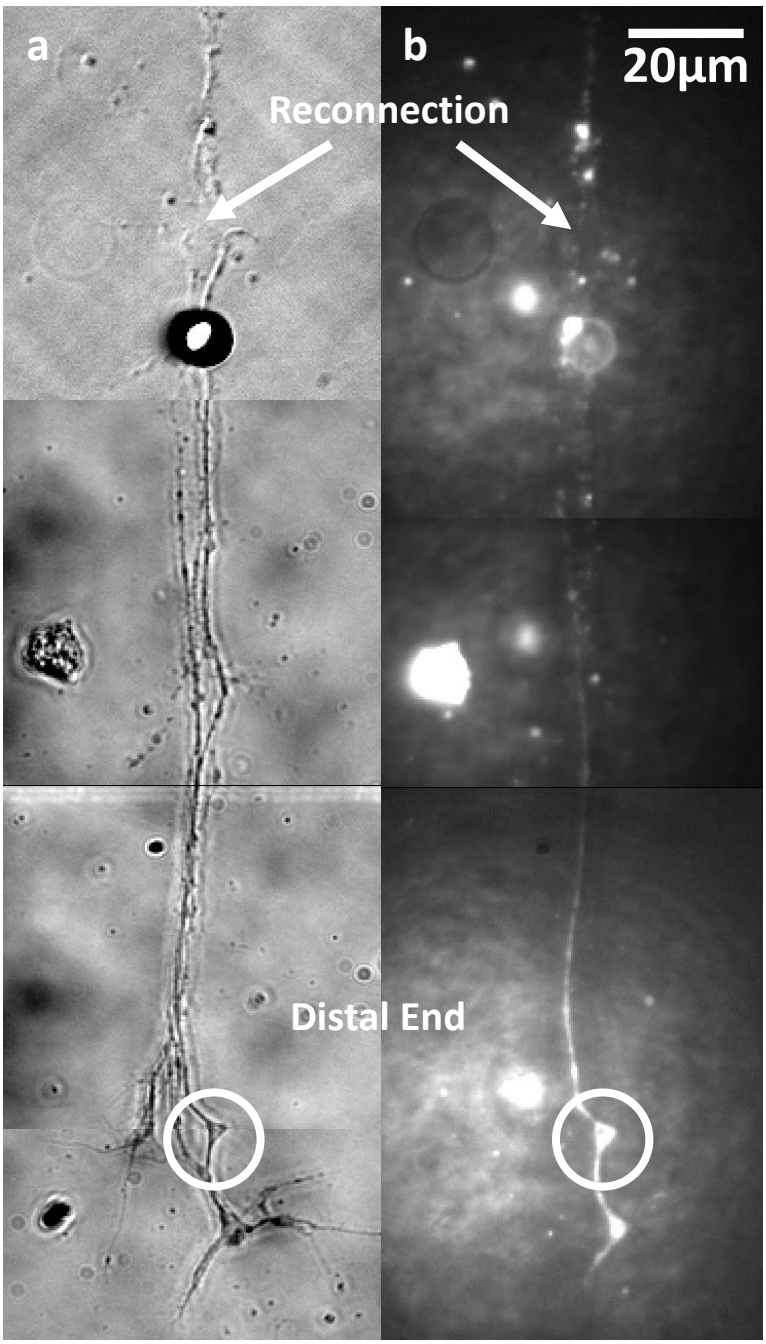

Figure 3.7 (a) Bright field image and (b) a fluorescent image of an axotomized axon who's proximal and distal ends were reconnected using our micromanipulation technique. After reconnection, a membrane impermeable dye was put into the cell body. Since there is clearly fluorescence in the distal end, this means that the proximal and distal ends have fused.

In sections 3.2 and 3.3, we used a Maxwell viscoelastic model (figure 3.8b) to fit force data and actin movement data respectively. In the constant velocity extension curves in figure 3.2b, the force increases, indicating stretch. This provides the motivation for the elastic component in the Maxwell model. The viscous component allows viscous flow to relax the spring, shown by the force plateau in figure 3.2b. Solving for the force as a function of extension at constant speed gives equation 3.2 which was used to fit the data in figure 3.2b. Since the neurite is well modeled as a spring and dashpot in series, it seems reasonable to model the transport of actin along the length of the neurite similarly. One spring and dashpot in series is mathematically equivalent to many connected smaller Maxwell elements. Since we are examining the actin movement throughout the length of the neurite, we propose a viscoelastic model consisting of many Maxwell elements in series[95] and derive the displacement of each element as a function of time (the model in figure 3.8a shows only the springs to make the visualization of each spring's displacement easier to follow).

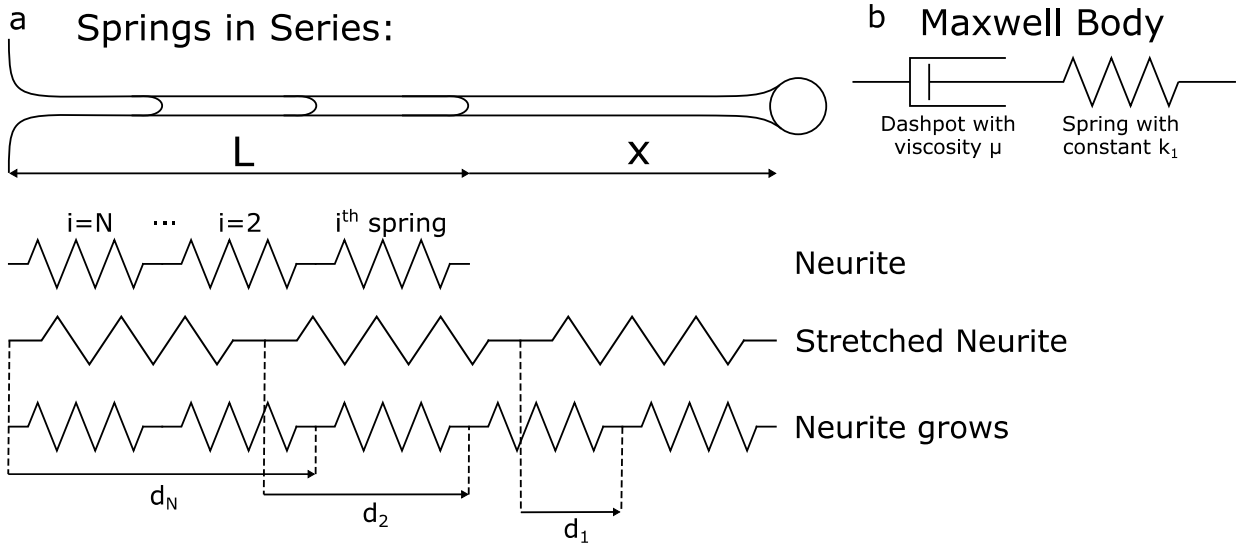

Figure 4.8. Physical model of the neurite during extension: (a) When modelling the neurite as many springs (and dashpots, not shown) in series, we can predict where each spring will be relative to each other in the neurite by calculating d_i as a function of d_{i-1}. (b) Maxwell viscoelastic body: the movement of the actin in time cannot be instantaneous because there is viscous flow. We model this by putting a dashpot in series with each spring in the neurite.

The flow of actin into the neurite occurs after the neurite is extended and the springs are stretched out (figure 3.8a). The tension from the stretching pulls more material into the neurite

by overcoming the viscous resistance, relieving tension and effectively elongating the neurite. Each spring in the neurite will feel the same force and will be stretched equally because the springs are arranged in series. In figures 3.8a and 3.4d, we see that the total displacement d_i of the proximal springs (those closest to the axon-neurite junction) will be much larger than the displacement of the distal springs (those closest to the bead).» To be clear, despite the proximal springs having a larger displacement, they are not stretched any more than the distal springs. This is because the springs are in series, not parallel and because there is no dissipation of force along the length of the spring as there would be if the neurite was adhered to the surface.[55] «The full displacement of the ith spring is equal to the total amount of stretch of all the springs in front of it:

$$d_i(t) = \frac{i}{N}x - ix_i(t) \tag{3.4}$$

Here, N is the total number of springs in the neurite, x is the total amount of initial stretch in the neurite, and x_i is the instantaneous stretch in each spring. Each elastic spring element is accompanied by a viscous element (modelled by a dashpot) to represent the resistance of the neurite to flow. Each spring and dashpot will experience the same amount of force, so that we can write the force applied on each element in the neurite as:

$$F_i = k_s x_i = \mu_d(\dot{d}_i - \dot{d}_{i-1}) \tag{3.5}$$

We have assumed that the spring constant k_s and the viscosity μ_d of all constituents are the same, which agrees with the linear trend in figure 3.4d. Combining equations (3.4) and (3.5), and solving the resultant differential equation gives:

$$d_i(t) = \frac{ix}{N}\left(1 - e^{-\frac{k_s}{\mu_d}t}\right) \tag{3.6}$$

Which describes the displacement of the i^{th} element of the neurite as a function of time. Equation 3.6 is the same as equation (3.3), only we have now defined $A = ix/N$ and $\tau = \mu_d/k_s$. As noted in section 3.3, the characteristic time $\tau = \mu_d/k_s$ is a constant independent of the actin position in the neurite (figure 5c). This indicates that the tension is distributed equally throughout the

neurite, allowing all constituents to relax together, and providing evidence there is a similar composition along the length of the neurite. The neurite displays a remarkable ability to stretch itself, with the actin pulled mechanically into the neurite.

Equation 3.6 also indicates that the total movement of actin in the neurite should be smaller for actin that starts distally and that this should have a linear dependence. This is what we observe in figure 3.4d. The deviation of this line from the $y = -x$ line is the total length of springs in the neurite measured in equilibrium, $L = Nl$, where l is the length of one unstretched spring. In terms of variables defined in the model, figure 3.4d is a plot of $ix_i + L$ vs $(i/N)x$. As we would expect, neurites which were pulled a longer distance had both a longer length L and initial stretch x (data not shown).

The model describes all aspects of the data, providing evidence that the flow of actin is mechanically driven by the force applied to the neurite. The neurite does not grow at the pulling rate set by the user, but instead stretches, and later fills in with a characteristic time which depends on the spring constant and the viscous resistance. When compared to other mechanically induced growth in neurites, the effective growth rate of these neurites is similar. However, because we are able to pull much faster, this allows the possibility to wire a complex neural network in a comparatively small amount of time.»

We used a Maxwell model to describe the viscoelastic relaxation of the force during constant velocity extension curves in section 3.2, and this motivated us to again use a Maxwell model here to describe the viscoelastic flow of actin into the neurite guiding structure. The details of the model here do not allow the determination of the spring constant or the viscosity, whereas the force curves do. However, the characteristic time obtained here is equal to the spring constant divided by the viscosity, so it is possible to compare the characteristic times from the two separate experiments. The characteristic time for actin flow is 15.5±3min (±SE) compared to a value of only 50±20s (±SE) ($\tau = k_s/\mu_d = 2.8/0.056 = 50 \pm 20s$) for the experiments from section 3.2. These values are clearly not equal to within their uncertainties and their average values differ by an order of magnitude (the characteristic time for actin is 19 times larger than that of the force during constant elongation). This indicates that the viscoelastic behaviour shown by the forces measured in section 3.2 is not caused by the viscoelastic flow of actin, so are more

likely due to the flow of plasma membrane. Actin is then pulled into the guiding structure by the residual tension in the neurite which remains for a long time after pulling. Since we know from the live actin experiments that the neurite initially has a very small amount of actin, it is likely that the composition of the guiding structure is mainly plasma membrane with a small amount of cytoskeleton. This means the viscosity will be low, allowing for quick elongation.[55]

3.7 Optimal manipulation

«With our micromanipulation technique, we can pull at 0.5µm/s, meaning it would take 30 days of pulling time to wire the proposed multilayer perceptron network's 1.288 meters total length. This is prohibitively slow: The cells will die well before the 30 days of manipulations are complete, as the manipulation is not performed in an incubator with optimal conditions for neuron survival. A more realistic maximum time for completing these manipulations before the cells die is empirically about 24 hours; an effective speed up of about 30 times is thus necessary. The only solution to reduce the manipulation time by this much would be to pull multiple beads simultaneously.

The necessary criteria for wiring an arbitrary neural network are:

1. The setup must keep cells alive for many hours.
2. It must be possible to manipulate in all 3 dimensions.
3. Most importantly, as described in section 3.2, the method must be able to exert a large enough force to initiate and extend the neurites.

There are many techniques for manipulating microspheres in a dish. Optical tweezers can be multiplexed, but the trap force maximum is generally about 100pN and the laser can cause photodamage and heat the sample significantly, both leading to cell death.[100] Acoustic force spectroscopy and centrifugal force spectroscopy both lack multidimensional motion.[101,102] An atomic force microscope cantilever array has many positives, but it cannot effectively release the beads as these are usually glued to the end of the cantilevers.[103] By making a hole in the bottom of the cantilevers, it could be possible to use suction to pick up the beads, but this method still lacks independent control over each bead.[104] Magnetic traps have been multiplexed by

positioning a magnet far away from the beads, such that all beads feel the same field. However, the multiplexing abilities mean that the magnets are positioned quite far away such that the maximum force is 260pN, and in most systems significantly less.[105,106] The multiplexed traps also lack independent control as they exert the same force on all beads.

The best option seems to be to use 2-3 magnetic pole pieces similarly to Fass et al, 2003. Since the pole pieces are mounted on a micromanipulator, each pole piece would give control over another dimension, the pole pieces can be brought into proximity with the magnetic bead of choice (allowing a large range of force control and bead selectivity) and this method does not kill the cells. Using an electromagnet, the force dependence on distance is a power law[107] which allows manipulating specific beads based on proximity to the pole pieces. Also, the force depends linearly on the current flowing through the solenoid[107] allowing quick adjustments to the force applied. Using a 4.5µm bead, and by varying the distance and the current, it is possible to apply forces that range from 15pN up to many nanonewtons.[26]

This method could be multiplexed by picking up each bead in a column (see figure 3.1) in one pass, such that many beads will all be pulled together. An appropriate field gradient could be one where a bead 14µm away would feel a force of around 1nN, sufficient to initiate and extend a neurite. Using this field, a bead on an adjacent axon another 30µm away (and thus a total of 44µm away), would feel only 0.1nN force, so it would not be initiated. For reference, a bead 10, 20, 30, 40 and 50µm away from the pole piece would feel a force of 2.0, 0.5, 0.22, 0.12 and 0.078nN respectively. In the situation where a bead on an adjacent axon was for example only 20µm away, it could be inadvertently initiated. This should be avoidable though because each bead is placed on the axon by the user and the multi-electrode arrays are separated by 30µm (although some optimization might be necessary here). Using these parameters, many beads could be picked up sequentially and connected to their common destinations simultaneously. Each pass would thus connect one column of 16 neurons in the first layer to every neuron in the entire row of 15 neurons in the next layer.

Since the input neurons form a 16x16 square of neurons, each column of this square could be pulled at one time simply by picking up a bead and moving on to the next row of neurons to pick up the next bead and initiate another neurite. To connect these newly initiated neurites to

the dendrites of the next layer's neurons, the neurites could be connected by wedging them under a non-magnetic bead sitting on the target neuron's dendrites. In this way, the column of neurons will have their neurites connected to each neuron's dendrites in the next layer's row in one single pass. This would reduce the amount of pulling time from about 42 days in sequential pulling, as calculated at the beginning of this section, to about 10.3 hours. Of course, for this to work, 296 beads would have to be precisely placed on the axons and dendrites throughout the dish. Placing a bead takes about 1 minute, so this would add about 5 more hours. Adding another hour for the user to operate the setup and make decisions in real time implies that it should be possible to wire the entire circuit in only 17 hours. Based on these considerations, using multiple magnetic pole pieces to connect this circuit seems feasible.

3.8 A learning biological neural network

Once the neural network has been successfully wired, the connections will be initially firing randomly, and will not be able to process a hand-written digit. In an artificial neural network, teaching a neural network to recognize a digit is done through a method called backpropagation. Each input neuron receives a pixel value from 0 to 1 from the initial 16x16 image, and the signal is passed through the layers to the output layer. As the signal passes from one layer to the next, the activation energy (neuron initial value), the weight (factor multiplied with the activation energy) and the bias (offset added at the end) will be scaled to determine what value between 0 and 1 the next neuron will take.[88] Teaching the network adjusts those three variables for every connection in the network appropriately to maximize the chance of outputting the correct number. Backpropagation works by calculating the cost function (the sum of the difference between the output and the input), and figures out what values of activation energies, weights and biases will give the correct value. This is done by minimizing the gradient of the cost function on a large set of training data.

In a biological neural network, Hebbian theory says that neurons can adjust the strength of their connections by increasing the number of synaptic connections or by changing the nature of their synapse (eg. by increasing synaptic vesicle exocytosis) in a process called long-term

potentiation.[8,9] Long-term potentiation is analogous to increasing the weight of a connection in an artificial neural network. Pre- and post-synaptic neurons depolarizing together during a high frequency stimulation can cause long-term potentiation.[11] Certain pathways may be inadvertently strengthened, but with the multi-electrode array, those pathways can be discouraged by hyperpolarizing select cells, preventing them from being strengthened. Bienenstock, Cooper and Munro (BCM) developed a theory which builds on Hebbian theory and says that when a pre-synaptic neuron is stimulated, but the post-synaptic activity is below a certain threshold, long-term depression will occur.[10] Long-term depression is the functional opposite of long-term potentiation and is analogous to decreasing the weight of specific connections. By inducing either long-term potentiation or depression, specific connections can be either encouraged or discouraged.[11–13] Synaptic plasticity can be induced using other methods such as: the pairing of depotentiation in pre- and post-synaptic neurons,[108] using naturally occurring firing patterns to induce LTP,[109] or by using N-methyl-D-aspartate to induce LDP.[13] Non-synaptic forms of plasticity which affect all the synapses in a cell[110] or membrane geometric properties[111] also exist.

A significant difference between a neuron and a computer is that a neuron will only fire if it reaches a threshold polarization, and its strength of polarization is always the same, which means that the analog of activation energy in an artificial neural network is not the same as changing the strength of the action potential in a biological neural network. Instead, information is encoded through stimulation pulses.[112] We could make high frequency pulses in a biological neural network analogous to higher activation energies in an artificial neural network. The pixel values that were encoded in the artificial neural network with a value between 0 and 1 could instead be encoded using higher and lower frequency inputs. Since the multi-electrode array allows both the stimulation and recording of action potentials of all the neurons in the dish, the entire network could be analyzed with the gradient of the cost function as in an artificial neural network. By systematically changing the long-term potentiation and depression of specific connections, the network could then be trained using backpropagation.

Assuming an artificial neural network with the exact topography described in section 3.1 is successfully built, there will still be a number of challenges in the actual training of the neural

network and the interpretation of its outputs. These are challenges present in any artificial neural network, but with the added complexity that the network is slower to train, the activation energy here is encoded as a frequency and the neuron may compute information in a fundamentally different way.

The biggest challenge would be if the biological neural network is unable to learn at all and the error rate on the training dataset never decreases significantly (underfitting). The strength of the connections between neurons are altered by inducing physiological changes to each connection, meaning that the neurons will take much longer to train than an artificial neural network. This means that it may not be possible to do more than 1 epoch (i.e. one pass through the entire training dataset, which for the MNIST dataset is 60000 hand-written digits), and hence the data will be underfit.[14] To compensate for this limitation, it may be more efficient to increase the number of training examples between each change to connection strengths. Another reason the network is underfitting could be due to fundamentally different computational methods between an artificial neural network and a biological one (e.g. because the frequency of the signal may not encode the activation energies properly). We know there are differences in how the two networks compute, and this may necessitate a different approach for training the network. Rather than specifying the exact algorithm for computing to the network, letting it figure out how to best process the information itself might give insights into how a biological neural network naturally computes. However, this will be difficult as we do not yet have a clear idea of how the network computes, so it will be difficult to know how to train the network (i.e. what behavior to encourage or discourage).

The opposite scenario where the network performs well on training data but does not perform well on test data is called overfitting. In this case, the capacity of the network will need to be reduced. In an artificial neural network, one way this is done is by using different types of non-linear functions for calculating the activation energies.[14] However, for a biological neural network, the neuron fires if depolarized below a certain threshold and this is intrinsic to the neuron, so it is not possible to change this. Instead, other techniques for reducing the capacity of the network should be employed, such as reducing the number of neurons in the deep layers or reducing the number of epochs. Following these adjustments, if the network can successfully

classify the hand-written digits from the test dataset (10000 digits), then we can be satisfied that the network has truly learned how to perform a complex task. We believe that the process of getting to this point will be important in understanding the difference between the biological neural network and the artificial one.

We believe that building an artificial neural network from biological neurons will help to understand what is fundamentally different between a brain and a machine. We propose a method to train the network by using backpropagation, which is used on artificial neural networks, by systematically changing the weight of the connections between neurons and by using frequencies to encode what would normally be entered as the activation energies of an artificial neural network. We propose using a multi-electrode array, to record all action potentials and stimulate any neuron, which would allow us to measure and systematically change any of the weights of the connections between neurons, capabilities which are not currently available for any complex network. The bioengineering feat of wiring all the connections into a complex biological neural can be done by using our micromanipulation technique which can pull 300 times faster than average natural growth. We have shown that the maximum forces required to initiate and elongate these neurites is within the capabilities of a magnetic trap. We have developed a model which describes the remarkable mechanically induced growth in the neurite. Furthermore, we have shown that it could be possible to test the robustness of this network by axotomizing specific axons and then reconnecting them. We believe that all the necessary knowledge and technology is available to build and teach an artificial neural network from biological neurons which will allow new insights into computation and learning in both machines and in brains.»

4

4. Extending the neurite model

In the previous chapter, we characterized the remarkable growth of functional neurites with the goal of determining the parameter space for building a perceptron from real neurons. In this chapter, we hope to build a more complete mechanical model describing the neurites.

4.1 Initiation of the neurite

In section 3.2, we presented data for the initiation of neurites from large bundles of axons. In other experiments, we used a higher magnification (100x's) which helped to pull neurites from either very small bundles or single axons. The data obtained from large bundles of neurites (figure 3.2a) contains multiple bumps and discontinuities, whereas the data presented in this section consistently shows a single smooth bump in the force distance curve (figure 4.1a). This is because, in a bundle of axons, several neurites are initiated simultaneously, but with slight differences in position. This causes a broadening in the transition point between catenoid and

cylindrical tube. Here, the broadening is minimized because there are very few neurites being initiated so that the distance pulled is well-defined.

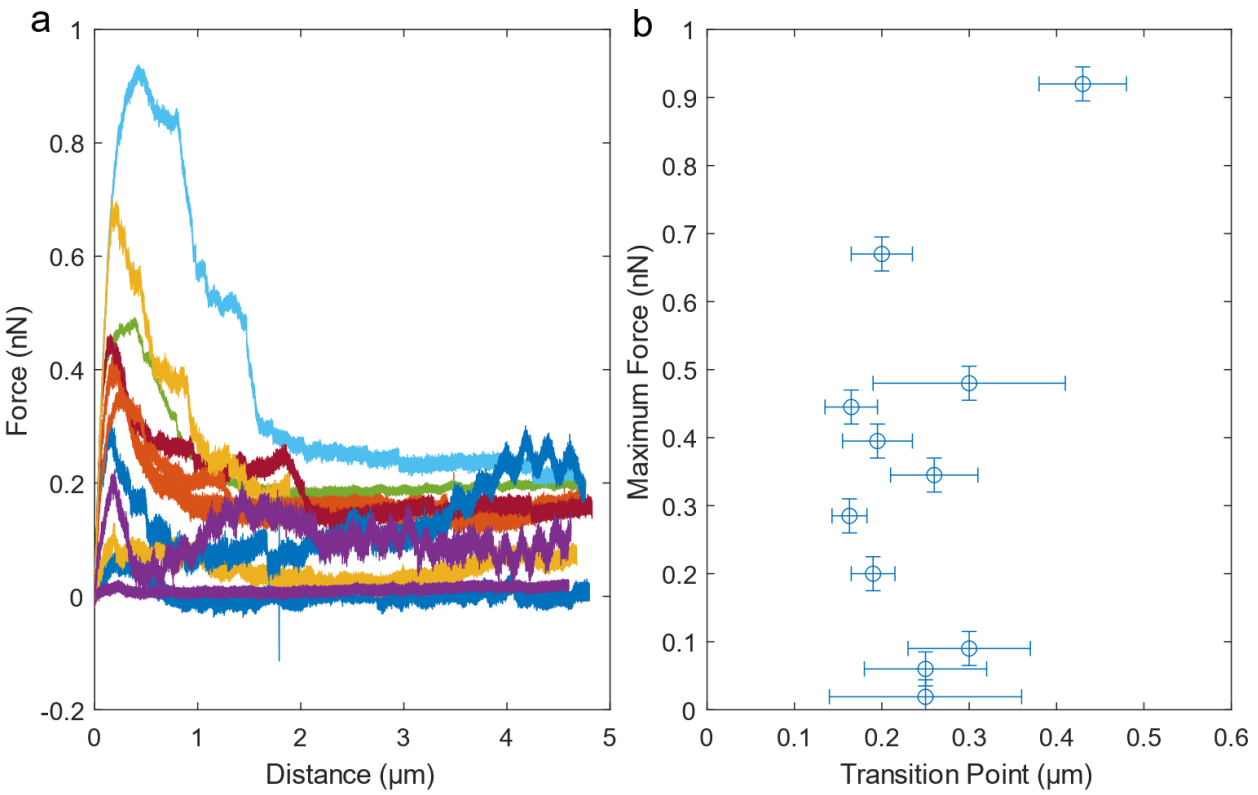

Figure 4.1. Neurite Initiation (a) Tension in the neurite as a function of distance pulled during neurite initiation for 10 different experiments on small bundles of axons. (b) The maximum tension in the neurite is plotted against the transition point from catenoid to tube of the neurite. Data was taken from (a).

The length at which the neurite transitions from a catenoid to a long tube is not statistical in nature, but rather, a well-defined point where the boundary conditions of the catenoid are no longer stable, so the structure collapses to a tube. In figure 4.1a, this point is well defined, and we can clearly see that the transition occurs at 0.25±0.08μm (±SD). If we remove the top point in figure 4.1b on the basis that it is an outlier and it is likely that multiple neurites are blurring the transition point (the top blue curve in figure 4.1a shows two large drops in force following the peak), the transition has even less variation: 0.23±0.05μm (±SD). The transition point was determined by median filtering the data around the peak, fitting a parabola to this data and finding the distance that corresponds to the maximum in the parabola. The uncertainty in the transition points in figure 4.1b is from the peaks not being smooth and from the zero point uncertainty. The zero point uncertainty in the position is due to the uncertainty in the zero point

in the force, which is why the three smallest forces have large uncertainties (the smallest forces have the least steep slope near zero, meaning that a small uncertainty in the force gives a large uncertainty in position). The determining factors for this transition point are the contact radius of the neurite with the bead, the radius at the point where the neurite protrudes from the axon, the bending rigidity of the neurite and the surface tension in the neurite.[65,66,113] Given the small variation in the transition point, we can assume that these variables do not vary greatly from experiment to experiment. This also means that the diameter of the neurite is likely quite constant.

Another point to note is that the force required to initiate a neurite was only 0.35±0.3nN (±SD). This should give a more appropriate maximum force needed to initiate a neurite than the value obtained from initiating neurites from large bundles. In the context of determining which techniques are suitable to wire a neural network with neurons, this would potentially allow the use of a larger number of possible techniques. In particular, mutliplexed magnetic traps and optical traps could possibly now be used as they can exert forces on the order of hundreds of piconewtons.[100,105,106]

4.2 Extending the neurite in steps

4.2.1 Tension in the neurite

In section 3.2, we showed that the neurite is a viscoelastic material which will initially stretch, but due to material flow, the tension is subsequently relieved. This was performed by extending neurites at a constant velocity. In this section, we extend the neurite in steps (see figure 4.2a). Similarly to section 3.2, the neurite here is initially stretched and then relaxes to a resting neurite tension with the addition of new material.

Figure 4.2b shows multiple increases in tension in the neurite, each corresponding to the extension of the neurite in a stepwise fashion. Due to the addition of new material, some of the tension is relieved. Not all the tension is released as the baseline tension increases slightly with each increase in length. The quick relaxation corresponds to the guiding structure described in sections 3.3 and 3.6, whereas the baseline tension provides the forces to pull the cytoskeleton

into the neurite. After long periods of time (tens of minutes-hours), we can visibly see in images the neurite relaxing and sometimes going slack on the surface of the slide, but for these time scales (minutes), the force appears constant.

4.2.2 Neurite stiffness

Another main characteristic of figure 4.2b is the relaxation after each step x_i. The relaxation happens on the order of tens of seconds, whereas the cytoskeleton takes tens of minutes to arrive. It is reasonable to believe then that this relaxation corresponds to that of the guiding structure described in section 3.6. As described before, this structure is assumed to consist mainly of plasma membrane with small amounts of cytoskeleton (we know it takes more than 10 minutes for the cytoskeleton to arrive and it continues to strengthen for hours after). Since these steps are very fast, we can obtain an effective spring constant for this guiding structure. This is done by dividing the tension in the neurite immediately after the step and dividing this by the step extension distance (5µm). Figure 4.2c clearly shows that the spring constant decreases with length. We assume that the decrease in spring constant is due to the addition of new material, not due to the neurite losing structural integrity. To show this, we use the same phenomenological model as in section 3.6 in which we modeled the neurite as many springs in series.

Here, we do not have information about each individual constituent along the length of the neurite as we did with the actin filaments distributed along the length of the neurite. We are only capable of measuring the global spring constant of the neurite. The global spring constant of the neurite k can be obtained as a function of material properties by considering the spring constant of each individual constituent k_i in series and in parallel. The equivalent spring constant k_j for one set of springs in series is given by:

$$\frac{1}{k_j} = \sum \frac{1}{k_i} = \frac{N}{k_i} \tag{4.1}$$

Where the unstretched length of the neurite L is given by $L = lN$, l is the size of each unstretched consituent and N is the total number of constituents as counted along the length of the neurite. The model and its variables are shown in figure 4.2d. This gives:

$$k_j = \frac{lk_i}{L} \tag{4.2}$$

Similarly for the springs in parallel, we have:

$$k = \sum k_j = \frac{N_A l k_i}{L} \tag{4.3}$$

Using a density ρ_A of total springs N_A in a cross-sectional area A, we insert $N_A = \rho_A A$ and get:

$$k = \frac{lk_i \rho_A A}{L} \tag{4.4}$$

Substituting in the macroscopic quantity, the elastic modulus $E = lk_i \rho_A$, gives:

$$k = \frac{EA}{L} \tag{4.5}$$

This predicts that the spring constant of the neurite should change with length if there is material flow and the constituents along the neurite remain the same. Obtaining the spring constant of the neurite is achieved simply by dividing the initial force due to stretching by the size of the step. This gives a spring constant for multiple lengths of neurite.

We assume that during longitudinal stretch, the area and elastic modulus will remain approximately constant while only the length will change. This allows us to fit equation 4.5 (plus a constant offset to the data as shown in figure 4.2c which is obtained from the fit to be 1.2±0.2x10^{-5}N/m). Although our model does not predict a constant offset, the offset may be the contribution to the spring constant from the rest of the neurite independent of the guiding structure (i.e. the small amount of cytoskeleton present). This constant could also be the source of increasing resting tension with neurite length discussed in section 4.2.1. Indeed, if the increase in resting tension is divided by the length, its spring constant is 1.1±0.2x10^{-5}N/m. This is equal to the spring constant offset mentioned above within uncertainty and is only 8% different.

We can see in figure 4.2c that the spring constant is inversely dependent on L, which indicates that the assumption that the cross-sectional area of the neurite is constant is a good one. The fitting parameter EA does however vary significantly from experiment to experiment (by one order of magnitude). The obvious explanation for this is due to a difference in diameter of neurite

or number of neurites. Since the spring constant depends linearly on area, two neurites would be twice as stiff as one, so a bundle of neurites would have a spring constant many times greater than a single neurite. The stiffness of the neurite would depend either quadratically or linearly on the radius if the constituents which contribute to the stiffness form a dense cylinder or a simple tube respectively. It is also possible that the elastic modulus is varying, but we do not expect different neurites to have very different compositions.

We would like to estimate the elastic modulus of the guiding structure by making some assumptions about the width and composition of the neurite. It is unlikely that the neurite will be thicker than an axon, which have a radius r of about 250nm,[114,115] and also unlikely that it will be smaller than the typical radius of tethers (tens of nanometers).[66] Furthermore, we have assumed before that the stiffness measurements made here are with respect to the guiding structure because the cytoskeleton requires tens of minutes to arrive. If this is the case, then plasma membrane gives the main contribution to the stiffness and the cross-sectional area of the neurite A is simply given by a tube:

$$A = 2\pi r w \tag{4.6}$$

Where the plasma membrane has a thickness w of about 10nm.[116] With these parameters, and using our one order of magnitude spread in EA, we get a value for the elastic modulus which is somewhere between 0.5-50x10^3Pa. These estimates are more likely to be overestimated because of the fact that there could be multiple neurites pulled. The lower bound of this estimate contains the elastic modulus of plasma membrane which is 1x10^3Pa.[116] We expect our guiding structure to be mainly plasma membrane with a small amount of cytoskeletal reinforcement, so an elastic modulus which is slightly larger than a tether makes sense.

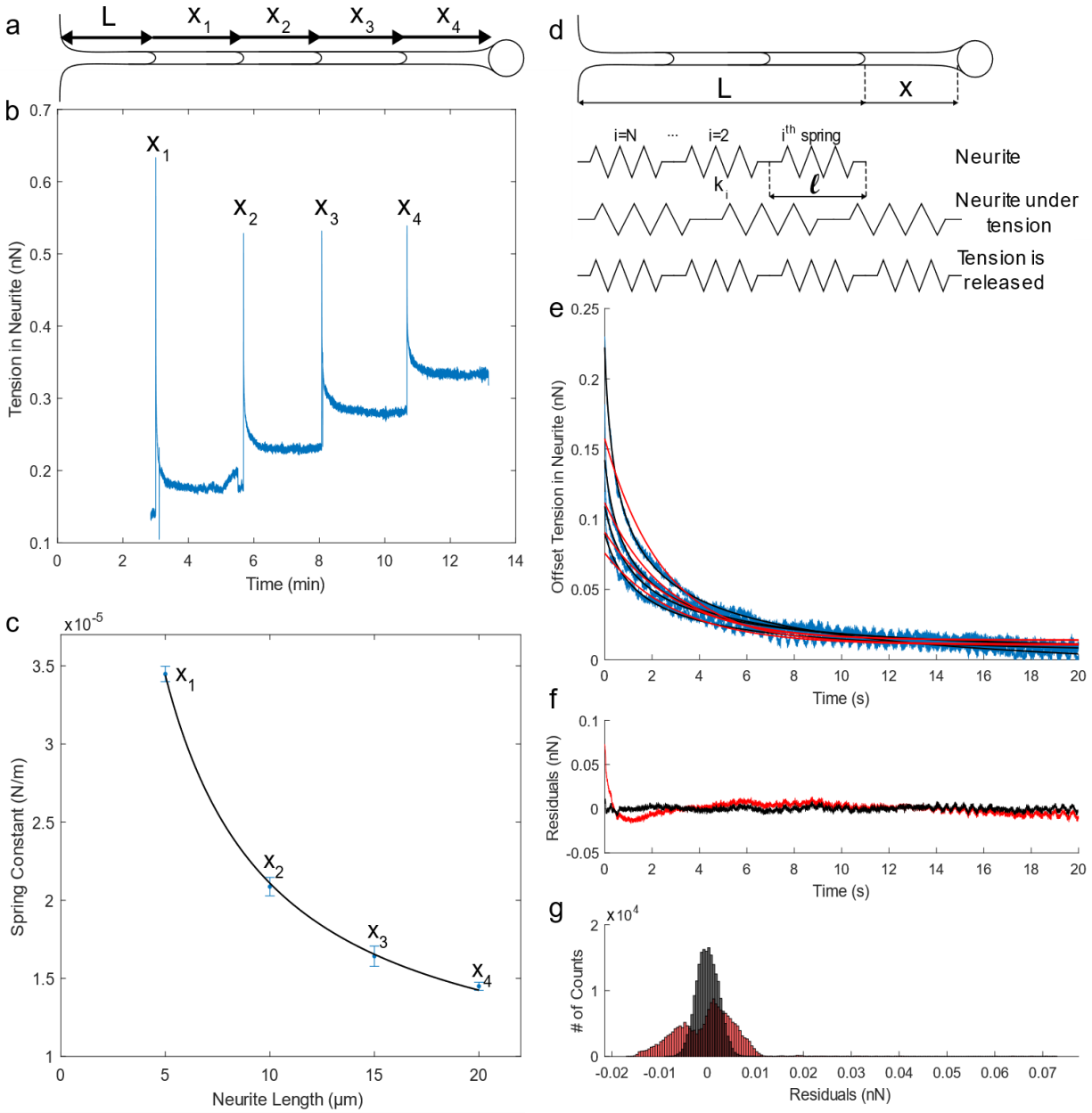

Figure 4.2 Extension of neurite in constant sized steps of x_i=5μm. (a) Cartoon of the neurite extended in constant sized steps. (b) Tension in neurite while being extended in constant sized steps. The first 3 minutes of the extension is omitted as this is the initiation of the neurite and this is not done by steps of 5μm, but rather at a constant speed of 0.1μm/s (see figure 5.1). (c) The spring constant of the neurite as a function of neurite length. The spring constant is obtained by dividing the increase in tension in the neurite by the size of extension step. The fit (black) shows the spring constant's inverse relationship with length of neurite as predicted by (d) our new model of the neurite as many springs in series which flow. Following the extension of the neurite, the springs are stretched, and the neurite is under tension. With time, the neurite relaxes, and the tension is released due to the addition of more springs. e) Data from b) but showing the data after each extension step and the data was offset such that all curves relax to 0nN. The data (blue) is fit with a Maxwell model (red) and our new model (black). For all lengths, our model fits the data better according to the Akaike Information Criteria which punishes our model for having one more variable. (f-g) The residuals and the histograms of the residuals taken from the first extension (x_1) show that our new model (black) is a better fit to the data than the Maxwell model (red).

4.2.3 Neurite relaxation

The spring constant and elastic modulus describe the neurite when it is statically stretched. However, the stretch relaxes temporally because the cell is a viscoelastic material. The most obvious way to attempt to describe this relaxation would be to use the same spring and dashpot Maxwell Model described in section 3.2. The solution is a simple exponential:

$$F(x) = F_0 e^{-\frac{k}{\mu}t} \tag{4.7}$$

Here, F is the force measured by the atomic force microscope, k is the global spring constant of the neurite, μ is the dashpot viscosity and t is the time. However, as shown in figure 4.2 e-g, the exponential qualitatively reproduces the correct shape, but does not fit the data well in this case. The reason for the model fitting poorly here, but well in section 3.2, is that the relative length of the neurite changes quickly when the neurite is pulled in steps as compared to the slower constant velocity extension in section 3.2. With this subtle change, the assumptions used to solve the Maxwell model break down.

The problem with the simple spring and dashpot model is that the strain $\epsilon = F/L$ is assumed to be a constant with time, but we know it not to be constant because the length of the neurite is changing (in the previous section, we showed that the spring constant is proportional to the inverse of the length). Given the conclusions of the previous section, a good alternate phenomenological model to propose would thus be one where the relaxation of the neurite is due to the addition of springs which lengthen the neurite and relieve the tension.

To achieve this objective, we use the model shown in figure 4.2d. The unstretched length of the neurite is L. There are N constituents, each contributing a stiffness k_i to the longitudinal stiffness k_j and have an unstretched, equilibrium length of l. After the neurite is stretched a distance x, we have a new length $L_s = L + x$. As before, $k_j = k_i/N$, so the global spring constant k and stretch x are given by the following two equations:

$$k = \frac{N_A k_i}{N} \tag{4.8}$$

$$x = L_s - lN \tag{4.9}$$

The tension in the neurite is given by Hooke's law $F = kx$. Substituting the previous two equations into Hooke's law gives:

$$F = N_A k_i \left(\frac{L_s}{N} - l\right) \tag{4.10}$$

Based on our results in section 4.2.2, the relaxation of the force is given by the addition of new springs that elongate the neurite. This implies that the only variable here that will depend on the time t is N, the total number of springs along the length of the neurite. If we assume viscous flow of new springs into the neurite, then the rate at which springs are added (i.e. N/t) should be proportional to the force applied multiplied by some term which characterizes the viscosity r_b. This is analogous to the situation for a dashpot element where the velocity is proportional to the force, which makes sense as we expect there to be some viscous element present here. Therefore, we expect the total number of springs to be equal to the initial number of springs N_i plus the new springs being pulled in:

$$N = N_i + r_b F t \tag{4.11}$$

Inserting this into equation 4.10, and solving for the force using the quadratic equation gives the force as a function of time:

$$F = \frac{\frac{L_i}{l} - r_b N_A k_i l t \pm \sqrt{\left(\frac{L_i}{l} + r_b N_A k_i l t\right)^2 + 4 r_b N_A k_i x_i t}}{2 r_b t} \tag{4.12}$$

The parameters that are known experimentally are L_i and x_i which are the initial length of the neurite before pulling and the size of the step respectively. $N_A k_i$ are effectively one parameter in the fit, and relate the spring constant of individual constituents k_i to the elastic modulus of the material. r_b is a viscous parameter with units of springs/nN·s and l is the equilibirum length of the individual constituents. Figure 4.2 e-g show how the data is fit much better by this model than the Maxwell model. In addition, the Akaike Information Criterion (AIC) is lower,[117] indicating that although there is an extra parameter, the model is still better.

The parameter extracted from four different neurites which describes the stiffness of the neurite, $N_A k_i$, is between 0.005-0.1N/m. Using the same assumptions as in section 4.2.2, but now

with the additional parameter l=0.5-5nm, we can calculate the elastic modulus with the formula (from equations 4.3 and 4.4): $E = lk_i N_A/A$. This gives an elastic modulus which is approximately 2-4 times larger than that calculated using the method from section 4.2.2. However, given that we have used multiple fit parameters to calculate the same value and the value is on the same order of magnitude, the results are not contradictory. Given that we used the equilibrium length l to calculate an elastic modulus which is comparable to that obtained in section 4.2.2, it is reasonable to trust this and the other parameters obtained from this fit. We can thus use the parameter l=0.5-5nm to try to understand what the length of each individual constituent contributing to the stiffness is. As the length is on the order of nanometers, not micrometers, we can conclude that the main constituent contributing to the stiffness is not the cytoskeletal elements or the cross-linkage between them, which are made of actin, microtubules and neurofilament and all have lengths on the order of micrometers. It seems more reasonable given that the length is on the order of nanometers that the main contribution to stiffness would be from the plasma membrane since typical phospholipid spacing is about 0.5nm[118] and our range is from l=0.5-5nm. In section 4.2.2, the lower bound of the elastic modulus of the neurite contained that of plasma membrane, suggesting that the guiding structure may be mainly plasma membrane with a small amount of cytoskeleton. Here, our fit parameter has a much smaller range of 0.5-5nm and the other candidates (ie. actin, microtubules and neurofilament) are about 1000 times larger than our range. Though not conclusive, this is a stronger indication that the guiding structure for the cytoskeleton in these neurites is (at least initially) mainly plasma membrane, with the cytoskeleton filling in and providing more support tens of minutes later.

The parameter r_b is a viscous term and ranges from 0.8-5x10^4 springs/nN·s. It is difficult to extract a value for the viscosity in normal units of nN·s/m because we do not know the origin of the viscosity (i.e. whether the resistance to flow is due to resistance between adjacent springs or with the interior or exterior of the membrane).

5

5. Conclusions and outlook

5.1 Conclusions

Building an artificial neural network from biological neurons is a huge task which will help us to understand both the brain and machines better. This requires the training and wiring of thousands of connections between hundreds of different neurons. If left alone, neurons will make connections almost randomly with many nearby neurons, so it is necessary to isolate them. However, neurons do not survive well if they are too isolated. They are extremely sensitive to environmental changes as they require the correct chemical cues and a pH, temperature and osmotic concentration in the optimal ranges. In sub-optimal conditions, they will die. Since neurons will not randomly form a complex network with 4215 different connections, we believe the use of manipulation techniques to wire them is more appropriate. Fass et al. 2003 already proposed a similar approach,[64] but their neurite pulling speeds are not fast enough to wire a complex network before all the neurons would be dead. Our group previously described a manipulation technique which would provide the speed-up needed to wire a multi-layer

perceptron capable of recognizing handwritten digits. We wanted to understand exactly why it was possible to pull so fast with the aim of improving the technique and using the details to describe exactly how to wire and train a complex neural network.

We have shown that it is possible to reliably pull at speeds as high as 0.5µm/s without the neurite breaking and with the consistent maturation of the neurite into a structurally stable axonal branch with cytoskeleton. We determined that the maximum forces needed to initiate and extend the neurites are on the order of 1nN or less. Using these parameters, we have determined that the most suitable currently available technology is that of a magnetic pole piece. By using multiple magnetic pole pieces simultaneously, three-dimensional control should be possible, which would allow the initiation, extension and connection of multiple neurites to multiple targets at once. We have determined that by growing neurons in a grid on a high-density multi-electrode array spaced only 30µm apart, the total time necessary for wiring the entire network of 496 neurons and 4215 connections is only 17 hours. This is below the maximum time of about 24 hours that neurons live happily in our live cell manipulation setup.

Once the network is correctly wired, we have proposed training it using backpropagation in an analogous way to training an artificial neural network. Whereas training an artificial neural network requires varying the values of the activation energies, weights and biases for the connections between nodes, we have proposed encoding the activation energies with frequencies (since neurons cannot vary the strength of an action potential) and the weights will correspond to the strength of the synaptic connections. By using a multi-electrode array, we could record all action potentials in the network, and use backpropagation to find which connections' strengths need to be changed. The connections will be strengthened or weakened by the careful spatio-temporal stimulation of connected neurons with the multi-electrode array, leading to long-term potentiation or depression. Once the network has been trained, the robustness of the network could be checked using our manipulation method to axotomize and reconnect axons. The process of trying to train this neural network will be difficult but it should help us to understand differences in computation between biological neural networks and artificial ones.

The rapid manipulation of neurites is crucial for wiring the network, so we have characterized it using various mechanical models. A PDL-coated bead left in contact with an axon will first form a synapse. Once the synapse is formed, we showed that the initiation of the neurite causes a large increase in force while the neurite is in the shape of a catenoid. Beyond a certain length, the catenoid boundary conditions are no longer stable and the neurite collapses into a cylindrical tube, corresponding to a decrease in tension.

We showed that it is possible to extend the neurite at a constant velocity or in steps. The neurite displays viscoelastic properties which are well described by a Maxwell model for constant velocity extension. However, modelling the neurite as many springs in series which are allowed to flow is a better model if the neurite is extended in steps. Both models give the same qualitative results, but the fact that the length changes so quickly when the neurite is extended in steps is likely the reason why the Maxwell model does not fit the data well in that case.

When the neurite is first extended, it forms a guiding structure which allows cytoskeleton to arrive later. We believe that the guiding structure is mainly composed of plasma membrane with a small amount of cytoskeleton because:

1) The F-actin fluorescent signal is initially quite weak, and we have showed that the actin cytoskeleton takes tens of minutes to arrive.

2) The guiding structure's viscoelastic characteristic time is 19 times smaller than that of the actin, indicating that the flow of actin is not responsible for the viscoelastic behaviour displayed during the initial extension of the neurite.

3) Using the many springs viscoelastic model on the guiding structure during step extensions predicts an elastic modulus consistent with the elastic modulus of plasma membrane, and a constituent spring size consistent with the phospholipid spacing in a lipid bilayer.

4) 0/4 neurites fixed within 3 minutes of initiation broke, compared to only 2/6 neurites fixed 30 minutes or more after initiation broke. All of the neurites broke during the Triton-X step which dissolves the membrane, indicating that the guiding structure lacked a reinforced cytoskeleton to prevent it from breaking.

When the neurite is first extended, we have showed that there is only a small amount of actin present, with the rest of the actin arriving tens of minutes later. As before, we modeled the

neurite using a Maxwell model. Similarly to O'Toole et al. 2008,[55] we treated the neurite in segments. We put many Maxwell elements in series to model the arrival of actin into the guiding structure. This model describes all aspects of the data and gives a characteristic time for actin arrival. Using actin arrival as a proxy for growth, we have similar growth rates to the maximum growth rates obtained by other groups. The crucial difference for wiring a neural network is that we are able to extend the neurite an order of magnitude faster compared to other groups whose neurites broke at these speeds. We believe the reasons for being able to pull so fast are that our neurite forms a synapse with the bead before pulling (which means the connection is strong), the neurite is initially small and largely devoid of cytoskeleton (which makes its viscosity small), and the neurite is suspended in solution (which prevents adhesion and a dissipation of speeds or force along its length).

5.2 Outlook

There are many next steps to take before we will be able to wire a neural network with neurons. Although we were pulling an order of magnitude faster than other groups and 300 times faster than regular axonal outgrowth, we may not have been pulling at the maximum speed. To find the maximum speed at which they can be pulled without breaking, we should systematically extend single neurites at higher speeds until they consistently break.

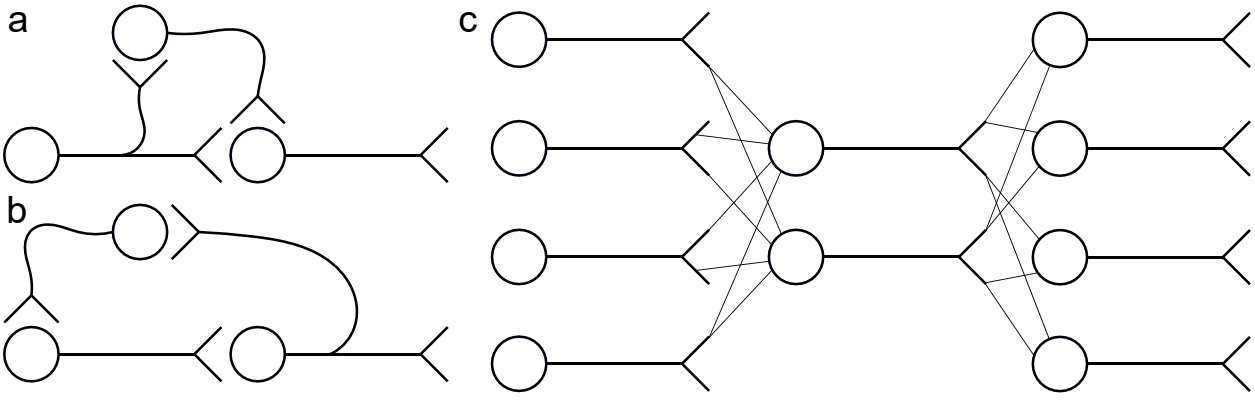

Figure 5.1 Simple neuronal circuits to wire before attempting the multi-layer perceptron. (a) Feedforward circuit (b) Feedback circuit (c) A 4-2-4 converter is a basic computer science circuit.

We observed the maturation of the neurites for as long as 15 hours. However, this was not long enough for the F-actin to reach a steady state. If the neurite's longevity could be extended

in the live manipulation setup or if the neurons are put back in the incubator and imaged periodically, we could determine how long it takes before the F-actin reaches a steady state. We also know other components of the cytoskeleton such as microtubules and neurofilaments are present in the neurite after many hours. It would thus be interesting to look at those components of the cytoskeleton to find when they arrive in the neurite, and how they mature.

The first step for wiring a neural network is to grow single, isolated neurons on a micro-electrode array. Next, it will be necessary to integrate multiple magnetic pole pieces for neurite manipulations. Using this setup, a small network such as a simple feedback or feedforward loop or a 4-2-4 converter (figure 5.1) should first be trained before moving on to the multi-layered perceptron (in a 4-2-4 converter, the four bits of information entered in the first layer of four neurons is encoded in the two neurons in the second layer, and then decoded back into the four neurons in the last output layer). Once we have built a multi-layered perceptron with neurons and trained it to recognize hand-written digits, we will be much closer to understanding the differences between the brain and machine than we are today.

6. References

[1] F.A.C. Azevedo, L.R.B. Carvalho, L.T. Grinberg, J.M. Farfel, R.E.L. Ferretti, R.E.P. Leite, W.J. Filho, R. Lent, and S. Herculano-Houzel, J. Comp. Neurol. **513**, 532 (2009).

[2] A. Araque, G. Carmignoto, P.G. Haydon, S.H.R. Oliet, R. Robitaille, and A. Volterra, Neuron **81**, 728 (2014).

[3] A. Volterra and J. Meldolesi, Nat. Rev. Neurosci. **6**, 626 (2005).

[4] I. Savtchouk and A. Volterra, J. Neurosci. **38**, 14 (2018).

[5] N.B. Hamilton and D. Attwell, Nat. Rev. Neurosci. **11**, 227 (2010).

[6] A. Longstaff, in 3rd ed. (Taylor & Francis, 2011).

[7] J.M. Tepper, C.J. Wilson, and T. Koós, Brain Res. Rev. **58**, 272 (2008).

[8] D.O. Hebb, *The Organization of Behavior; a Neuropsychological Theory.* (Wiley, Oxford, England, 1949).

[9] J.D. Sweatt, J. Neurochem. **139**, 179 (2016).

[10] E.L. Bienenstock, L.N. Cooper, and P.W. Munro, J. Neurosci. **2**, 32 (1982).

[11] T. V Bliss and T. Lomo, J. Physiol. **232**, 331 (1973).

[12] S.M. Dudek and M.F. Bear, Proc. Natl. Acad. Sci. U. S. A. **89**, 4363 (1992).

[13] H.-K. Lee, K. Kameyama, R.L. Huganir, and M.F. Bear, Neuron **21**, 1151 (1998).

[14] I. Goodfellow, Y. Bengio, and A. Courville, *Deep Learning* (MIT Press, 2016).

[15] A. Coates, B. Huval, T. Wang, D.J. Wu, A.Y. Ng, and B. Catanzaro, *Deep Learning with COTS HPC Systems* (2013).

[16] M.F. Hasan and Y. Berdichevsky, Micromachines **7**, 1 (2016).

[17] M. Ivenshitz and M. Segal, J. Neurophysiol. **104**, 1052 (2010).

[18] R. Singhvi, A. Kumar, G. Lopez, G. Stephanopoulos, D. Wang, G. Whitesides, and D. Ingber, Science **264**, 696 (1994).

[19] D.W. Branch, B.C. Wheeler, G.J. Brewer, and D.E. Leckband, IEEE Trans. Biomed. Eng. **47**, 290 (2000).

[20] W. Li, Z. Xu, J. Huang, X. Lin, R. Luo, C.-H. Chen, and P. Shi, Sci. Rep. **4**, 4784 (2015).

[21] J. Erickson, A. Tooker, Y.-C. Tai, and J. Pine, J. Neurosci. Methods **175**, 1 (2008).

[22] C. Wyart, C. Ybert, L. Bourdieu, C. Herr, C. Prinz, and D. Chatenay, J. Neurosci. Methods **117**, 123 (2002).

[23] E. Claverol-Tinturé, M. Ghirardi, F. Fiumara, X. Rosell, and J. Cabestany, J. Neural Eng. **2**, L1 (2005).

[24] T. Zhou, S.F. Perry, Y. Berdichevsky, S. Petryna, V. Fluck, and S. Tatic-Lucic, Biomed. Microdevices **17**, 2 (2015).

[25] O. Feinerman, A. Rotem, and E. Moses, Nat. Phys. **4**, 967 (2008).

[26] J.N. Fass and D.J. Odde, Biophys. J. **85**, 623 (2003).

[27] J. Zheng, P. Lamoureux, V. Santiago, T. Dennerll, R.E. Buxbaum, and S.R. Heidemann, J. Neurosci. **11**, 1117 (1991).

[28] C.S. Goodman and C.J. Shatz, Cell **72 Suppl**, 77 (1993).

[29] M. Tessier-Lavigne and C.S. Goodman, Science **274**, 1123 (1996).

[30] O. Marín and J.L.R. Rubenstein, Nat. Rev. Neurosci. **2**, 780 (2001).

[31] K. Xu, G. Zhong, and X. Zhuang, Science **339**, 452 (2013).

[32] D.B. Arnold and G. Gallo, J. Neurochem. **129**, 213 (2014).

[33] S. Roy, **212**, 131 (2016).

[34] P.C. Letourneau, in *Results Probl. Cell Differ.* (2009), pp. 265–290.

[35] A. Akhmanova and M.O. Steinmetz, Nat. Rev. Mol. Cell Biol. **9**, 309 (2008).

[36] A. Yuan, M. V. Rao, Veeranna, and R.A. Nixon, J. Cell Sci. **125**, 3257 (2012).

[37] C.L. Smith, J. Cell Biol. **127**, 1407 (1994).

[38] T. Slaughter, J. Wang, and M.M. Black, J. Neurosci. **17**, 5807 (1997).

[39] J.T. Kevenaar and C.C. Hoogenraad, Front. Mol. Neurosci. **8**, 1 (2015).

[40] E.W. Dent and F.B. Gertler, Neuron **40**, 209 (2003).

[41] D.M. Suter and P. Forscher, J. Neurobiol. **44**, 97 (2000).

[42] D. Bray, J. Cell Biol. **56**, 702 (1973).

[43] D. Bray, Dev. Biol. **102**, 379 (1984).

[44] S.S. Lim, K.J. Edson, P.C. Letourneau, and G.G. Borisy, J. Cell Biol. **111**, 123 (1990).

[45] S. Chang, T.M. Svitkina, G.G. Borisy, and S. V. Popov, Nat. Cell Biol. **1**, 399 (1999).

[46] G. Maheshwari, G. Brown, D.A. Lauffenburger, A. Wells, and L.G. Griffith, J. Cell Sci. **113 (Pt 10)**, 1677 (2000).

[47] K.E. Miller and M.P. Sheetz, J. Cell Biol. **173**, 373 (2006).

[48] P.C. Letourneau and A.H. Ressler, J. Cell Biol. **98**, 1355 (1984).

[49] B.J. Pfister, A. Iwata, D.F. Meaney, and D.H. Smith, J. Neurosci. **24**, 7978 (2004).

[50] D.H. Smith, Prog. Neurobiol. **89**, 231 (2009).

[51] J.R. Loverde and B.J. Pfister, Front. Cell. Neurosci. **9**, 1 (2015).

[52] S. Okabe and N. Hirokawa, J. Cell Biol. **117**, 105 (1992).

[53] S. Okabe and N. Hirokawa, J. Cell Biol. **120**, 1177 (1993).

[54] S. Chang, V.I. Rodionov, G.G. Borisy, and S. V Popov, J. Neurosci. **18**, 821 (1998).

[55] M. O'Toole, P. Lamoureux, and K.E. Miller, Biophys. J. **94**, 2610 (2008).

[56] C.E. Morris and U. Homann, J. Membr. Biol. **179**, 79 (2001).

[57] M. Hammarlund, E.M. Jorgensen, and M.J. Bastiani, J. Cell Biol. **176**, 269 (2007).

[58] J. He, R. Zhou, Z. Wu, M.A. Carrasco, P.T. Kurshan, J.E. Farley, D.J. Simon, G. Wang, B. Han, J. Hao, E. Heller, M.R. Freeman, K. Shen, T. Maniatis, M. Tessier-Lavigne, and X. Zhuang, Proc. Natl. Acad. Sci. **113**, 6029 (2016).

[59] S.C. Sidenstein, E. D'Este, M.J. Böhm, J.G. Danzl, V.N. Belov, and S.W. Hell, Sci. Rep. **6**, 26725 (2016).

[60] T.J. Dennerll, P. Lamoureux, R.E. Buxbaum, and S.R. Heidemann, J. Cell Biol. **109**, 3073 (1989).

[61] S. Chada, P. Lamoureux, R.E. Buxbaum, and S.R. Heidemann, J. Cell Sci. **110**, (1997).

[62] P. Lamoureux, S.R. Heidemann, N.R. Martzke, and K.E. Miller, Dev. Neurobiol. **70**, 135 (2010).

[63] P. Lamoureux, G. Ruthel, R.E. Buxbaum, and S.R. Heidemann, J. Cell Biol. **159**, 499 (2002).

[64] J.N. Fass, Investigation of Neurite Initiation and Elongation for Neural Network Engineering, University of Minnesota, 2003.

[65] T.R. Powers, G. Huber, and R.E. Goldstein, Phys. Rev. E **65**, 11 (2002).

[66] I. Derényi, F. Jülicher, and J. Prost, Phys. Rev. Lett. **88**, 4 (2002).

[67] A.L. Lucido, F. Suarez Sanchez, P. Thostrup, A. V. Kwiatkowski, S. Leal-Ortiz, G. Gopalakrishnan, D. Liazoghli, W. Belkaid, R.B. Lennox, P. Grutter, C.C. Garner, and D.R. Colman, J. Neurosci. **29**, 12449 (2009).

[68] M. Aeschlimann, Biophysical Models of Axonal Pathfinding, University of Lausanne, 2000.

[69] M. Aeschlimann and L. Tettoni, Neurocomputing **38**–**40**, 87 (2001).

[70] M. O'Toole, Models of Axonal Elongation and Transport, Michigan State University, n.d.

[71] M.H. Magdesian, G.M. Lopez-Ayon, M. Mori, D. Boudreau, A. Goulet-Hanssens, R. Sanz, Y.

Miyahara, C.J. Barrett, A.E. Fournier, Y. De Koninck, and P. Grutter, J. Neurosci. **36**, 979 (2016).

[72] M.H. Magdesian, M. Anthonisen, G.M. Lopez-Ayon, X.Y. Chua, M. Rigby, and P. Grütter, JoVE e55697 (2017).

[73] G. Binnig, C.F. Quate, and C. Gerber, Phys. Rev. Lett. **56**, 930 (1986).

[74] R. Hooke, *Lectures de Potentia Restitutiva, or, Of Spring* (1678).

[75] G. Meyer and N.M. Amer, Appl. Phys. Lett. **53**, 1045 (1988).

[76] T. Ando, N. Kodera, E. Takai, D. Maruyama, K. Saito, and A. Toda, Proc. Natl. Acad. Sci. U. S. A. **98**, 12468 (2001).

[77] J.E. Sader, J. Appl. Phys. **84**, 64 (1998).

[78] J.E. Sader, J.W.M. Chon, and P. Mulvaney, *Calibration of Rectangular Atomic Force Microscope Cantilevers* (1999).

[79] C.P. Green, H. Lioe, J.P. Cleveland, R. Proksch, P. Mulvaney, and J.E. Sader, (2004).

[80] M. Anthonisen, M. Rigby, M.H. Sangji, X.Y. Chua, and P. Grütter, J. Mech. Behav. Biomed. Mater. **98**, 121 (2019).

[81] R.J. Cannara, M. Eglin, and R.W. Carpick, Rev. Sci. Instrum. **77**, pages (2006).

[82] J.S. Goldman, M.A. Ashour, M.H. Magdesian, N.X. Tritsch, S.N. Harris, N. Christofi, R. Chemali, Y.E. Stern, G. Thompson-Steckel, P. Gris, S.D. Glasgow, P. Grutter, J.-F. Bouchard, E.S. Ruthazer, D. Stellwagen, and T.E. Kennedy, J. Neurosci. **33**, 17278 (2013).

[83] *P-2000 Laser Based Micropipette Puller System Operation Manual* (2010).

[84] S. Gomis-Rüth, M. Stiess, C.J. Wierenga, L. Meyn, and F. Bradke, Nat. Protoc. **9**, 1028 (2014).

[85] M.E. Morris, J. Leblond, N. Agopyan, and K. Krnjević, J. Neurophysiol. **65**, 157 (1991).

[86] S.M. Potter and T.B. Demarse, **110**, 17 (2001).

[87] T.J. Kurtti, S.P.S. Chaudhary, and M.A. Brooks, In Vitro **11**, 274 (1975).

[88] M.A. Nielsen, (2015).

[89] Y. Lecun, L. Bottou, Y. Bengio, and P. Haffner, Proc. IEEE **86**, 2278 (1998).

[90] L.R. Varshney, B.L. Chen, E. Paniagua, D.H. Hall, and D.B. Chklovskii, PLOS Comput. Biol. **7**, e1001066 (2011).

[91] M.H. Magdesian, M. Anthonisen, G. Monserratt Lopez-Ayon, X.Y. Chua, M. Rigby, and P. Grütter, J. Vis. Exp. **2017**, (2017).

[92] Y.F. Dufrêne, T. Ando, R. Garcia, D. Alsteens, D. Martinez-Martin, A. Engel, C. Gerber, and D.J. Müller, Nat. Nanotechnol. **12**, 295 (2017).

[93] O. Rossier, D. Cuvelier, N. Borghi, P.H. Puech, I. Derényi, A. Buguin, P. Nassoy, and F. Brochard-Wyart, Langmuir **19**, 575 (2003).

[94] J. Schmitz, M. Benoit, and K.E. Gottschalk, Biophys. J. **95**, 1448 (2008).

[95] W. Findley, J. Lai, and K. Onaran, **19**, 118 (1978).

[96] N. Chakrabarty, P. Dubey, Y. Tang, A. Ganguly, K. Ladt, C. Leterrier, P. Jung, and S. Roy, J. Cell Biol. jcb. 201711022 (2018).

[97] W.C. Chang, E. Hawkes, C.G. Keller, and D.W. Sretavan, Wiley Interdiscip. Rev. Nanomedicine Nanobiotechnology **2**, 151 (2010).

[98] B. Neumann, K.C.Q. Nguyen, D.H. Hall, A. Ben-Yakar, and M.A. Hilliard, Dev. Dyn. **240**, 1365 (2011).

[99] G.A. Neil and U. Zimmermann, Methods Enzymol. **220**, 174 (1993).

[100] K.C. Neuman and A. Nagy, Nat. Methods **5**, 491 (2008).

[101] G. Sitters, D. Kamsma, G. Thalhammer, M. Ritsch-Marte, E.J.G. Peterman, and G.J.L. Wuite, Nat. Methods **12**, 47 (2015).

[102] D. Yang, A. Ward, K. Halvorsen, and W.P. Wong, Nat. Commun. **7**, 11026 (2016).

[103] R. McKendry, J. Zhang, Y. Arntz, T. Strunz, M. Hegner, H.P. Lang, M.K. Baller, U. Certa, E.

Meyer, H.-J. Güntherodt, and C. Gerber, Proc. Natl. Acad. Sci. U. S. A. **99**, 9783 (2002).

[104] O. Guillaume-Gentil, E. Potthoff, D. Ossola, C.M. Franz, T. Zambelli, and J.A. Vorholt, Trends Biotechnol. **32**, 381 (2014).

[105] K.C. Johnson, E. Clemmens, H. Mahmoud, R. Kirkpatrick, J.C. Vizcarra, and W.E. Thomas, J. Biol. Eng. **11**, 47 (2017).

[106] N. Ribeck and O.A. Saleh, Rev. Sci. Instrum. **79**, 094301 (2008).

[107] A.R. Bausch, W. Möller, and E. Sackmann, Biophys. J. **76**, 573 (1999).

[108] B. Gustafsson and H. Wigström, J. Neurosci. **6**, 1575 (1986).

[109] O. Paulsen and T.J. Sejnowski, Curr. Opin. Neurobiol. **10**, 172 (2000).

[110] G.G. Turrigiano, K.R. Leslie, N.S. Desai, L.C. Rutherford, and S.B. Nelson, Nature **391**, 892 (1998).

[111] D. Debanne, G. Daoudal, V. Sourdet, and M. Russier, J. Physiol. **97**, 403 (2003).

[112] P.D. Maia and J.N. Kutz, J. Comput. Neurosci. **36**, 141 (2014).

[113] B. Pontes, N.B. Viana, L.T. Salgado, M. Farina, V.M. Neto, and H.M. Nussenzveig, Biophysj **101**, 43 (2011).

[114] M.H. Magdesian, F.S. Sanchez, M. Lopez, P. Thostrup, N. Durisic, W. Belkaid, D. Liazoghli, P. Grütter, and D.R. Colman, Biophys. J. **103**, 405 (2012).

[115] M. Pesaresi, R. Soon-Shiong, L. French, D.R. Kaplan, F.D. Miller, and T. Paus, Neuroimage **115**, 191 (2015).

[116] R.M. Hochmuth, N. Mohandas, and P.L. Blackshear, Biophys. J. **13**, 747 (1973).

[117] H. Bozdogan, Psychometrika **52**, 345 (1987).

[118] P.C. Nelson, M. Radosavljevic, and S. Bromberg, *Biological Physics : Energy, Information, Life* (W.H. Freeman and Co., New York, 2008).